Interaction between the vascular endothelial glycocalyx and flow *in vitro*

by Miao Lin

Supervisor: Professor Wen Wang

Submitted for the Degree of Doctor of Philosophy
School of Engineering and Materials Science
Queen Mary University of London

2016

Abstract

Vascular diseases, such as stroke and heart attacks, account for more than 50% of abnormal death worldwide. The cause of these diseases is linked to malfunctions of vascular endothelial cells, in particular the endothelial glycocalyx. This study investigates the location and stability of the endothelial glycocalyx under different flow conditions *in vitro*.

AFM (Atomic Force Microscopy) micro indentation is carried out on endothelial cell membrane to determine its Young's modulus. The Young's modulus of the glycocalyx layer is then deduced from measurements on cell membranes with, and those without, the glycocalyx layer. Heparan sulphate (HS) is an important component of the glycocalyx and can be removed by the enzyme heparinase-III (Hep-III). Our results show the glycocalyx on cultured Human Umbilical Vein Endothelial Cells (HUVECs) has a Young's modulus of ~0.64Kpa. We further observe how the Young's modulus of the endothelial cell membrane decreases with time, as the glycocalyx layer redevelops, following its removal by Hep-III.

Steady and oscillatory shear stimulations are used in flow chamber experiments. Under 24 hours' steady shear stimulation (12.6 dyn/cm^2), cells are seen to elongate and reorient parallel to the flow direction. The glycocalyx is seen to shift to the peripheral region of the cell surface. With actin depolymerisation treatment, significant shedding of the glycocalyx from the luminal surface of the cell is observed. This occurs together with the loss of focal adhesions on the basal membrane. When endothelial cells are subjected to 24 hours' oscillating shear stress, the size of the cell increases as the oscillatory reversal time (time between changes in oscillatory flow direction) increases. Measurements are taken with oscillatory flow reversal programmed at 5s, 10s and 15s. The angle (between the long axis of the cell and the flow direction) and the aspect ratio (long axis vs short axis) change from 41.57° and 1.72 : 1 (static) to 40.18° and 3.26 : 1 (5s), 36.71° and 4.17 : 1 (10s), 26.5° and 4.39 : 1 (15s). Both the height and the area of the cell increase.

The Young's modulus of the endothelial cell membrane is measured under oscillatory flows with different reversal time and compared to that under static flow conditions. An increase in the Young's modulus is observable under oscillatory flows, with the most significant change occurring at the edge (i.e. periphery) of the cell membrane area. As the oscillatory reversal time increases from 5s to 15s, the Young's modulus of the cell membrane increases. In the apical areas of the cell membrane, the increase is less significant. These results indicate that the thickness of the glycocalyx decreases as cells are exposed to oscillatory flows, and the loss is most significant in the peripheral region of the cell membrane. As the oscillatory reversal time increases from 5s to 15s, so the loss in the glycocalyx increases.

Acknowledgements

I would like to express my enormous gratitude to my supervisor, Professor Wen Wang, for his guidance, supervision and encouragement throughout my PhD project. I am really appreciative of everything he has taught me, his patience and support at every step of the experiment.

I am grateful to Dr. Asa Barber and Dr Núria Gavara, who are responsible for AFM in School of Engineering & Materials Science (SEMS) at Queen Mary University of London (QMUL), and supported me on AFM during the PhD project.

I would like to thank all the staff in SEMS of Queen Mary University of London: especially engineering technicians Mr Dennis Ife and Ms Jun Ma, for their help in manufacturing and development of the flow experiment; and Dr. Dongsheng Wu, who gave me training and support with super-resolution microscopy. I thank Dr. Zofia Luklinska and Mr Russell Bailey in Scanning Electron Microscope (SEM) and AFM imaging.

Many thanks to the group members in the Biofluids and Cell Mechanics Laboratory: Dr. Yankai Liu, Dr. Ke Bai, Dr. Hong Chang, Dr. Devendra Deo, Dr. Weiqi Li, Dr. Lin Qiu, Dr. Zhengjun Lv, Dr. Xia Chen, Ms Piaopiao Luo, Mr. Wenjie Zhu, Ms Rebecca Norton for happy memories of the time we spent together.

Furthermore, I would like to thank my parents, for their selfless love and support throughout my life. Finally, the deepest gratitude goes to my husband and my lovely daughter. I could not have finished my project without their support and smiles.

Table of contents

Abstract I
Acknowledgements III
Table of contents IV
List of abbreviations VII
List of tables IX
List of figures X
1 Introduction 1
1.1 Endothelium 2
1.1.1 Endothelial cell structure and function 4
1.1.2 Vascular tone 5
1.1.3 Coagulation and anti-thrombotic function 6
1.1.4 Role in inflammation 7
1.1.5 Role in fluid transport 8
1.1.6 Neoangiogenesis 9
1.2 Structure and composition of the endothelial glycocalyx layer 10
1.2.1 Proteoglycans 10
1.2.2 Glycosaminoglycan chains (GAGs) 13
1.2.3 Glycoproteins 16
1.3 Structure and thickness of the endothelial glycocalyx 18
1.3.1 The structure of the endothelial glycocalyx 18
1.3.2 Factors affecting the thickness of the endothelial glycocalyx 21
1.4 Functions of the endothelial glycocalyx 26
1.4.1 Permeability barrier 26
1.4.2 Immuno-modulator 28
1.4.3 Mechanotransduction 30
1.5 The role of the endothelial glycocalyx in vascular pathology 38
1.5.1 Atherosclerosis 39
1.5.2 Diabetes 42
1.5.3 Cancer 42
1.6 Aims and Objectives 43

2. Materials and method....44
2.1 Cell culture....44
2.1.1 Culture medium preparation....44
2.1.3 Cells....45
2.1.4 Cell subculture....46
2.2 Cryopreservation and reawakening of HUVECs....48
2.3 Immuno-fluorescent staining of HUVECs....49
2.4 Enzyme treatment of glycocalyx....50
3. Mechanical properties of the endothelial cell glycocalyx in vitro....54
3.1 Introduction....54
3.2 AFM and cantilever....56
3.2.1 Two AFM scanning modes used for imaging and mechanical property examination....60
3.2.2 Cell morphology imaging....61
3.2.3 Calibration of the cantilever....62
3.2.4 Calculation of the Young's modulus....68
3.3 Results....69
3.4 Discussion....73
4. Effect of oscillatory flow on morphological change of endothelial cells....75
4.1. Introduction....75
4.2 Methodology....76
4.2.1 Design of the flow experiment....76
4.2.2 Preparation of experiment....80
4.2.3 Calculation of the shear stress....81
4.2.4 Shear stimulation of HUVECs....82
4.3 Results....83
4.3.1 Steady flow stimulation....83
4.3.2 Oscillatory flow stimulation....87
5. Effect of oscillatory flows on the distribution of the glycocalyx....102
5.1 Introduction....102
5.2 Results....103
5.2.1 Confocal images....103
5.2.2 Super-resolution images....111

6. Discussion and future work 122
7. References:.....127

List of abbreviations

Acrylonitrile butadiene styrene	ABS
actin cortical web	ACW
atomic force microscopy	AFM
blood brain barrier	BBB
bovine aortic endothelial cells	BAECs
bovine lung microvascular endothelial cells	BLMVECs
Bovine Serum Albumin	BSA
Chondroitin sulphate	CS
claudin-5	CLDN5
Confocal laser scanning microscopy	CLSM
dense peripheral actin bands	DPABs
4',6-Diamidino-2-Phenylindole, Dilactate	DAPI
Dimethyl sulfoxide	DMSO
electron microscopy	EM
endothelial cell	EC
endothelial cell growth factor	ECGF
epidermal growth factor	EGF
Fluorescein isothiocyanate–dextrans	FITC-dextrans
glucuronic acid	GlcA
Glycoprotein Iib	GPIIb
glycosaminoglycan chains	GAGs
Heparan sulphate	HS
heparinase-III	Hep-III
human umbilical vein endothelial cells	HUVECs
hyaluronan or hyaluronic acid	HA
intercellular adhesion molecule 1	ICAM-1
Interleukin 1	IL1
intima-to-media ratio	IMR
low density lipoproteins	LDLs
macrophage inflammatory protein-2	MIP-2
matrix metalloproteinases	MMPs
Micro-particle image velocimetry	PIV
mucosal vascular addressin cell adhesion molecule **1**	MAdCAM-1
N-acetyl-glucosamine	GlcNAc
nitric oxide	NO
Paraformaldehyde	PFA
Phosphate-Buffered Saline	PBS
Plasminogen activator inhibitor-1	PAI-1
platelet/endothelial cell adhesion molecule 1	PECAM-1

polymethylmethacrylate	PMMA
Potassium Phosphate monobasic	KH_2PO_4
Prostacyclin, or prostaglandin I_2	PGI_2
rat fat-pad endothelial cells	RFPECs
receptor tyrosine kinases	RTKs
short consensus repeat	SCR
Sodium Bicarbonate	$NaHCO_3$
Sodium Phosphate dibasic	Na_2HPO_4-$7H_2O$
stress fibres	SFs
structured illumination microscopy	SIM
superoxide dismutase	SOD
tumour necrosis factor alpha	TNF-α
Universitat Autònoma de Barcelona	UAB
vascular cell adhesion molecule 1	VCAM-1
vascular endothelial growth factor	VEGF
vascular lumen	VL
Wheat Germ Agglutinin	WGA

List of tables

Table 2. 1 The complements for endothelial cell growth factor preparation. ...44
Table 2. 2 Reagents for HUVECs culture medium preparation. 44
Table 2. 3 The chemicals for cell culture.....46
Table 2. 4 The consumables for cell culture. 46
Table 2. 5 The staining reagents for HUVECs. 49
Table 2. 6 The targeting elements corresponding to different staining reagents. 49
Table 2. 7 The types of enzymes. 50

Table 4. 1 Equipment and materials for the flow chamber experiment assembly. 80
Table 4. 2 Shear stress calculations for the steady flow section of the experiment. 81

List of figures

Figure 1. 1 Major types of core protein in human cells include the membrane spanning syndecans, the glypicans, and the matrix localized perlecan. 11
Figure 1. 2 Schematic images for syndecan structure. Red shows the part in the cytoplasmic area, green denotes the glycosaminoglycan chains (Tkachenko, Rhodes et al. 2005). 12
Figure 1. 3 Schematic representation for the components of the glycocalyx on the luminal surface of endothelial cells (Tarbell and Pahakis 2006). 13
Figure 1. 4 Schematic images for the procedure of HS chain formation (Bernfield, Götte et al. 1999). 14
Figure 1. 5 Cleaving sites of HS chain (Lopes, Dietrich et al. 2006). 15
Figure 1. 6 Electron microscope image of a goat coronary capillary suggesting a brush like structure for the glycocalyx (van den Berg, Vink et al. 2003). 19
Figure 1. 7 Pictures taken via electron microscopy show the quasi-hexagonal arrangement of the endothelial glycocalyx (Squire, Chew et al. 2001). ... 19
Figure 1. 8 Image to show the first drawn model of endothelial glycocalyx structure..... 20
Figure 1. 9 Schematic images for common region (I), sinus region (II) and flow divider region (III) in carotid artery (van den Berg, Spaan et al. 2006). ... 22
Figure 1. 10 Comparison of the thickness of endothelial glycocalyx between ex vivo and in vitro model. EG, endothelial glycocalyx; VL, vascular lumen (Chappell, Jacob et al. 2009). 25
Figure 1. 11 Effect on NO2 production under shear stress after different enzyme treatments to degrade specific glycocalyx components (Pahakis, Kosky et al. 2007). 32
Figure 1. 12 Thi et al.'s "bumper-car" model showing the structural reorganization of the endothelial cells under flow. 34
Figure 1. 13 Model for glycocalyx redistribution under flow (Yao, Rabodzey et al. 2007). 37
Figure 1. 14 Light microscopic images of red blood cells flowing through capillary, showing a gap which is understood to represent the glycocalyx layer. 40

Figure 1. 15 EM images of stained luminal surface of mouse carotid arteries and a graph showing the measured thickness of the glycocalyx for varying location and diet. 41

Figure 2. 1 Confluent HUVEC after 7 days' culture in passage 6 (left) and passage 15 (right) showing normal HUVECs on left and cell differentiation in the right image. 45
Figure 2. 2 Trypsinization. Left image: cells in culture prior to addition of trypsin. Right image: after the addition of trypsin. 47
Figure 2. 3 Microscope image for HUVECs in passage 7 after 10 mins of sub-culture. 48
Figure 2. 4 Neuraminidase of influenza virus (Colman 1994). 51
Figure 2. 5 the chemical structure of N-Acetylneuraminic acid. 51
Figure 2. 6 The chemical structure of heparan sulphate. 52

Figure 3. 1 Schematic diagram of AFM working process. The detector receives the reflected laser signal from the cantilever tip pushing on the HUVECs membrane. 56
Figure 3. 2 The complete system for AFM.....57
Figure 3. 3 The sample platform is mounted on top of the specific z-piezo element, which enables the operator to make tiny adjustments to move the sample up or down into position. 57
Figure 3. 4 The specialist scanning sensor head for liquid state work. 58
Figure 3. 5 Contact mode(left) and tapping mode (right) of AFM. 60
Figure 3. 6 AFM height image (left) and phase image (right) for HUVECs after 8-day cell culture. 61
Figure 3. 7 Cantilever calibration process. 62
Figure 3. 8 Diagrams to show the pure indentation depth calculation process.65
Figure 3. 9 Image from indentation test on HUVECs with deflection-piezo displacement curves. 66
Figure 3. 10 Force-distance curve for HUVECs with 8 culture days. 67
Figure 3. 11 AFM images of HUVECs. 70

Figure 3. 12 The Young's modulus of HUVECs membrane in vitro for untreated and Hep-III treated HUVECs cultured for 4 days (control) and 8 days. ...71

Figure 4. 1 Schematic for steady flow stimulation. 76
Figure 4. 2 Structure of the flow chamber (expanded view). 77
Figure 4. 3 Structure of the flow chamber assembly (side view). 78
Figure 4. 4 schematic diagram for oscillatory flow stimulation. 79
Figure 4. 5 The relationship between height differential for two reservoirs and shear stress. 82
Figure 4. 6 Microscope images for 5 hrs' luminal flow stimulation 83
Figure 4. 7 Microscope images for 24 hrs' luminal flow stimulation. 84
Figure 4. 8 Chart showing average cell areas, analyzed using ImageJ for different timescales of luminal shear stress application. 85
Figure 4. 9 Chart showing average cell perimeters, analyzed using ImageJ for different timescales of luminal shear stress application. 85
Figure 4. 10 Chart showing average change in angle of orientation of the cell, analyzed using ImageJ for different timescales of luminal shear stress application 86
Figure 4. 11 Chart showing average change in aspect ratio of the cell, analyzed using ImageJ for different timescales of luminal shear stress application 87
Figure 4. 12 Microscope images for 5 hrs' oscillating flow stimulation experiment. 88
Figure 4. 13 Chart showing change in average area of the cell, analyzed using ImageJ for different reversal timescales of oscillatory shear stress (5 hrs' experimental duration).....89
Figure 4. 14 Chart showing change in average perimeter of the cell, analyzed using ImageJ for different reversal timescales of oscillatory shear stress (5 hrs' experimental duration). 90
Figure 4. 15 Chart showing change in average angle of cell orientation, analyzed using ImageJ for different reversal timescales of oscillatory shear stress (5 hrs' experimental duration). 91

Figure 4. 16 Chart showing change in average aspect ratio of cell, analyzed using ImageJ for different reversal timescales of oscillatory shear stress (5 hrs' experimental duration). 92
Figure 4. 17 Microscope images for 24 hrs' oscillating flow stimulation experiment. 94
Figure 4. 18 Chart showing change in average area of the cell. 95
Figure 4. 19 Chart showing change in average perimeter of the cell. 96
Figure 4. 20 Chart showing change in average angle of orientation of the cell. 97
Figure 4. 21 Chart showing change in average aspect ratio of the cell. 98
Figure 4. 22 The Young's modulus of HUVECs at different regions of the cell membrane, in vitro.....100

Figure 5. 1 CLSM images of glycocalyx on live HUVECs under static (no flow) conditions. 104
Figure 5. 2 the formatted sequential images for samples of HUVECs under oscillatory shear stress, with a control group cultured for the same time in static no-flow) conditions. 106
Figure 5. 3 Formatted sequential images for samples of HUVECs under oscillatory shear stress, with a control sample incubated in static medium (no flow). 108
Figure 5. 4 Formatted sequential images for samples of HUVECs under oscillatory stress, with a control sample incubated in static medium (no flow). 110
Figure 5. 5 Comparison of CLSM images and super-resolution images to show overview and detail of various locations within the sample.....113
Figure 5. 6 2D super-resolution image for control sample of HUVECs cultured for 8 days. Scale bar=10μm. 115
Figure 5. 7 Formatted super-resolution images. 116
Figure 5. 8 Formatted super-resolution images. 118
Figure 5. 9 Formatted super-resolution images. 120

1 Introduction

The vascular endothelium, as the innermost layer of the blood vessel, is in direct contact with the blood, controls vessel permeability and determines the interaction between blood cells and the vessel wall. It has an irreplaceable role in many vascular events such as blood-tissue exchange, inflammatory response, tissue homeostasis, fibrinolysis, coagulation, vasotonus regulation, the vasodilatation of various tissues and angiogenesis (Risau and Flamme 1995, Reitsma, Slaaf et al. 2007). It has been described as a unique organ system (Orr, Wang et al. 2000).

There is a brush-like structure on the luminal surface of the endothelial cells called the endothelial glycocalyx. The endothelial glycocalyx layer is continuously modified by proteoglycans, glycosaminoglycans and glycoproteins. The physiological functions of the endothelium are determined by the glycocalyx layer (Pries, Secomb et al. 2000), which acts as a barrier between the blood and vascular tissues. The endothelial glycocalyx layer also generates a measurable response to mechanical stimulation, functioning as a mechanotransducer e.g. in its role within the body's inflammatory responses (Michel and Curry 1999, Levick and Michel 2010, Oberleithner, Peters et al. 2011).

Stasis (or disruption) of flow, endothelial injury and hypercoagulability are the three main contributory factors for thrombosis. Further, vascular dysfunction, especially endothelial cell dysfunction, has been shown to cause cardiovascular disease through atherosclerosis, diabetes and inflammation (Mulivor and Lipowsky 2004, van Golen, van Gulik et al. 2012).

Thus it is anticipated that focusing on the effect of disturbed flow on the endothelial glycocalyx will advance our knowledge towards prevention and treatment of atherosclerotic and other vascular diseases (Flaherty, Pierce et al. 1972, Aird 2012, Chatterjee and Fisher 2014).

1.1 Endothelium

The endothelium is a thin layer of cells located on the luminal surface of blood and lymphatic vessels. This layer is made up of a continuous micromolecular structure of cells, cross linked with each other (Michiels 2003). The vascular endothelial cell is in direct contact with the blood; the basic function of the endothelium is as a partially permeable barrier, allowing substances to transfer between the blood itself and the blood vessels, including the tissue around them. The permeability of the endothelium near to wound sites plays an important role within the body's inflammatory responses; surrounding tissue will become swollen if endothelium permeability increases over a certain limit. This and other endothelial processes are governed by mechanotransduction: signalling pathways which begin with physical stimuli and end in biochemical responses such as protein expression.

The endothelium is known to play an important role in a number of human pathologies including as previously noted atherosclerosis, stroke and heart attack; Alzheimer's disease and vascular dementia, and a number of viral transmission routes including HIV, hepatitis C, rubella, dengue, herpes simplex infection, the related Zika virus and associated increased risk of Guillain-Barré Syndrome, and human cytomegaloviruses (Visser, Tracy et al. 1988, Grundy, Lawson et al. 1998, Hürlimann, Weber et al. 2005, Jarvis and Nelson 2007, Bentz and Yurochko 2008, Grammas 2011, Fletcher, Wilson et al. 2012, Perelygina, Zheng et al. 2013, Beatty, Puerta-Guardo et al. 2015, Hamel, Dejarnac et al. 2015).

In an adult human body, the total surface area of the endothelium is approximately 350 m^2. Yet because the tissue is so difficult to access, relatively little is understood about its structure and function. Endothelial cells are generated from the hemangioblast, a mesodermal progenitor cell (deriving from the splanchnopleuric mesoderm) which may differentiate to form either an endothelial cell or haematopoietic cell (Choi, Kennedy et al. 1998). The haematopoietic cells may develop into white or red blood cells: endothelial cells may differentiate into mesenchymal or intimal smooth muscle cells, a process that underpins embryonic development but which may also continue to be relevant in adult life within pathologic settings, including pulmonary hypertension, atherosclerosis, wound

healing and inflammation (Arciniegas, Sutton et al. 1992, Mironov, Rekhter et al. 1995, Romero, Zhang et al. 1997, Lee, Kotliarova et al. 2006, Qiao, Nishimura et al. 2014). Further, the endothelial cell's ability to change phenotype is an important consideration and may be a limiting factor in the reliability of some work carried out on culture cells.

Both biomechanical and biochemical forces affect the development of the endothelium: shear stress, cyclical strain, growth factors, cytokines, gas composition and hormones all play important roles (Masuda, Kawamura et al. 1989, Shyy, Hsieh et al. 1994, Shalaby, Rossant et al. 1995, Tricot, Mallat et al. 2000, Michiels 2003, Asada, Paszkowiak et al. 2005). These factors can determine not only the phenotypic qualities including the size and shape of the endothelial cell, and characteristics such as cell proliferation, apoptosis and survival time, but also its mRNA and functions such as protein expression, regulation of vascular tone, and haemostasis, the process that governs clotting of the blood in response to damage to vessel walls and bleeding injuries.

As an example, the endothelium's vital role in embryonic development is governed by growth factors which bring order and organization to the process of vasculature growth. VEGF (vascular endothelial growth factor), angiopoietins and ephrins are three types which play vital roles in vascular development and remodelling. VEGF triggers vasculogenesis, the arrangement of endothelial cells into immature vessels. This takes place via an interaction between the VEGF and receptor tyrosine kinases (RTKs) on the cell surface. Experiments with mice show that any disruption of genes related to VEGF will lead to the failure of vasculogenesis (Shalaby, Rossant et al. 1995, Elhadj, Akers et al. 2003). VEGF-A, binding to receptors including VEGFR2 (VEGF Receptor 2), is not only helpful in forming the tubular structure of the vessel where the endothelial cells are found, but also induces endothelial proliferation and migration. Another of the growth factors, angiopoietin, has effects similar to VEGF. The interactions between ANG1 (angiopoietin-1) and RTKs lay the foundations for blood vessel stability. Another important condition for vascular development is the presence of ephrins, which control angiogenic remodelling (the development of new blood vessels from existing vessel tissue which is the only means of vascular development in the adult) at its early stages through endothelial cell functions

including sprouting and branching (Carmeliet 2000). Ephrins can also help us to distinguish between embryonic arterial and venous vessels at a very early stage of development, through the vessels' different distribution patterns of ephrin B2 (present only in primordial arterial vessels) and the receptor Eph-B4 (detected only in primordial venous vessels)(Brambilla, Brückner et al. 1996, Wang, Chen et al. 1998, Adams, Wilkinson et al. 1999).

It has also been observed that there are differences in phenotype, morphology and function between endothelial structures in different locations, such as venous and arterial endothelium. There are many phenotypes of endothelial cells, which are influenced by the extracellular environment: for example, liver sinusoidal endothelium shows typical heterogeneity for endothelium cells in its reaction to differences in the micro and macro environment (Aird 2007, Aird 2007, Yano, Gale et al. 2007). This heterogeneity has been cited by scholars including Auerbach *et al.* to support the contention that cultures from multiple organ beds should be used in experimental study of the endothelium (Auerbach, Alby et al. 1985). Aird has noted that this argument is somewhat undermined by endothelial cells' ability to change phenotype *in vitro*, which means cell cultures cannot be relied on to maintain their identity (Aird 2007).

1.1.1 Endothelial cell structure and function

The structure of the overall endothelium (a combination of the intercellular connections and individual cell morphology) can be differentiated into two types: fenestrated endothelium (whose underlying basement membrane may be of continuous or discontinuous structure, but which contains fenestrae or holes that allow molecules to cross the permeable barrier rapidly), and non-fenestrated continuous endothelium with a continuous basement membrane and tight connections between the cells. The non-fenestrated continuous endothelium is distributed not only in the capillaries of the brain, skin, heart and lung, but also in arteries and veins. The fenestrated endothelium is normally found in areas where constant filtration takes place, or where there is increased transport between inner and outer layers of the endothelium, such as capillaries of the exocrine and endocrine glands, gastric and intestinal mucosa, choroid plexus, glomeruli, and a

subpopulation of renal tubules (Aird 2012). Fenestrated continuous endothelium promotes the exchange of molecules between sinusoid blood vessels and surrounding tissue due to its porous structure. Some research shows that transendothelial transport is more regulated and unidirectional in areas of distribution of the fenestrated continuous endothelium (De Keulenaer, Chappell et al. 1998, Hsiai, Cho et al. 2002, Elhadj, Akers et al. 2003). The capillaries in the *lamina propria* of the human small intestine confirm this: the fenestrated structure is shown on the side that faces the absorptive epithelial layer of the mucosa. Variations between vascular beds show a very strong connection with the density of fenestrae. For example, the fenestra density in the jejunal is double that of pancreatic capillaries.

There is another type of endothelial cell structure, the discontinuous endothelium, which is found in certain sinusoidal vascular beds such as that of the liver. Significantly larger fenestrations, up to 100-200 nm in diameter, have been shown in these discontinuous liver sinusoidal endothelial cells as compared with the fenestrated continuous endothelium. Liver sinusoidal endothelial cells lack diaphragms, and gaps exist between individual cells. This extremely porous structure may be assumed to contribute to the bidirectional exchange of fluids, solutes and particles which supports the liver's function as both "sieve" and "scavenger" (Braet and Wisse 2002).

1.1.2 Vascular tone

The tone of vascular vessels is dependent on the activity of their smooth muscle cells, which changes in response to acetylcholine stimulation in the intima (inner layer), where the endothelium is located. Conversely, vascular tone may be regulated by the endothelium itself, through the secretion of mediators. For instance, oxygen derived from nitric oxide (NO), a free radical gas dissolved in the blood, synthesized with L-arginine in the endothelium through a process of NO synthase to produce endothelium derived relaxing factor (Palmer, Ferrige et al. 1987). This relaxing factor has a short half-life time to activate a rapid short dilation mechanism in the vascular vessels. Although it is regulated by shear stress, it is the relaxing factor that is fundamentally responsible for maintaining the vessel's vascular tone,

and to this end a basic level of the relaxing factor is continuously secreted by the endothelium. PGI_2 (Prostacyclin, or prostaglandin I_2) is another vasodilator, whose function is to relax the smooth muscle cells of the vascular wall, produced in the endothelium. It plays a role in the regulation of resting vascular tone (Furchgott 1983). Increased quantities of PGI_2 is synthesized in response to the presence of a number of substances that bind to the endothelial cell, such as thrombin, arachidonic acid, and histamine etc. (Moncada, Herman et al. 1977, Furchgott 1983).

Endothelium derived vasoconstrictive factors will be released in pathophysiological situations. In other words, endothelin is released when there is high blood pressure or hypoxia. Endothelin is considered not to be stored in the endothelial cells, but to be secreted from the non-luminal side of the endothelium, acting on the muscle cells surrounding the vessel in order to protect the vessel walls from overexpansion.

1.1.3 Coagulation and anti-thrombotic function

Numerous factors are secreted by endothelial cells to stabilize anti-coagulating and anti-thrombotic processes in the blood through the regulation of platelet function and other mediators. Under healthy conditions, this anti-coagulate/anti-thrombotic state will be maintained. Conversely, the endothelium can enter a pro-coagulant, pro-thrombotic state to deal with vessel damage or stimulation from cytokines or other pro-inflammatory mediators. PGI_2 and NO are the two main antiplatelet agents (Furchgott 1983). The coagulation process is influenced by both factors, and especially by the synthesis of the two. Thus, the extent of formation of intravascular thrombi will be limited by these factors or by their synthesis. Under healthy conditions, the activity of numerous anti-coagulant pathways is promoted by flow of the blood over the endothelial cells. The protein C/protein S pathway is the most important of these because it is indispensable for blood coagulation through inactivating co-factors (Heemskerk, Bevers et al. 2002).

The endothelial cell surface structure is composed partly of glycosaminoglycan receptors, such as thrombomodulin which has a similar structure to heparin. These receptors are the main sites for inactivating thrombin, along with antithrombin which is produced through liver secretion. When thrombin binds together with

thrombomodulin, it assists it to cleave and activate protein C (Esmon and Owen 1981). Furthermore, the receptors can inactivate clotting factors Va, VIIIa and PAI-1 (Plasminogen activator inhibitor-1), which has benefits for the blood in maintaining the non-thrombotic fluid state. The endothelium also secretes an inhibitor to the tissue factor pathway, taking a part in the prevention of coagulation by inhibiting Factor VIIa (Stern, Nawroth et al. 1985). However, the substances secreted will be changed through the activation of either histamine or thrombin (Lorant, Patel et al. 1991). Histamine is released from mast cells in response to tissue damage due to foreign pathogens. This process assists the endothelium to transform the blood vessel into a pro-thrombotic, pro-proliferative and vasoconstricting state (Van De Voorde and Leusen 1983). In addition, white blood cells have the ability to adhere to the endothelium in this state of activity, due to the neutrophil adhesion produced from a change on the surface of the endothelium through the reaction between the syntheses of platelet activating factor, which binds to P selectin on the surface of the endothelial cell, and Glycoprotein IIb (GPIIb), CD154 (on the platelet surface) (Gawaz, Langer et al. 2005).

1.1.4 Role in inflammation

Endothelial cells coordinate the recruitment of inflammatory cells if there is tissue injury or infection. At the same time, they are connected with leukocytes through cytokines and the production and release of growth factors. Many of these processes are modulated by nitric oxide (NO) production in the endothelium, and NO is known to regulate inflammation in low concentrations, but can be toxic and pro-inflammatory in large amounts (Guzik, Korbut et al. 2003). Interleukins and chemokines are synthesized and secreted by the endothelial cells when activated. Furthermore, the endothelial cells respond to stimulation by cytokines. For example, interaction between cells, proliferation and survival of the endothelial cells are influenced by TNF-α (tumour necrosis factor alpha) or IL1 (Interleukin 1). The migration of leucocytes, too, depends on recognition of endothelial cells through glycoproteins on the membrane. Selectins initialize the tethering of the leukocyte to the endothelial cell surface. The leucocyte is caught by transmembrane glycoproteins and delivered from the vascular system to the place of tissue injury or

infection. Cell adhesion molecules on the surface of endothelial cells are our main evidence for recognition.

1.1.5 Role in fluid transport

The endothelium is responsible for effective transport through the transfer medium of the blood in order to maintain the correct volume, concentration and composition of tissue (Sumpio, Riley et al. 2002). The regulated transport of fluids and solutes between blood and tissues is the reason for its partial permeability. The endothelium's permeability can be separated into two different types: basal and inducible. The second type (inducible permeability) will be discussed at the end of this section. The first type (basal) ensures that the flow of material between the blood and underlying interstitium is continuous, even though flow volume is physiologically regulatable. This activity occurs mainly in the capillaries, which are the major sites of exchange within the circulatory system. The ultimate function of the transition of materials between cells and blood is carried out by the capillary wall, and this overall transition is called ultramicroscopic circulation. Essential nutrients are carried by the red blood cells: blood gases, by the plasma (Curry and Michel 1980).

It is known that macromolecules are transported across the barrier by the transcellular route, the "shuttle service" across the endothelial barrier provided by membrane-bound vesicular carriers such as caveolae (Deanfield, Donald et al. 2005). Small solutes and fluids depend on the other, paracellular route, moving passively across the barrier. There are two different types of mechanism that may be involved in transcellular transport of macromolecules. The first type, receptor-dependent mechanisms, includes carrier-mediated transcytosis. The second, receptor- independent mechanisms, includes fluid-phase transcytosis (Stevens, Garcia et al. 2000, Komarova and Malik 2010).

The differences in permeability observed across the endothelium probably depend on the phenotype differences of endothelial cells in response to differing environments, the different properties in junction areas, the presence or absence of fenestrae, and the differences in activity of the transcytotic machinery. Interestingly,

the size and level of complexity of junctions are inversely proportional to the endothelial permeability. Arteries are a useful example to prove this, because there are highly developed tight junctions and low permeability under the same conditions. The research shows the absence of claudin-5 (CLDN5), which is an integral component of tight junctional regions, correlates to a selective impairment in blood brain barrier (BBB) function against small, but not large, molecules (Yuan, Le Bras et al. 2012). Research on mice involving the systemic administration of anti-VE-cadherin antibodies demonstrates a significant increase in vascular permeability in the lung and heart; this evidence shows the importance of the adherens junctions in mediating site-specific permeability (Carmeliet, Lampugnani et al. 1999). Increased permeability of fluids and small solutes (not macromolecules) is observed in the continuous fenestrated endothelium: the more fenestrae, the higher the permeability. Site-specific transcytosis may result from differences in the range of caveolae-associated membrane receptors even through the correlation between the number of caveolae and segmental permeability is relatively poor.

The upper limit of the endothelium's permeability is observed in inducible permeability, which occurs in situations of acute or chronic inflammation. From fundamental research into the basal level of permeability, inflammation is a well-known cause of vasodilation and the leakage of capillaries (Curry and Michel 1980). The main area where inducible permeability occurs is the postcapillary venule. Based on conventional opinion, inflammatory factors including histamine, serotonin, bradykinin, substance P and VEGF induce endothelial cell (EC) retraction and the formation of intercellular gaps: the release of the inflammatory factors can lead to increases both in transcellular vascular leakage and of the passage of macromolecules through the transendothelial fenestrate (Wedmore and Williams 1981). Permeability-enhancing agents, by contrast, operate by increasing transcellular permeability but do not induce the formation of intercellular gaps.

1.1.6 Neoangiogenesis

Endothelial cells play a part not only in permeability, but also in angiogenesis and vasculogenesis through VEGF and angiopoietin secretion. This is an established area for oncology research which targets the vessels pervading the tumour, since tumour

progression is dependent on the oxygen and nutrient supply and removal of waste products provided by vascular support vessels (Nishida, Yano et al. 2006).

1.2 Structure and composition of the endothelial glycocalyx layer

The glycocalyx is a part of the endothelial cell membrane, located on the luminal surface of the blood vessel. The glycocalyx layer is estimated to be about 500nm in thickness. Research has begun to discover some of its various structural properties. There is a wide range of membrane-bound molecules involved in the endothelial glycocalyx layer, which may be separated into three different types: proteoglycans, glycosaminoglycan chains (GAGs) and glycoproteins. Each of them will be discussed in the following sections.

1.2.1 Proteoglycans

Proteoglycans are glycoproteins, composed of a core protein covalently attached with O-glycosyl linkage c to one or more long chain glycosaminoglycans. These long chain GAGs are unbranched carbohydrate polymers (Pries, Secomb et al. 2000). The research shows that proteoglycans influence cell growth through various growth factors that bond to them, including fibroblast growth factor (Presta, Statuto et al. 1992), platelet-derived growth factor (Raines and Ross 1992) and transforming growth factor (Segarini, Rosen et al. 1989). The core proteins of proteoglycans play an important role as the foundation of the glycocalyx's structure for sulphated GAG attachment.

Proteoglycans are described and differentiated according to the way their core proteins differ, both in size, and in the number of GAG chains that attach to them. The major core protein families include transmembrane syndecans, glypicans which bind to the cell membrane, and matrix localized perlecans. Syndecans and glypicans are incorporated in the cell membrane; perlecans are not (Rosenberg, Billingsley et al. 1997).

Figure 1.1 shows the various specialized sites for GAG chain attachment on core proteins in proteoglycans.

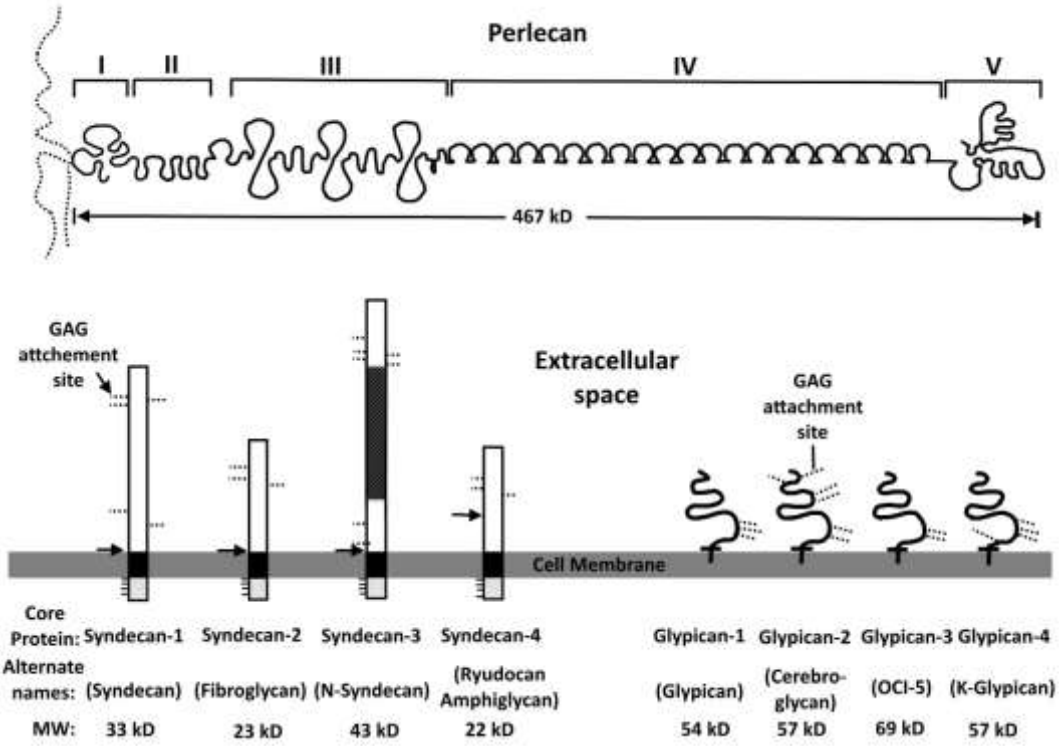

Figure 1. 1 *Major types of core protein in human cells include the membrane spanning syndecans, the glypicans, and the matrix localized perlecan. (Rosenberg, Billingsley et al. 1997).*

The dotted lines show the specific sites for GAG attachment. The pure black colour indicates the homologous transmembrane domain; the stippled area denotes the intracellular domain and the dotted area shows the conserved tyrosines in syndecans

All of the syndecans are type I transmembrane proteins (Carey 1997): the membrane-spanning domain is the site of the strong connection between syndecans and cell membrane. Syndecan-1, syndecan-2, and syndecan-4 are the three different types of syndecan that are expressed by endothelial cells. Figure 1.2 shows that each syndecan has several sites for GAG attachment, occurring near the N terminus and distal to the apical surface. Heparan sulphates are the main GAGs that attach to the syndecans but other types of GAGs are capable of attachment as well (Rosenberg, Billingsley et al. 1997, Tkachenko, Rhodes et al. 2005). Extending into the cell

cytoplasm, the tail of the syndecan is associated with the endothelial cell cytoskeleton. This is why some researchers have identified a need to investigate whether syndecans play a role in cytoskeleton reorganization through molecules including tubulin, dynamin, and α-actinin (Yoneda and Couchman 2003).

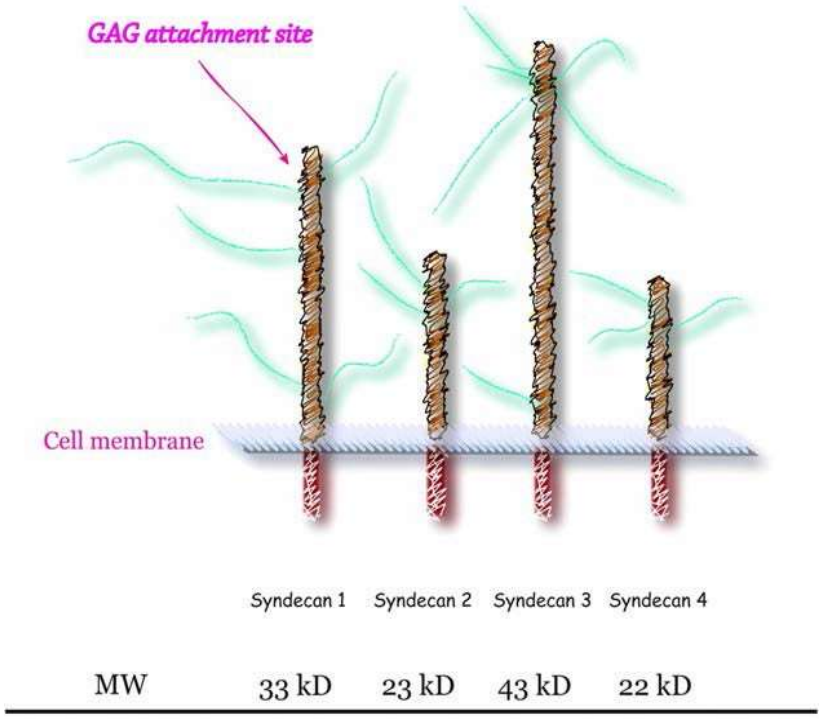

Figure 1. 2 *Schematic images for syndecan structure. Red shows the part in the cytoplasmic area, green denotes the glycosaminoglycan chains (Tkachenko, Rhodes et al. 2005).*

Glypican-1 is the only glypican which is expressed by the endothelial cells (Rosenberg, Billingsley et al. 1997) and its three to four sites for GAG chain attachment support only heparan sulphate GAG chains, no other types. These are situated close to the cell membrane (Fransson, Belting et al. 2004). A glycosylphosphatidylinositol anchor attaches glypican to the membrane, close to lipid rafts which are rich in cholesterol and sphingolipid. These lipid rafts include caveolae (formed from caveolin-1 protein) as a subset. Caveolin-1 is a cholesterol carrier that forms cave-like structures in the plasma membrane (van Deurs, Roepstorff et al. 2003). linked and supported by the actin cytoskeleton of the cells. It is in the region of plasma membrane where the caveolin-1 is present that glypicans and heparan sulphate chains may usually be found attached.

Perlecan, which is associated with the basement membrane, is the third type of core protein expressed by the endothelial cell. There are five different regions for attachment sites on perlecan's core protein. These sites are receptive to GAG chains, O-linked nonsulphated oligosaccharides and long chain fatty acids. Perlecan interacts with components such as collagens, laminin and others (Murdoch, Dodge et al. 1992).

1.2.2 Glycosaminoglycan chains (GAGs)

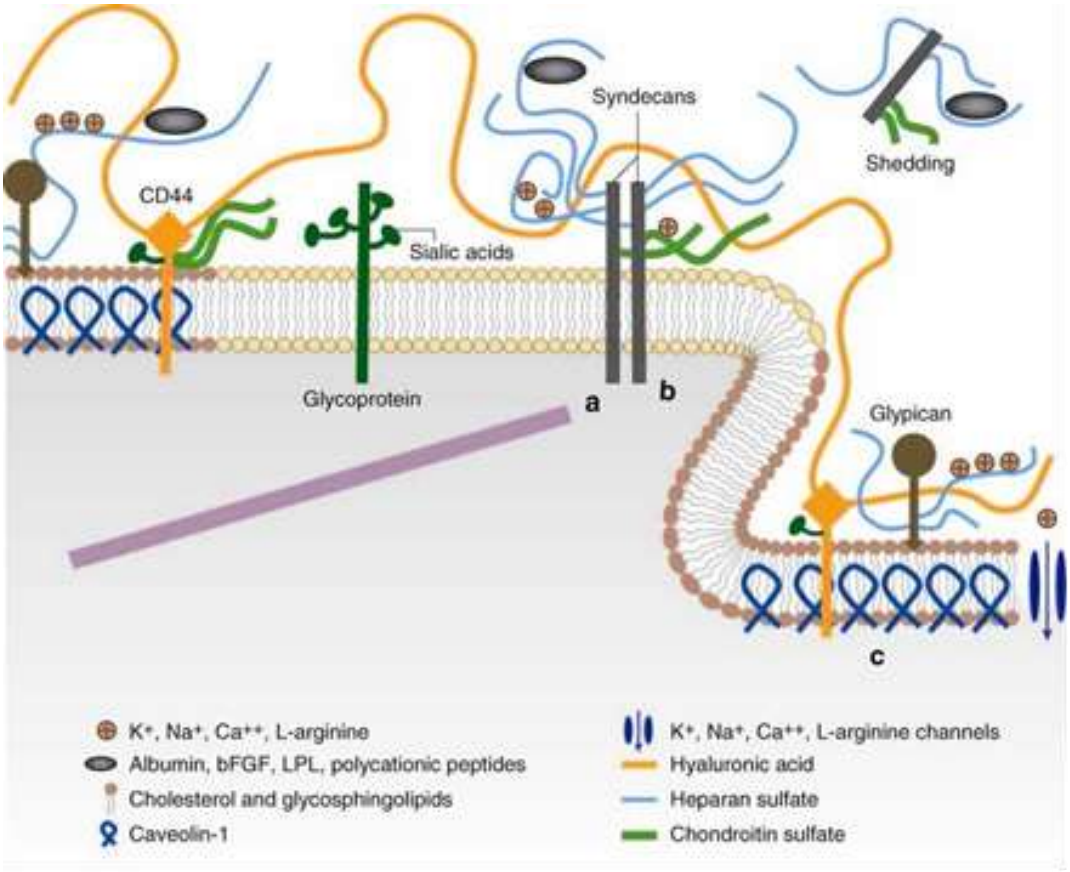

Figure 1. 3 *Schematic representation for the components of the glycocalyx on the luminal surface of endothelial cells (Tarbell and Pahakis 2006).*

GAGs, the components which attach to the core protein of proteoglycans, are polysaccharides that form part of the extracellular matrix (ECM) (Jackson, Busch et al. 1991). Heparan sulphate, chondroitin sulphate, dermatan sulphate, keratan sulphate, and hyaluronan are the five GAGs found in the endothelial glycocalyx. The length of these GAG chains varies and is affected by sulphation and/or deacetylation (Reitsma, Slaaf et al. 2007). Figure 1.3 is a schematic image to show

components of the glycocalyx on the luminal surface of endothelial cells (Tarbell and Pahakis 2006).

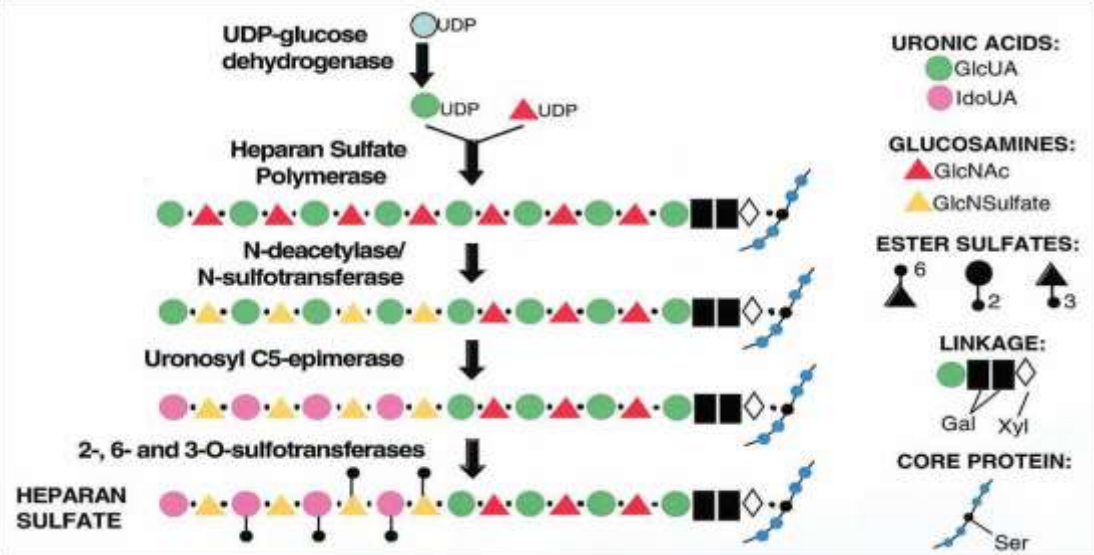

Figure 1. 4 *Schematic images for the procedure of HS chain formation (Bernfield, Götte et al. 1999).*

Heparan sulphate (HS) is the most common type of GAG and makes up 50-90% of all GAGs in the vascular system (Oohira, Wight et al. 1983, Ihrcke, Wrenshall et al. 1993, Pries, Secomb et al. 2000). The figure above shows the process of HS chain formation: it is polymerized from a repeating disaccharide unit of glucuronic acid (GlcA) and N-acetyl-glucosamine (GlcNAc), through a series of changes in cis- and trans-Golgi which preserve the units near the C-terminus while the units near the amino-terminus end become increasingly sulphated (Bernfield, Götte et al. 1999). This assembly of sulphated residues results in the mature HS bearing high negative charges at physiological pH value.

HS lyases are chemicals which can selectively cleave HS bonds at various sites on the GAG chains: the following image shows the cleavage sites (Lopes, Dietrich et al. 2006). HS lyases are used commercially to cleave HS bonds, usually through selective cleavage of the α-1, 4-glycosidic bonds between uronic acid and glucosamine (Nader, Porcionatto et al. 1990, Lopes, Dietrich et al. 2006, Fux, Ilan et al. 2009). One example of such HS lyases, Heparitinase I, acts specifically upon the unmodified area which is rich in N-acetyl-glucosamine; another, heparitinase II,

prioritises N,6-sulphated glucosaminido-glucuronic acid linkages (Linhardt, Turnbull et al. 1990). HS chains can only be totally degraded in the presence of both. Some research shows that nonspecific proteases also play a role in HS chains being fully released from the cell surface, through the proteolytic cleavage of core proteins (Ihrcke, Wrenshall et al. 1993). The experimental methodology for the research presented in this project uses heparinase-III to cleave less sulphated HS chains in the glycocalyx in order to allow measurement of the endothelium thickness and Young's modulus with, and without, the glycocalyx and hence to deduce the thickness of the glycocalyx layer.

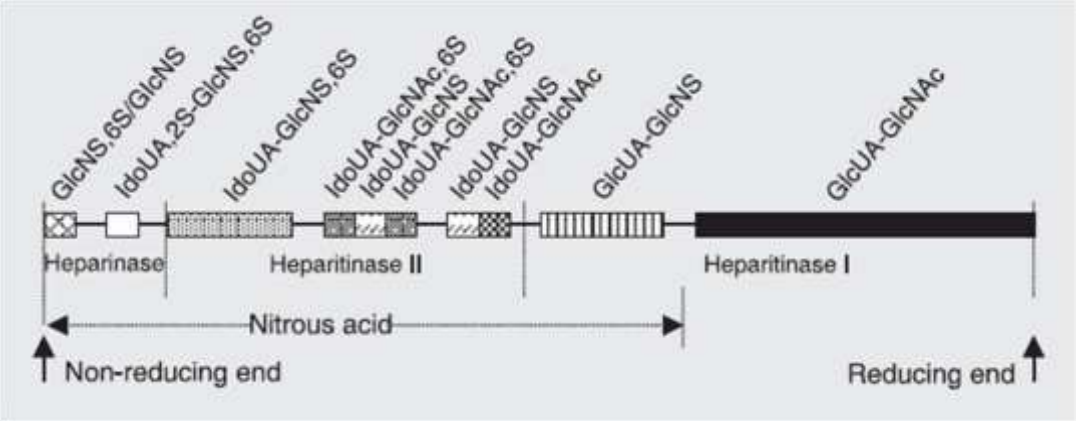

Figure 1. 5 *Cleaving sites of HS chain (Lopes, Dietrich et al. 2006).*

Chondroitin sulphate (CS) makes up 15-24% of the proteoglycans and is another common type of GAG present in the endothelial glycocalyx (Rapraeger, Jalkanen et al. 1986). The amount of CS present is proportion to HS at a ratio of 1:4 (Megens, Reitsma et al. 2006). CS can be separated into three different types, A, B and C, by variations in the sulphation sites: chondroitin sulphate type B is also known as dermatan sulphate. Chondroitinase ABC acts on, but is not specific to, β-1,4-galactosaminic bonds. It cannot be prevented from acting on HA chains as well, due to the structural analogy between CS and HA chains (Yamagata, Saito et al. 1968, Hamai, Hashimoto et al. 1997).

In the main, these two types of GAG chains are attached to the transmembrane syndecans and the core protein of membrane-bound glypicans (Pries, Secomb et al. 2000).

The third type of GAG chain, hyaluronan (HA or hyaluronic acid), is distinctive in a series of ways. It is synthesized in the plasma membrane, rather than the Golgi apparatus as HS GAG chains are. It is significantly longer than sulphated GAGs, reaching up to 25,000 disaccharide repeats. The exact site of its attachment is as yet unknown, in comparison to HS attachment which is well understood: it is believed that HA bonds either to the endothelial cell membrane receptor CD44 (Nandi, Estess et al. 2000), or alternatively to the HA synthases, which are the integral membrane proteins located on the cytosolic side of the endothelial cell membrane (Weigel and DeAngelis 2007) or even possibly exists as a very viscous solution surrounding the cell membrane area (Scott 1989). Like the HS and CS GAG chains, HA carries a negative charge, but in this case the negative polarity derives from carboxyl residues in glucuronic acid.

The final two types of GAG chain, dermatan and keratin sulphate, are present among the endothelial cells, in smaller degrees than CS or HS (Mulivor and Lipowsky 2004). Dermatan sulphate is sometimes described as a type B CS. There is less research for keratan sulphate's physiological and pathophysiological role.

The tissue's location, and changes in physiological state, are factors affecting the number of GAGs that attach to the core proteins. The expression of proteoglycans in the endothelium is also dependent on a range of stimuli. Tumor necrosis factor-α (TNF-α) is understood to regulate endothelial expression of syndecans by increasing syndecan-2 expression and decreasing syndecan-1 expression (Halden, Angelika et al. 2004). The level of syndecan-4 will be increased in states of arterial injury (Geary, Koyama et al. 1995) or acute myocardial infarction (Li, Brown et al. 1997).

1.2.3 Glycoproteins

Glycoprotein and proteoglycan are considered the foundations of the endothelial glycocalyx for their structural function connecting the glycocalyx and the endothelial cell membrane. The endothelial glycoproteins have small molecular size, with only 2-15 sugar residues and branched carbohydrate side chains. Their structure shows a heavy concentration of sialic acids, a family of various sugar units with a nine-carbon spine that are found on almost all animal cells and typically attach to the outermost

ends of protein chains. Among other effects, sialic acid contributes to the negative electrical charge at the glycocalyx tips, producing the repulsion between individual tips which gives a bush- or brush-like structure which will be discussed below (Varki 2008). Important glycoprotein groups found in the endothelial glycocalyx are components of the coagulation and fibrinolysis system (Megens, Reitsma et al. 2006) and adhesion molecules: these include the selectin family, integrin family and the immunoglobulins. Adhesion molecules have a positive effect on cell recruitment from the bloodstream to surrounding tissues, and on cell signalling which assists with tissue repair and immunity among other functions.

The selectins family are common molecules with tails extending to the cytoplasm of the endothelial cells. There is an C-type lectin domain at the amino-terminus, an EGF-like domain and multiple short consensus repeat (SCR) units involved in the structure of each tail (Tedder, Steeber et al. 1995). The structures on the tails have advantages for carbohydrate group binding to glycosylated proteins or lipids. E-selectin and P-selectin, the two members of the selectin family observed in the vascular endothelium, have vital importance for leukocyte–endothelial cell interactions, which enable inflammatory and immune responses among others. P-selectin is the main adhesion receptor in this region which shows interactions with leukocytes on acutely inflamed endothelial cells *in vivo* (Sperandio 2006). There is an epidermal growth factor (EGF)-like domain in the structure of P-selectin, which has been shown to take part in ligand recognition and cell adhesion (Kansas, Saunders et al. 1994). A notable feature of E-selectin is its spontaneous assembly and expression on the endothelial cell surface, and this process can be enhanced through stimulus from cytokins such as interleukin-1, tumor necrosis factor α, and lipopolysaccharide (Jung and Ley 1997).

Integrins are widely distributed on endothelial cells, white blood cells and platelets. The integrin $\alpha_V\beta_3$ is expressed on the endothelial cell membrane and plays a crucial mediating role in platelet–endothelial cell interactions. The adhesion of activated platelets to the intact endothelium is dependent on the interaction between integrin $\alpha_V\beta_3$ and the immunoglobulin intercellular adhesion molecule 1 (ICAM-1) (Bombeli, Schwartz et al. 1998, Xiong, Stehle et al. 2003). Immunoglobulin is another glycoprotein family that includes intercellular adhesion molecules 1 and 2 (ICAM-1

and -2), vascular cell adhesion molecule 1 (VCAM-1), and platelet/endothelial cell adhesion molecule 1 (PECAM-1). All types of immunoglobulin function as ligands for integrins on the leukocytes and platelets. Thus they are not only the major mediator for leukocyte adhesion to the endothelium, but also the passage for leukocyte transport to inflammation areas (Müller, Hermanns et al. 2002, Reitsma, Slaaf et al. 2007).

1.3 Structure and thickness of the endothelial glycocalyx

1.3.1 The structure of the endothelial glycocalyx

In 1966, Luft found that the image of the glycocalyx on the luminal surface of the endothelial cell could be obtained through electron microscopy (Luft 1966). However, limited detail of the structure was understood until recently, key contributions including the 'fibre matrix' theory describing vascular permeability developed in 1980 (Curry and Michel 1980) and the work of Satcher *et al*. in 1997 describing the fine cytoskeletal structure of cultured bovine aortic endothelium (Satcher, Dewey et al. 1997). The first model of the glycocalyx's structure was presented by Squire's research group in 2001 and amended by Weinbaum *et al* two years later (Squire, Chew et al. 2001, Weinbaum, Zhang et al. 2003).

Figure 1.8 shows the evidence found by Squire *et al* that there are regular spaces of around 20nm within the various glycocalyx areas (scale bar shows 200nm in white colour) in specimens under electron microscopy. The spaces are clearly observed running not only in parallel directions, but also perpendicular. In other words, the team's foundational theory for the structure of the glycocalyx is that the glycocalyx is a three dimensional meshwork in all directions with 20nm between the 'meshes' indicated with white parallel lines on the figure (Squire, Chew et al. 2001). Conversely, other imaging suggests a brush-like structure for the glycocalyx (Figure 1.6).

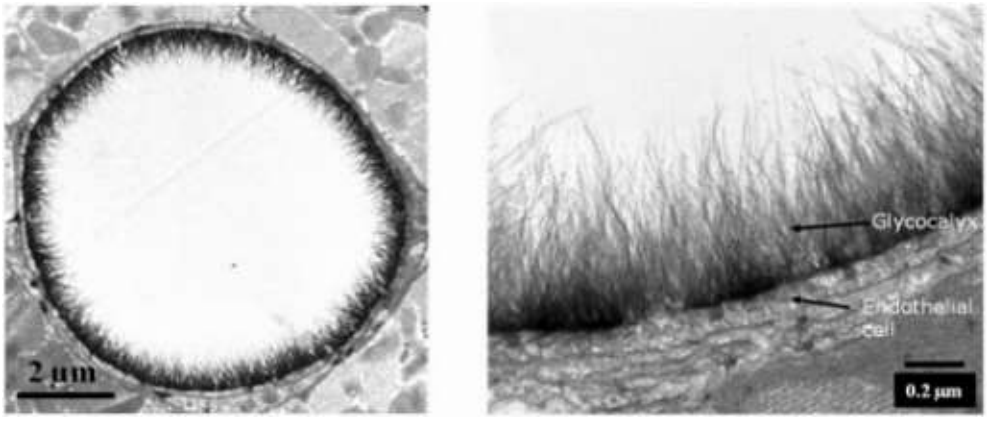

Figure 1. 6 *Electron microscope image of a goat coronary capillary suggesting a brush like structure for the glycocalyx (van den Berg, Vink et al. 2003).*

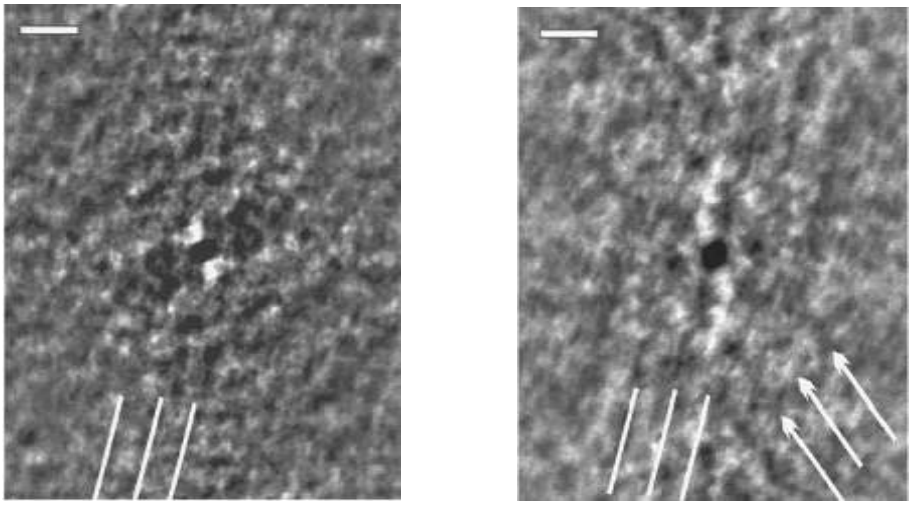

(A) **(B)**

Figure 1. 7 *Pictures taken via electron microscopy show the quasi-hexagonal arrangement of the endothelial glycocalyx (Squire, Chew et al. 2001).*

Weinbaum *et al* proposed in 2003 a refinement of Squire *et al'*s model which sought to reconcile the observations of the bush- or brush-like and matrix-like structures for the glycocalyx (Weinbaum, Zhang et al. 2003). Based on the model of the glycocalyx structure that had been presented by Squire *et al* two years earlier, and the posited structure of actin cytoskeleton linkage between glycocalyx and cell membrane, figure 1.7b shows how Weinbaum *et al* redrafted Squire *et al's* model. Their model shows a complex distributed cytoplasmic structural actin network (DCSA) as the connection between the apical and basal cell membranes. The structure provides a mechanism for transmitting mechanical forces between the cells.

Furthermore, it shows a signalling pathway from cell membrane to nucleus. In the model that Squire *et al* presented, the thickness of the endothelial glycocalyx structure is less than 200nm: this layer of glycocalyx is shown with fibrous structures which exhibit periodicities at each 20nm in both parallel and perpendicular directions connected to the endothelial cell surface. There is also a quasi-hexagonal lattice structure shown between the groups of endothelial glycocalyx macromolecules, with the distance between the centres of each bush- or brush-like structure being around 100nm (Squire, Chew et al. 2001).

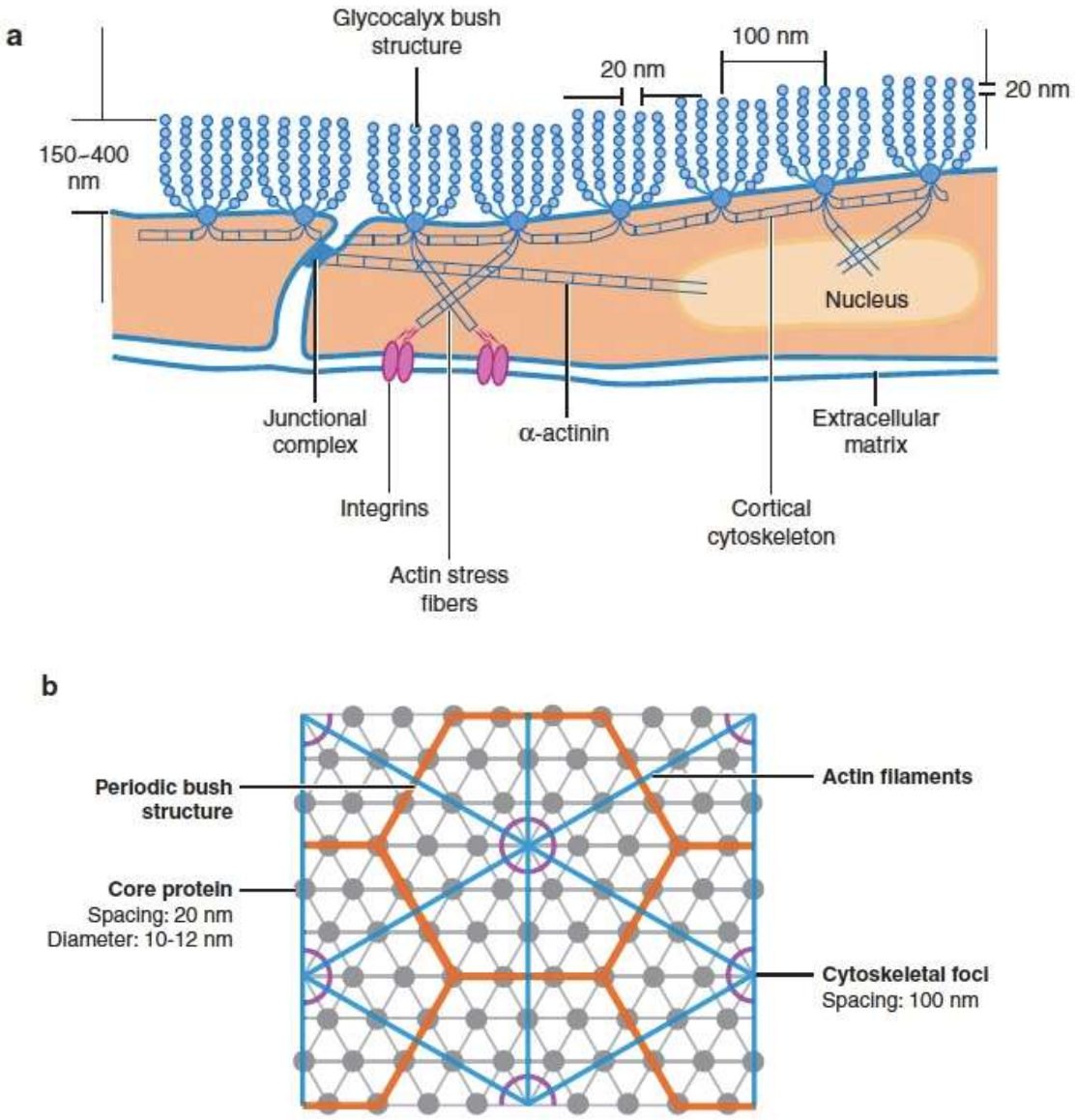

Figure 1. 8 *Image to show the first drawn model of endothelial glycocalyx structure (Weinbaum, Zhang et al. 2003).*

(a) the original model presented (Squire et al., 2001) to show the bush- or brush-like structure of the endothelial glycocalyx and the glycocalyx linked actin cytoskeletons to the nucleus and cell membranes (b) simplified face view of idealized model which shows the quasi-hexagonal lattice structure presented between the groups of endothelial glycocalyx macromolecules.

This model of the endothelial glycocalyx's structure aims to show how its macromolecules are organized on the luminal surface and proposes structural connections between this surface and the cortical cytoskeleton underlying the endothelial cell. This is the first model to show the organization of the matrix of the endothelial glycocalyx while also describing a relationship of linkage between the core proteins of the proteoglycans and the underlying cortical cytoskeleton.

It has been shown that the physiological functions of endothelial cells can be influenced by enzymes that act to degrade the structure of the glycocalyx layer. For example, the hydraulic conductivity of the vessels will be increased by pronase treatment of the endothelial glycocalyx (Adamson and Clough 1992). There is an increasing research focus on the interaction between structure and function in the glycocalyx.

1.3.2 Factors affecting the thickness of the endothelial glycocalyx

The vascular system contains many different types of blood vessels. Their diameter increases from venule to vein, vena cava, then decreases from elastic artery to muscular artery, arteriole and capillary (Wiedeman 1963). Haldenby et *al* indicated through electron microscopy (EM) that the thickness of the glycocalyx on rabbit carotid was 81±2nm and the thickness on coronary artery was 40±2nm (Haldenby, Chappell et al. 1994). Subsequently, van Haaren *et al.*, Gao and Lipowsky demonstrated through dye-exclusion and immunostaining a similar difference in glycocalyx thickness of rat mesentery vessels (van Haaren, VanBavel et al. 2003, Gao and Lipowsky 2010). Their results showed that the thickness of the glycocalyx

increases proportional to the diameter of the lumen (van Haaren, VanBavel et al. 2003, Gao and Lipowsky 2010, Yen, Cai et al. 2012). Varying thickness of the glycocalyx is also observed in vessels of similar diameter and showing similar speed and viscosity of blood flow, but of different phenotypes: for instance, the glycocalyx is slightly thicker in venules than in arterioles (Smith, Long et al. 2003, Savery and Damiano 2008). Glycocalyx thickness is also influenced by patterns of blood flow. Van den Berg et al. undertook a comparison of glycocalyx in different regions in the murine carotid artery via EM (van den Berg, Spaan et al. 2006).

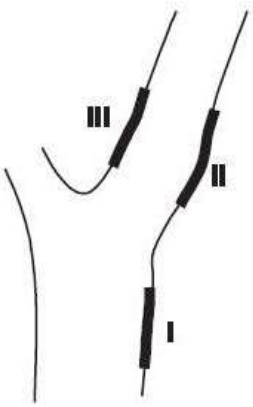

Figure 1. 9 *Schematic images for common region (I), sinus region (II) and flow divider region (III) in carotid artery (van den Berg, Spaan et al. 2006).*

Figure 1.9 shows three different regions in the murine carotid artery: the common region, sinus region and flow divider region. There is a laminar flow in the common region and flow divider region: a turbulent flow is present in the sinus region. There is a very significant difference in the thickness of glycocalyx between regions depending on the types of flow present there. The thickness was 399±174nm in the common region, 73±36nm in the sinus region under turbulent flow, and 308±185nm in the flow divider region. A difference in glycocalyx thickness between atheroprotective and atheroprone regions was further confirmed by van den Berg *et al*. and Reitsma *et al*. through confocal microscopy and two-photon microscopy (van den Berg, Spaan et al. 2009, Reitsma, Vink et al. 2011).

Different methods of detection are a potential factor influencing the measured thickness of the glycocalyx. In early studies, EM was the method used to visualize

the glycocalyx, because the glycocalyx is negatively charged, so it can be visualized due to the binding of cationic molecules. The samples for EM detection were slices of vessels taken after dehydration. It is now known that dehydration causes various types of damage to samples: especially the glycocalyx, where integrity is compromised through dehydration. This may explain why results obtained via EM show a wide range, from within the tens to a hundred nanometres. There are different ways to avoid the effects of dehydration, such as the improvement of sample preparation in EM measurement, or other methods such as dye-exclusion (van Haaren, VanBavel et al. 2003, Gao and Lipowsky 2010). FITC-dextran (70 ~150kD) is used in dye-exclusion technique. At the first stage, the samples of the vessel are perfused with FITC-dextran. FITC-dextran, a fluorescent substance, cannot penetrate into the glycocalyx because its molecule size is much larger than the spaces in the glycocalyx structure. So after treatment, the region without fluorescence denotes the glycocalyx and its thickness can be measured. Compared with EM detection, dye-exclusion technique is a more accurate way to determine the thickness of glycocalyx (van Haaren, VanBavel et al. 2003).

Micro-particle image velocimetry (PIV) is another detection method for glycocalyx thickness (Smith, Long et al. 2003, Savery and Damiano 2008). In PIV technique sample preparation, a small amount of fluorescent micro-particles is injected into the blood vessels. The particles' flow dynamics can be recorded as a velocity profile to derive the hydrodynamic properties of the glycocalyx. This method gives information on the regions near the vessel wall, providing better resolution for both small and large vessels.

Yet another experimental technique is to target the components of the glycocalyx through immunostaining, so that the whole glycocalyx layer can be detected by confocal microscope or two-photon microscope.

The sample preparation of the dye-exclusion technique and PIV technique do not require dehydration, and the means of visualization is much easier than the EM technique. The range of glycocalyx thickness detected by those two techniques is between 1μm and several microns after staining. Although full resolution is provided by both these two microscopes, the depth of penetration is different. The

confocal microscope utilizes single-photon excitation with a common range from 400-500nm, so the penetration depth is limited and only used *in vitro* or *ex vivo.* The two-photon microscope utilizes excitation of two low energy photons with a larger range from 700-1000nm so the penetration depth is increased to 1mm, enabling it to be used *in vivo* without cutting the blood vessels open. (Megens, Reitsma et al. 2006, Reitsma, Vink et al. 2011).

Cultured endothelial cells are widely used to investigate the functions of glycocalyx on endothelial cells, but more recent research has demonstrated important differences in glycocalyx thickness between cultured and natural endothelial cells which may significantly weaken these experimental results. Using the micro-PIV technique to allow measurements to be taken *in vivo*, Potter and Damiano developed research on the differing thickness of glycocalyx between natural endothelium and cultured endothelial cells (Potter and Damiano 2008). The glycocalyx thickness measurement was obtained by comparison after hyaluranon or CS cleaving. The thickness of the glycocalyx in mouse cremaster muscle venules was measured at 0.52±0.28μm through measurements of the layer directly afterwards. By contrast, very little differential in thickness was found on cultured human umbilical vein endothelial cells (HUVECs), with a difference of only 0.03±0.04μm observed. The same happens in cultured bovine aortic endothelial cells (BAECs) where the measured thickness of glycocalyx was just 0.02±0.0.04μm. In followup research, the thickness of regenerated glycocalyx 1, 3, 5 and 7 days after cleaving was measured, to demonstrate significant deficiency in the glycocalyx regeneration properties of cultured cells compared to natural endothelium (Potter, Jiang et al. 2009). These results clearly show the striking difference between *in* or *ex vivo* and *in vitro* models, and cast doubt on the physiological relevance of samples produced *in vitro* under standard cell culture conditions. Although the research compared endothelial glycocalyx from different sizes of vessel (venules *in vivo* and vein/aortic cells *in vitro*), it is unlikely that this caused the differences observed, since the glycocalyx layer is known to be thicker in larger vessels *in vitro*.

A further conspicuous example presented by Chappell *et al.* of the difference in thickness between *ex vivo* and *in vitro* samples, measured using EM, is shown in Figure 1.10 (Chappell, Jacob et al. 2009). This research used human umbilical

cells *ex vitro* and HUVECs to establish a direct comparison between similar blood vessels.

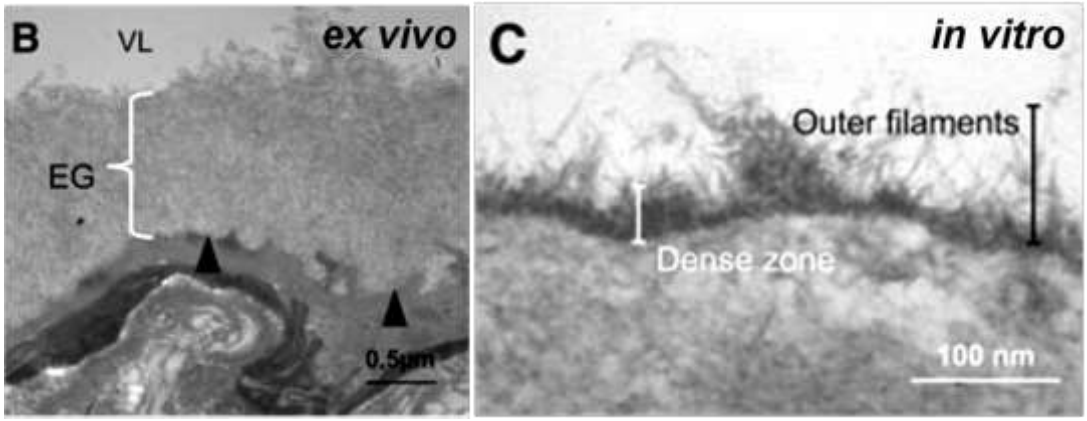

Figure 1. 10 *Comparison of the thickness of endothelial glycocalyx between ex vivo and in vitro model. EG, endothelial glycocalyx; VL, vascular lumen (Chappell, Jacob et al. 2009).*

Image B shows the thickness of glycocalyx in human umbilical vein endothelium was 878±612nm whereas cultured HUVECs (image C) had a layer 29.4±5.8nm thick. The result was clearly smaller than the measurement from the *ex vivo* sample even when the outer filaments were included as part of the *in vitro* thickness measurement, giving a measurement for the HUVECs averaging at 119±39.1nm. The research from Chappell *et al.* additionally showed that HS and syndecan-I can be detected after immunostaining whether in the *ex vivo* or *in vitro* mode.

Chappell's important results suggest that the method of measurement (PIV or EM) is not strongly relevant in the deficiency of glycocalyx thickness observed in cultured cells. They pose challenges for future research to discover ways of refining lab culture conditions, in order to enable the synthesis of a more physiologically relevant hydrodynamic glycocalyx surface layer for *in vitro* research into glycocalyx-mediated mechanisms of endothelial cell function.

1.4 Functions of the endothelial glycocalyx

Endothelial cells are located between blood vessels and the blood flow: research is required on the role(s) played by the glycocalyx in structural and functional changes in the endothelium. The glycocalyx works as a permeability barrier, immune-modulator and mechano-sensor and -transducer. It is well known that the morphology and functions of endothelial cells are influenced by flow shear stress. The responses affected by blood shear stress include cell morphology changes, proliferation rate and other changes in biochemical signaling activities (Dewey, Bussolari et al. 1981, Ebong, Spray et al. 2008, Lopez-Quintero, Amaya et al. 2009).

1.4.1 Permeability barrier

Micro-vessels take charge of exchange between blood and tissues. Oxygen/carbon dioxide, nutrients and chemical waste can transfer between them through micro-vessels. The Starling principle states that the filtration rate is proportional to the net pressure difference between the hydrostatic and oncotic pressures across the vessel wall (Starling 1896). Michel and Weinbaum modified the Starling principle with a different definition for Starling forces, taking the location for the hydrostatic and oncotic pressure measurements not across the whole vessel wall, but across the glycocalyx layer (Michel and Feron 1997, Weinbaum 1998). This was a development for the spatially heterogeneous micro-structural model for endothelial cells; the model was refined again to include an increased importance for inter-endothelial clefts and tight junctions alongside the glycocalyx (Hu and Weinbaum 1999).

The increased importance of the glycocalyx in the revised method for calculating Starling forces indicates that it is necessary to undertake further research on the endothelial glycocalyx, including analysis of its effect on the regulation of transvascular transport. FITC-dextrans (Fluorescein isothiocyanate–dextrans**)** were the first fluorescents successfully used to determine the permeability of the glycocalyx and to suggest a role for hyaluronan in the assembly of the matrix (Henry and Duling 1999). Types of FITC-dextran that had a molecular weight of

70kDa or higher had not penetrated the endothelial membrane after 90mins of dye infusion: this experiment took place on hamster cremaster muscle microvessels which were 15μm in diameter. The exclusion of 70kDa and 145kDa FITC-dextrans was shown to be reduced after the samples were treated by *Streptomyces* hyaluronidase for at least 1 hour. The HA matrix can be digested by *Streptomyces* hyaluronidase, producing pores that increase the permeability of the glycocalyx to smaller FITC-dextrans molecules. The larger sized molecules continue to be excluded, showing no effect from HA digestion. At this stage, the filtration properties of the glycocalyx were maintained by the interaction between the remaining components such as HS and CS. In small arteries with a diameter around 150μm, the exclusion of FITC-dextrans of different molecular weight has been observed as well. Van Haaren et al. did a similar experiment with 4.4kDa, 50kDa and 148kDa FITC-dextran, the results showed 50kDa dextran can partially penetrate the endothelial glycocalyx over time (van Haaren, VanBavel et al. 2003). However, these experiments did not accurately define the size of pores on the glycocalyx because there was a large range of size difference between the 50kDa and 70kDa FITC-dextrans.

The size of pores is not the only factor affecting permeability. Vink and Duling focused on fibrinogen of 340kDa molecular weight and 67kDa albumin. Both proteins demonstrated penetration through the glycocalyx with a halftime at 40mins of the whole 3 hours' exposure. Both of them carried negative charges due to a low isoelectric point of pI4.7~5.2 (Vink and Duling 2000). Even when 70kDa dextran was combined to the albumin, giving a total molecular mass of ~140kD, penetration still occurred. These experiments strongly indicated that interaction between plasma proteins and the glycocalyx plays a decisive role in plasma protein transport into the cells.

The pore size of the glycocalyx, affinity with plasma molecules, and negative charge are identified as three factors for permeability of the glycocalyx. A number of vascular diseases develop following damage to the glycocalyx, which allows plasma molecules to cross the permeable barrier more readily than in healthy vessels.

1.4.2 Immuno-modulator

The process by which leukocytes are delivered from the blood to wound sites, leukocyte extravasation, happens in a series of steps including chemoattraction, rolling, tight adhesion, locomotion and transendothelial migration. Several of these processes are influenced by the glycocalyx, for example, the transendothelial migration of the leukocyte. It has been demonstrated that degrading the glycocalyx structure, using component cleavage such as HS, prevents the leukocytes from migrating through the glycocalyx layer to the laminal surface where they would normally be released to act at inflammation sites. HS cleavage actually exacerbated the inflammation (Mulivor and Lipowsky 2002, Schmidt, Yang et al. 2012) suggesting that healthy glycocalyx normally plays a role in anti-inflammation (Lipowsky 2011).

One of the functions for the endothelial glycocalyx is to separate the leukocytes and vessel wall, acting as a barrier. The coordination of cellular adhesion molecules plays a crucial role on leukocyte-endothelial cell adhesion. However, the communications between adhesion molecules can be disturbed by changes to the glycocalyx, suggesting that it is involved in modulating normal communications. Rolling of leukocytes, the second of the steps in extravasion, is brought about through binding between P-selectin on activated endothelial cells and ligand on leukocytes. There are nine consensus domains within the extracellular domain of P-selectin on the long tail of the GAG chain, but only a fully exposed domain can actually bind with a ligand: the glycocalyx's bush- or brush-like structures mask many of these nine domains, reducing the number actually available for combination with ligands to ≥5 (Patel, Nollert et al. 1995). Ushiyama et al. determined that the length of the extracellular domain of P-selectin was 38nm and the limit length for combination was 19nm (Ushiyama, Laue et al. 1993). Ebong et al. demonstrated that the thickness of the glycocalyx was 1μm on average, but some of the brush-like structures can measure up to 5-10μm (Ebong, Macaluso et al. 2011). This suggests that the whole of the P-selectin structure is masked by the glycocalyx, whose thickness is at least 20 times larger than the length of P-selectin plus its ligand (P-selectin + ligand, 50-60nm: glycocalyx thickness, up to 10μm with average thickness 1μm). Furthermore, the length of L-selectin, which binds with

ligand MAdCAM-1 (mucosal vascular addressin cell adhesion molecule **1)** on leukocytes, was 10-15nm extended from the endothelial cell surface, thus these structures are similarly shielded within the glycocalyx network (Briskin, McEvoy et al. 1993). Shedding of the endothelial glycocalyx has been observed to occur *in vivo* in response to inflammation among other pathological events (Henry and Duling 2000, Mulivor and Lipowsky 2004). Lipowsky further suggests this process is governed by matrix metalloproteinases (MMPs), a family of over two dozen zinc dependent proteases activated from proenzymes on the endothelial cell surface (Lipowsky 2011). Lipowsky et al had demonstrated that inhibition of MMPs decreased the velocity of leukocyte rolling (Lipowsky, Gao et al. 2011). While the processes at work are not fully understood, Lipowsky suggests in his later 2011 paper that MMPs may promote two opposite effects: a) cleaving the glycocalyx to reveal more adhesion molecules for the bonding of leukocytes, thus promoting white blood cell rolling and firm adhesion: and b) conversely, MMP may slow down rolling by preventing the accumulation of ligands that promote it.

In conclusion, there are two ways to improve communication with adhesion molecules: extend the length of microvilli from leukocytes (Sasaki, Okouchi et al. 1998, Zhao, Chien et al. 2001), or reduce the thickness of the masking glycocalyx.

Early studies of the glycocalyx identified anti-inflammatory functions, but more recent research suggests there are also pro-inflammatory functions of HS binding domains in chemokine and adhesion molecules on leukocytes (Lortat-Jacob, Grosdidier et al. 2002). Neutrophil infiltration is influenced by HS; infiltration is reduced when the endothelial sulphation process, essential to synthesis of HS, is prevented by genetic mutation in mice (Wang, Fuster et al. 2005). The absence of HS reduces three important processes, L-selectin-mediated rolling, chemokine-activated tight adhesion and transcytosis. All of these pro-inflammatory processes that promote neutrophil infiltration are therefore shown to be dependent on HS in the glycocalyx. Hayashida *et al* investigated the effects of cleavage of the entire HS chain *in vivo* in mice, by inactivating the ectodomains for syndecan-1, one of the major HS proteoglycans discussed above (Hayashida, Parks et al. 2009). They demonstrated that shortage of syndecan-1 is associated with high levels of CXC chemokines KC (CXCL1, CXC ligand 1) and MIP-2 (macrophage inflammatory

protein-2), extreme neutrophilic inflammation, and lethal organ damage at multiple sites. In conclusion, HS plays a role in both pro-inflammatory and anti-inflammatory processes, and is known to be involved in every stage of inflammatory responses (Parish 2006).

Little is known about the functions of the glycocalyx in pro-inflammation and anti-inflammation and how the different functions are activated. Research is needed that focuses on the functions of individual glycocalyx components in inflammation. Lipowsky notes that modelling based on observations of *in vitro* cell cultures, which as discussed above fail to replicate the structure and composition of glycocalyx *in vivo,* is likely to be inadequate in this complex area (Lipowsky 2011).

1.4.3 Mechanotransduction

The morphology and functions of endothelial cells are regulated by shear stress from blood flow. Thus, shear stress plays an important part in vascular regulation, remodelling and disease. The term 'mechanotransduction' describes the transduction mechanism from biomechanical forces to biochemical signals. In early research, theoretical models were used to predict the action of the endothelial glycocalyx in mechanotransduction (Secomb, Hsu et al. 2001, Weinbaum, Zhang et al. 2003). The undamaged glycocalyx layer was predicted to form a strongly protective barrier against shear stress to the endothelial cell membrane. The shear stress will be completely absorbed within the endothelial glycocalyx, applying little or no pressure on the endothelial cell membrane. The endothelial cell membrane will experience a larger force from shear stress if the glycocalyx is degraded. However, PGI_2 transduction requires a more complicated explanation that allows for shear stress to be communicated to the membrane.

Enzymes that selectively degrade specific components of the glycocalyx have been used experimentally to show that the endothelial glycocalyx plays a crucial role in mechanotransduction. An experiment presented by Pohl et al. shows that flow-dependent vasodilation is blocked after 0.2U/ml neuraminidase treatment for 30mins to cleave SA in mesenteric arteries of rabbit (Pohl, Herlan et al. 1991). NO,

the endothelium derived relaxing factor, and PGI_2 are the two factors controlling flow-dependent vasodilation, thus this research suggests that one or both are promoted by presence of SA. In further work, the shear-induced release of NO was restrained by 2U/ml neuraminidase pretreatment for 40mins, but no effect was shown on the release of PGI_2, in rabbit femoral arteries (Hecker, Mulsch et al. 1993).

The GAGs also play a role in shear-induced NO production, ie in vasodilatory processes. After 14μg/ml hyaluronidase treatment on canine femoral arteries for 20mins, shear-induced NO production is decreased to 20% of the previous level (Mochizuki, Vink et al. 2003).

When bovine aortic endothelial cells (BAECs) are treated with 15mU/ml Hep-III for 2 hours *in vitro*, shear-induced NO production is 100% suppressed within 3 hours. The reason for this should be that HS cleavage through Hep-III damages the structural integrity of the glycocalyx (Florian, Kosky et al. 2003). Oscillatory shear stress at 10±15 dyn/cm^2 was found that the oscillatory conditions promoted more NO release than steady shear stress in 20dyn/cm^2. This NO production result from oscillatory shear stress was also sensitive to Hep-III. Pahakis *et al.* systematically compared the effect on release of NO of digesting individual components of the glycocalyx in BAECs *in vitro* (Pahakis, Kosky et al. 2007). The results showed significant inhibition of NO release after neuraminidase, hyaluronidase and Hep-III treatment with shear stress applied, however no effect was produced by chondroitinase treatment. Figure 1.11 shows the data comparison after the different treatments.

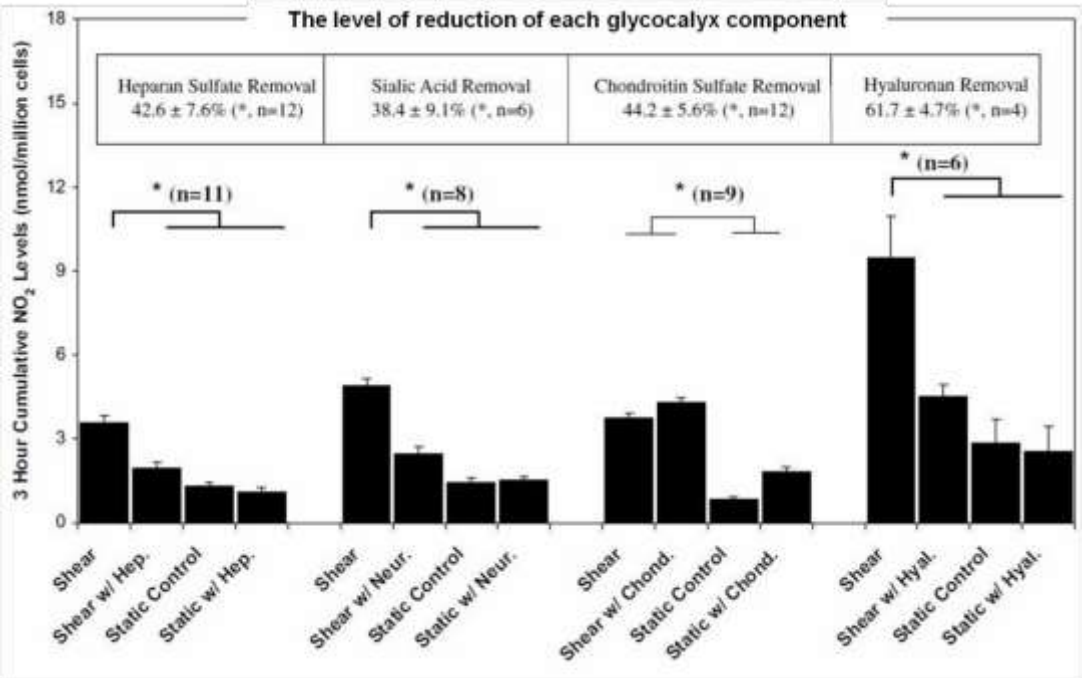

Figure 1. 11 *Effect on NO2 production under shear stress after different enzyme treatments to degrade specific glycocalyx components (Pahakis, Kosky et al. 2007).*

The data above shows approximately 50% suppression of NO_2 production under shear stress after application of enzyme treatment to remove HS, SA and hyaluronan, demonstrating that these three glycocalyx components have unique roles in mechanotransduction and make broadly equal contributions. CS removal, by contrast, does not suppress NO_2 production.

Research suggests that there are at least two separate processes for mechanotransduction at work in the endothelium: one for shear-induced NO transduction, which can be suppressed by enzyme cleavage and is therefore shown to occur in the glycocalyx, likely by a glypican-caveolae-endothelial NO synthesis mechanism; and another for PGI_2 release, which is not suppressed by enzyme cleavage (Pahakis, Kosky et al. 2007, Ebong, Lopez-Quintero et al. 2014). It may be hypothesized that shear dependent PGI_2 mechanotransduction is not dependent on the glycocalyx and originates in shear stress effects on the basal surface of the endothelium, but if so, then an explanation is needed for how the shear stress is transmitted to the basal surface to trigger the mechanotransduction (Hecker, Mulsch et al. 1993, Pahakis, Kosky et al. 2007). There is some evidence of sensitivity to

mechanical stress in the focal adhesions on osteoblasts, likely through a mechanical equilibrium between the basal and apical surfaces (Norvell, Ponik et al. 2004, Ponik and Pavalko 2004). Extrapolating this result to endothelial focal adhesions, Pahakis et al. hypothesized an explanation for PGI_2 mechanotransduction that is not dependent on the healthy glycocalyx.

The shear stress response of the endothelial cytoskeleton, that is the microfilament and microtubules, and its associated structures of cell-cell junctions and focal adhesions, has been recognized as an important focus for research seeking to understand the endothelium's remodelling processes and their contribution to vascular diseases. The relationship of the glycocalyx to the cytoskeleton and its role in these processes had been poorly understood until Squire et al. showed that the glycocalyx's structure has an underlying periodicity, with regular gaps of around 20nm between actin filaments arranged in a hexagonal meshwork, possibly also organized in larger clusters indicating a cytoskeletal scaffold in the submembrane (Squire, Chew et al. 2001). A further study by Thi *et al.*, to investigate how the glycocalyx communicates shear stress to the basal membrane for the stimulation of PGI_2 production, shows that exposure of rat fat-pad endothelial cells (RFPECs) with an intact glycocalyx to uniform shear stress, and especially to high shear stress gradients, leads to the disruption of dense peripheral actin bands (DPABs) bounding the cell, and the formation of stress fibres (SFs) to stabilise the cell in their absence (Thi, Tarbell et al. 2004). This process is blocked under Hep-III treatment to cleave the HS GAG chains and break down the glycocalyx. SFs are understood to be bristle like, communicating shear stress through the actin cortical web, from flow forces acting on its tip at the apical membrane, into the basal membrane where the other end of the stiff actin fibre is attached to the focal adhesion site (see Figure 1.12).

This important study focused on all of the actin structures in the endothelium: the actin cortical web (ACW) underlying the glycocalyx; the DPAB around each cell; and vinculin, paxillin, ZO-1, and Cx43, the associated binding partners of the α-actinin-bundled SFs, observed at the focal adhesions on the basal membrane and at sites on the apical membranes. Observation of changes to the cytoskeletal reorganization in the presence or absence of glycocalyx concluded that the glycocalyx plays little or no role in the organization of focal adhesions on the basal

membrane, as indicated by vinculin and paxillin distribution. ZO-1 and Cx43 expression can be used as a marker to demonstrate whether stable junctions between cells are able to form: ZO-1 serves to organize tight junction proteins, and link them with F-actin; Cx43 is a gap junction protein.

Thi et al. further proposed a "bumper-car" model for describing the structural organization of the endothelial cells, with implications for the way that cells reorient under oscillatory or turbulent shear flow and also for the way that shear stress is transmitted via the glycocalyx to the basal membrane (Thi, Tarbell et al. 2004).

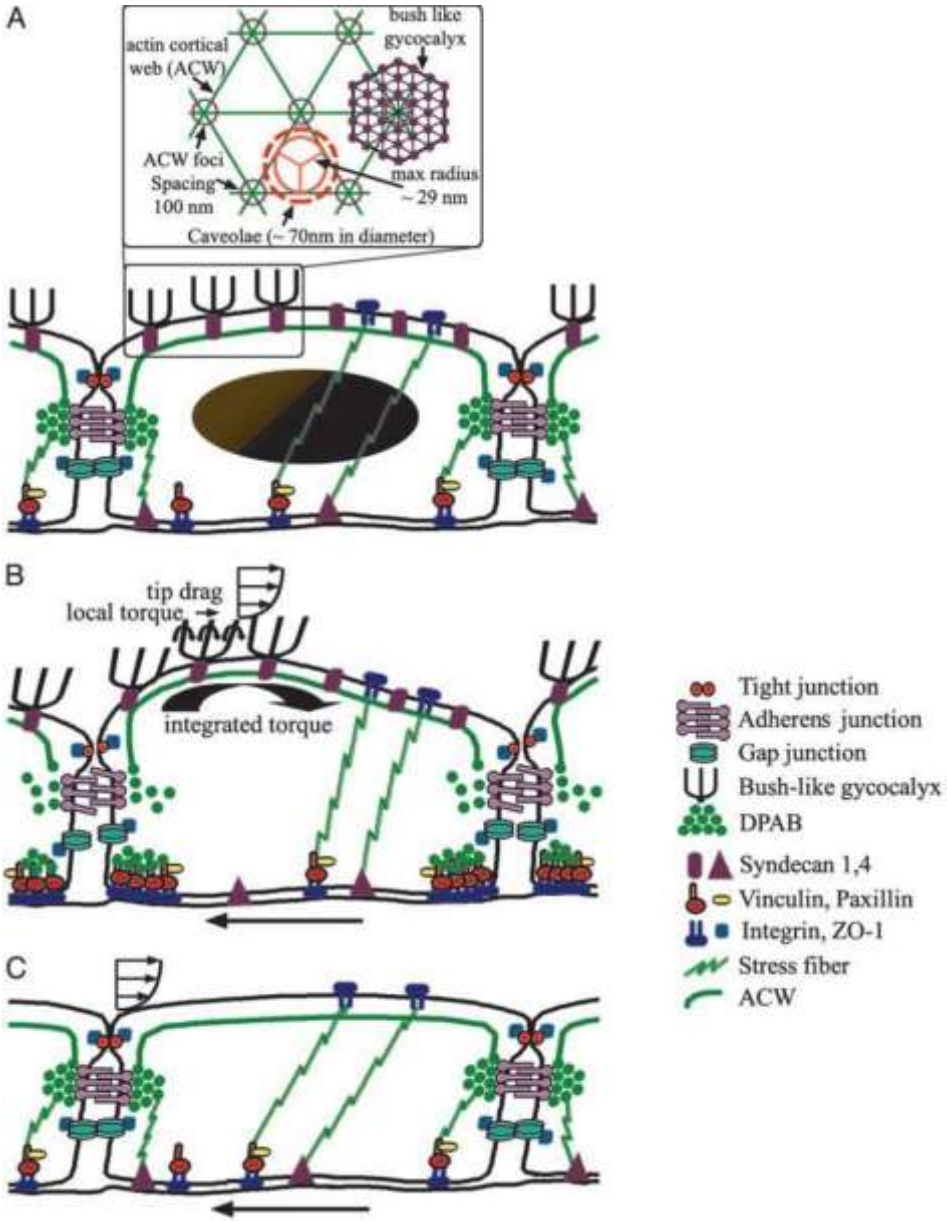

Figure 1. 12 *Thi et al.'s "bumper-car" model showing the structural reorganization of the endothelial cells under flow (Thi, Tarbell et al. 2004).*

A shows the confluent control state, B and C show adaptation steps predicted for intact (B) and compromised (C) endothelial glycocalyx in response to fluid shear stress.

The model hypothesizes that the endothelial cells are weakly held in place on the basal membrane by interactions between the DPAB, tight junction proteins, and the SF connections to focal adhesions: and that the actin cortical web that underlies the glycocalyx on the apical surface functions as a single unit with the DPAB, capable of moving sideways or of rotating slightly, parallel to the basal surface. Under shear stress on the tips of the core proteins in the bush- or brush-like structures of the glycocalyx at the periphery of the cell, the tips are pushed sideways exerting torque on the ACW. Under high shear stress gradients, the multiplied torque exerted by a number of core proteins will act to cause rotational force on endothelial cells. When the forces experienced are strong enough to break the junctional bonds, the glycocalyx then plays an essential role in recruiting the DPAB fragments to form new stress fibres, anchoring to new focal adhesions promoted by vinculin, that temporarily stabilize the cell against radical changes to its shape. If the cell is in an area where there is uniform shear stress, then once the cell's new shape and position is stable, these temporary stress fibres break down, vinculin at the periphery is dispersed, and the protein components are re-used to form a new DPAB for the cell. This process is shown to be governed by the glycocalyx because it can be suppressed by the action of Hep-III. However when the cell is in a region with a high shear stress gradient, the changes to stress fibres are predicted to be permanent, as shown by others with 24- to 30-h studies (Davies, Remuzzi et al. 1986, Girard and Springer 1995, DePaola, Davies et al. 1999, Thi, Tarbell et al. 2004).

As discussed above, Thi *et al.*'s model provides a theoretical explanation for the cytoskeletal processes reorganizing the alignment of cells along the shear flow vector (remodelling). In a further study by Yao *et al.*, Hep-III cleavage to degrade the glycocalyx was shown to suppress cell alignment over 24h and with 15dyn/cm^2 shear stress stimulation (Yao, Rabodzey et al. 2007).

It has previously been observed that there are changes to cell morphology as well as alignment under shear stress. MJ Levesque and RM Nerem noted that the shape of

cells appeared more polygonal under low shear, more ellipsoidal (i.e. elongated) under high shear stress (Levesque and Nerem 1985). BAECs grown on plastic coverslips were exposed to shear stress levels of 10, 30, and 85 dynes/cm2 for periods up to 24 h,, demonstrating a) that endothelial cells orient with the shear flow direction, b) cells elongate more quickly than they realign with the flow direction, c) endothelial cells become more elongated under higher shear stress, and d) a strong correlation is found between the degree of alignment and the shape of the cell. Merks *et al*. demonstrated using HUVECs that the elongation of the cell during remodelling is a key step in vasculogenesis to achieve stable vascular network growth *in vitro* (Merks, Brodsky *et al*. 2006). Yao et al. among others demonstrated that Hep-III treatment of both BAECs and HUVECs to remove the HS proteoglycan structures of the glycocalyx suppressed both the elongation and alignment responses (Yao, Rabodzey et al. 2007). In 2014, Ebong *et al*. investigated the role of HS and syndecan-1 in glycocalyx-mediated mechanotransduction mechanisms for elongation as well as alignment (Ebong, Lopez-Quintero et al. 2014). The team hypothesized that as syndecans have a known relationship with the cytoskeleton, they play a role in mechanotransduction processes governing elongation and alignment: particularly syndecan-1, which lies on the apical surface in direct contact with the shear flow. In contrast, glypican which has no known relationship with the cytoskeleton would not be involved in these processes. This study using BAECS under 3h-24h of shear stress found that HS-removal by Hep-III cleavage reduces elongation and abolishes alignment of the cells, demonstrating that HS is essential to both processes. This team separately tested inactivation of syndecan-1 and of glypican-1, and found that. syndecan-1 silencing completely suppresses both elongation and alignment. Glypican-1 silencing did not produce similar effects.

Endothelial cell migration is a further process that is crucial to angiogenesis and wound healing and that depends on cytoskeletal reorganization. A study by Moon et al. demonstrated, through comparisons between BAECS with intact glycocalyx and with glycocalyx depleted using heparinase-II, that HS proteoglycans are important for cell adhesion rate and strength, formation of SFs and the size of FAs (Moon, Matsumoto et al. 2005). The study further demonstrated the importance of HS proteoglycans in controlling cell migration under steady shear flow by slowing the

speed of migration and giving it directional focus in the direction of the shear flow. These are hypothesized to be key mechanotransduction processes for angiogenesis.

Yao *et al*. extended this line of enquiry, demonstrating with both BAECs and HUVECs that confluent endothelial cells respond quickly to flow by slowing their migration speed by 40% during the first few hours (the migration speed then recovers), and increasing cadherin in the cell-cell junctions: both these processes were suppressed by Hep-III treatment. A further interesting observation was the redistribution of HS proteoglycans to the cell junctional regions, away from the nucleus, after 24h of flow application. The team hypothesized that this might be an adaptive mechanism by the cell, to lessen the shear stress gradient that the apical surface undergoes (Figure 1.13).

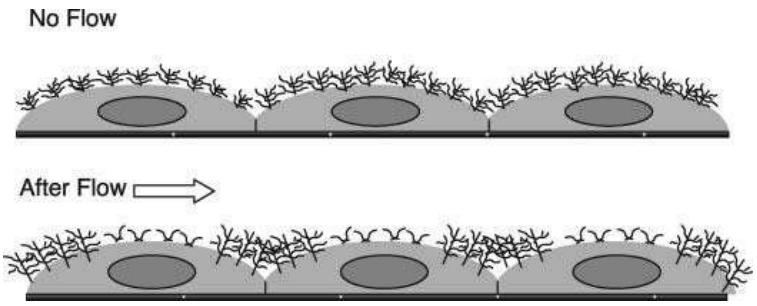

Figure 1. 13 *Model for glycocalyx redistribution under flow (Yao, Rabodzey et al. 2007).*

Bai and Wang then used WGA labelling and immunofluorescent staining of HUVECs under confocal microscopy to give quantitative measurements for the distribution of the glycocalyx by two methods: a) percentage area of the cell membrane covered by glycocalyx, and b) the ratio of WGA intensity between the apical and edge regions of the cell (Bai and Wang 2012). Their study showed that after 24h of shear flow stimulation, the area of glycocalyx distribution was decreased significantly, recovering another 24h after the removal of shear stress.

Following this, a study by Zeng and Tarbell examined the adaptive remodelling of the glycocalyx over time (Zeng and Tarbell 2014). In previous work, the team had shown that within 30 minutes of shear flow beginning, HS clustered at cell junctions, apparently via the mobility of GPI-anchored glypican-1 in lipid membrane rafts

(Zeng, Adamson et al. 2013). By contrast, syndecan-1 seemed to be fixed in position, as did the HS-attached glypican-1 that was bound to caveolae, i.e. protein-based membrane rafts, which are anchored to the actin cytoskeleton by caveolin-1. The team's 2014 study on RFPECs and BAECs built on this: as previously, within 30 minutes of shear flow beginning, HS, CS, glypican-1 and syndecan-1 were observed to be concentrated at the edge regions of the cell, but after 24h of shear flow, in addition to the HS clusters which were sustained at the cell boundary, all four components had returned to a much more even distribution across the apical region, close to the baseline measurement. This suggests that the glycocalyx responds to the onset of shear flow with new synthesis of HS which contributes to the restoration of levels in the apical region, while the original HS is deployed to the protein structures in the edge region. The mechanisms and function of this process of deployment of HS structures to the edge region, and new synthesis of HS in the apical region, are not yet clear, but the team hypothesizes that the dynamic reorganization of the glycocalyx, its associated membrane rafts and the actin cytoskeleton may underlie the way transduction mechanisms in the endothelium change through time, and may therefore be relevant to underlying causes of pathologies including stroke, diabetes and hypertension. They further suggest that way the glycocalyx reorganizes over time may be relevant to other endothelial functions such as selective permeability and leucocyte adhesion.

1.5 The role of the endothelial glycocalyx in vascular pathology

Previous sections have noted that the endothelium is known or suspected to play a role in various pathologies. This section will focus on inflammation and on changes to the vascular wall, and will examine the role of the glycocalyx in atherosclerosis, diabetes and cancer cell metastasis.

1.5.1 Atherosclerosis

The normal functions of the endothelial glycocalyx include inflammatory processes regulating vasonconstriction and vasodilation: damage to the glycocalyx initiates a number of processes and events that promote or worsen atherosclerosis. Atherosclerosis may be predicted by endothelial dysfunction before it can be diagnosed through angiography or ultrasound detection of structural changes to the blood vessel wall (Davignon and Ganz 2004). One of the earliest signs for atherosclerosis are decreased in production of NO (the glycocalyx-produced relaxing factor which controls vasodilation).

The link between atherosclerosis and the circulation of low density lipoproteins (LDLs) in the blood is well established. LDLs accumulate on the vessel luminal wall under sites of endothelial damage, to form atherosclerotic lesions or plaques which eventually begin to protrude into the blood vessel, impeding blood flow and narrowing the vessels. Lowering the concentration of circulating LDL and cholesterol levels can reduce the progression rate of atherosclerosis and may even cause the condition to regress (Skogsberg, Lundström et al. 2008).

The connection between high concentrations of LDL in the blood and damage to the glycocalyx was made by Vink et al., who demonstrated partial degradation of the glycocalyx in endothelial hamster cremaster muscle capillaries under clinically relevant doses of oxidized LDL: see Figure 1.14 (Vink and Duling 2000). This may be linked to the inflammatory processes which are understood to underlie atherosclerosis: systemic bolus injection of Ox-LDL was shown by Lehr et al to be associated with increased leukocyte adhesion in small arteriole and venule endothelium, which can be suppressed by vitamin C or superoxide dismutase (SOD) (Lehr, Seemüller et al. 1993). Liao and Granger also observed that SOD prevents Ox-LDL–induced leukocyte adhesion and endothelial albumin leakage (Liao and Granger 1995).

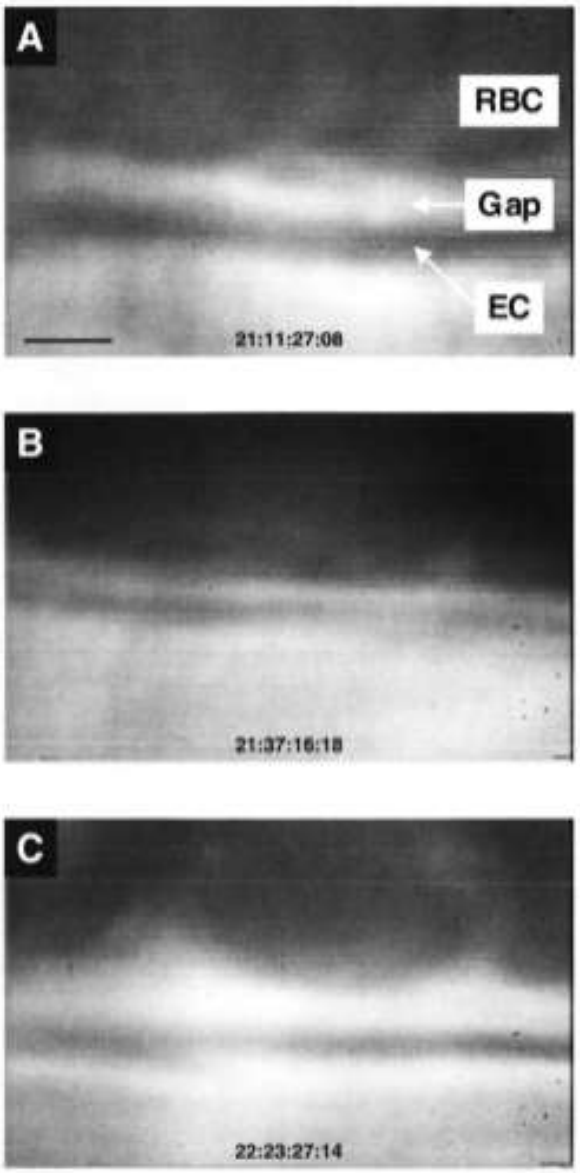

Figure 1. 14 *Light microscopic images of red blood cells flowing through capillary, showing a gap which is understood to represent the glycocalyx layer. (Vink and Duling 2000)*

A, B, and C show the gap narrowing (i.e. the glycocalyx degrading) at 0, 24, and 70 minutes, respectively, after application of Ox-LDL. Calibration bar in A represents 2 μm

A study by van den Berg *et al* tracked two atherogenic risk factors and their effects on glycocalyx structure: an internal factor, the vascular site/morphology, and an external factor, high fat/cholesterol diet (van den Berg, Spaan et al. 2006). Zarins *et al.* had earlier proposed that flow turbulence at arterial branches and curvatures should be predictive of a higher likelihood of development of atherosclerotic lesions at these sites (Zarins, Giddens et al. 1983). These atherosclerotic lesions are detectable as visual changes in the vascular wall, and can be quantified as the ratio between the

thickness of the intima (endothelial) layer and the tough elastic media layer of the vessel. Increases in the intima-to-media ratio (IMR) have been shown to be associated with increased risk of atherosclerosis and cardiovascular disease.

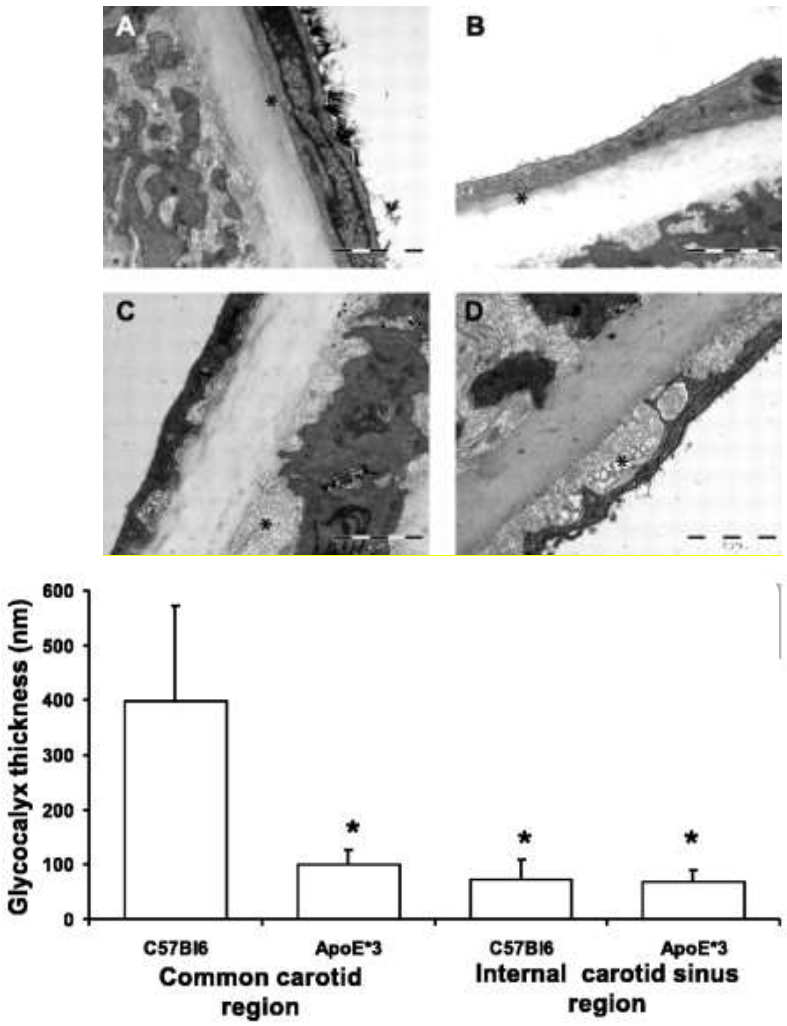

Figure 1. 15 *EM images of stained luminal surface of mouse carotid arteries and a graph showing the measured thickness of the glycocalyx for varying location and diet(van den Berg, Spaan et al. 2006).*

Images A and C above show the low risk region modelled by common carotid: images B and D show high risk internal carotid artery sinus regions. A and B show the effects of normal diet, C and D of atherogenic diet, and asterisks mark the position of the subendothelial matrix layer. Calibration bar in A, B, C and D represents 2 μm.

The van den Berg *et al* study used mouse common carotid artery as a model for a low risk region, and mouse internal carotid artery sinus as a high-risk region. Their

results showed that the glycocalyx loses thickness as the IMR increases, ie the vessel wall thickens or the artery 'hardens' (see Figure 1.15). This suggests that protective functions of the glycocalyx are reduced in areas of higher atherogenic risk. The study further demonstrated that the high-fat, high-cholesterol diet also reduced the thickness of the glycocalyx.

1.5.2 Diabetes

Diabetes is a condition caused by lack of insulin production, or insulin resistance, leading to hyperglycaemia. It frequently leads to cardiovascular complications because the endothelium is readily damaged by excess concentrations of glucose in the blood, making atherosclerosis more likely. Hyperglycaemia has also been shown to significantly inhibit NO synthase enzyme activity in BAECs and to contribute to degradation of GAGs (Ceriello, Giugliano et al. 1983, Du, Edelstein et al. 2001).

1.5.3 Cancer

Selectins, or adhesion molecules, in the glycocalyx have been shown to play an important role in the metastasis of cancer, where cancer cells are migrated via the same mechanisms that promote leukocyte tethering and transendothelial migration (Lafrenie, Buchanan et al. 1993, Okegawa, Pong et al. 2004). Tumour cells that have broken away and are circulating freely in the blood are normally eliminated rapidly; the few that are able quickly to adhere at a new site in the vasculature and pass through the wall of the blood vessel to initiate a new tumour colony will show a selective advantage (Zetter 1993).

Many cancers demonstrate a probability of metastasis to one or more specific organs, and this may be explained by interactions between the particular cancer and structures on the endothelial and/or sub-endothelial cells that are specific to the target organs (Orr, Wang et al. 2000). The relationship between processes in the endothelial cells, including the glycocalyx, and the cancer cells is complex and interdependent.

1.6 Aims and Objectives

The aim of this PhD project is to investigate the location and stability of the endothelial glycocalyx under different flow conditions *in vitro*.

The objectives of this project are:

- To investigate changes in mechanical properties of the endothelial glycocalyx, i.e. the Young's modulus, using Hep-III enzyme treatment. The result is compared to that from an earlier study using neuraminidase.
- To observe the endothelial glycocalyx under static, steady and oscillatory shear flows.
- To investigate the distribution of glycocalyx on the endothelial cell membrane following overnight oscillatory shear stimulation, using AFM indentation and super resolution confocal microscopy.

2. Materials and method

2.1 Cell culture

2.1.1 Culture medium preparation

Aseptic conditions are vital for the preparation of HUVEC culture medium. A perfect complex medium contains the basic medium, antibiotics and extra nutrients. Endothelial cell growth factor (ECGF) is one of the extra nutrients used in the complex medium. The reagents for ECGF preparation are shown below.

Reagent	Company	Working Amount
β-endothelial cell growth factor	Sigma	25μg
Bovine neural tissue	Sigma	75mg
Heparin	Sigma	25KU
Thymidine	Sigma	28.1mg
dH_2O	Millipore	40ml

Table2. 1 *The complements for endothelial cell growth factor preparation.*

The mixture of all the reagents shown in the table above must be divided into 1ml per vial and kept in freezer storage at -80° C. When the complex culture medium is prepared, 1ml of this ECGF must be added to the other ingredients of endothelial cell culture medium, as listed in Table 2.2.

Reagent	Company	Working Amount
Medium 199, HEPES (No.22340/22350)	Invitrogen	500ml
L-Glutamine-Penicillin-Streptomycin solution	Sigma	5ml
Fetal bovine serum	Sigma	56ml
ECGF supplement	Sigma	1ml

Table2. 2 *Reagents for HUVECs culture medium preparation.*

Either of two different types of medium 199 is used, according to the purpose of the cell culture. The first is buffered with Sodium Bicarbonate ($NaHCO_3$) and is specific for seeding cell culture inside the incubator, which requires CO_2 for pH value maintaining (Invitrogen, M199, No.22340). The second is buffered with Sodium Phosphate dibasic (Na_2HPO_4-$7H_2O$) and Potassium Phosphate monobasic (KH_2PO_4) for pH maintenance where 5% CO_2 concentration is not required (Invitrogen, M199, No.22350). The complex culture medium is the mixed with the reagents listed in Table 2.2, then separated into 50ml aliquot for the experiment, to manage the risk of contamination.

2.1.3 Cells

The cells used in this project are Human Umbilical Vein Endothelial Cells (HUVECs) (primary pooled) purchased from Lonza (CC-2517, Lonza Cologne AG, Germany). The HUVECs are cultured in a flask or on a glass slide at 37°C in incubator with a 5% CO_2 concentration applied. The culture medium for HUVECs is changed every 2-3 days.

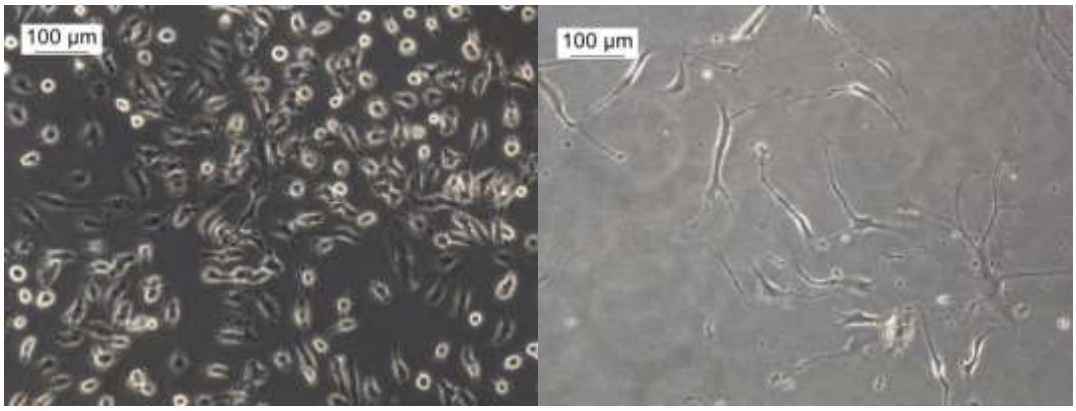

Figure 2. 1 *Confluent HUVEC after 7 days' culture in passage 6 (left) and passage 15 (right) showing normal HUVECs on left and cell differentiation in the right image.*

HUVECs will be discarded after 10 passages due to the risk of cell differentiation. The figure shown above illustrates the difference between normal HUVECs and HUVECs with cell differentiation.

2.1.4 Cell subculture

HUVECs are subcultured until 80% confluence is observed in the flask. Higher confluence than this may lead to cell death as growth in cells leads to overcrowding in the sample and weaker cells experience breaking of the structures that attach them to the glass surface. The tables below show the chemicals and consumables needed for cell culture.

Chemicals	Company	Dilution
Phosphate-Buffered Saline with Ca2+ Mg2+	Invitrogen	-
Phosphate-Buffered Saline without Ca2+ Mg2+	Invitrogen	-
ProLong® Gold reagent	Invitrogen	-
Trypsin-EDTA solution	Sigma	-
Paraformaldehyde (PFA)	Sigma	4%
Triton X-100	Sigma	0.10%
Bovine Serum Albumin (BSA)	Sigma	1%
Dimethyl sulfoxide (DMSO)	Sigma	-
Agar	Sigma	2%

Table2. 3 *The chemicals for cell culture.*

Product	Company	Size
Nunc™ Cell Culture Treated Flasks with Filter Caps	Thermo Scientific	25cm^2
Nunc™ Cell Culture Treated Flasks with Filter Caps	Thermo Scientific	75cm^2
Nunc™ Cell-Culture Treated 24-well plates	Thermo Scientific	1.92cm2 per around well
Coverslips	VWR	18×24×0.13 mm
Coverslips	VWR	Ø13×0.13mm
Centrifuge tubes	VWR	15ml
Centrifuge tubes	VWR	50ml
Serological pipettes	VWR	10ml

Table2. 4 *The consumables for cell culture.*

Prior to cell culture, every chemical must be pre-warmed to 37°C. At the beginning of the sub-culture, the culture medium must be removed and the cells gently washed with 2-3ml PBS for 10 seconds (3-5 ml PBS if the size of the flask is 75cm^2). Then

the PBS is discarded, and 1ml (2-3 ml) of Trypsin added into the flask. Trypsin is a protease that cleaves the protein bonds attaching the cells to the tissue culture plastic and to each other. It can only be left on cell cultures for a short time: if the time period is exceeded, the level of cell damage will kill the cell. Therefore, it is a very important rule for cell culture only to trypsinize one flask at a time. The whole process of trypsinization can be observed via microscope as below.

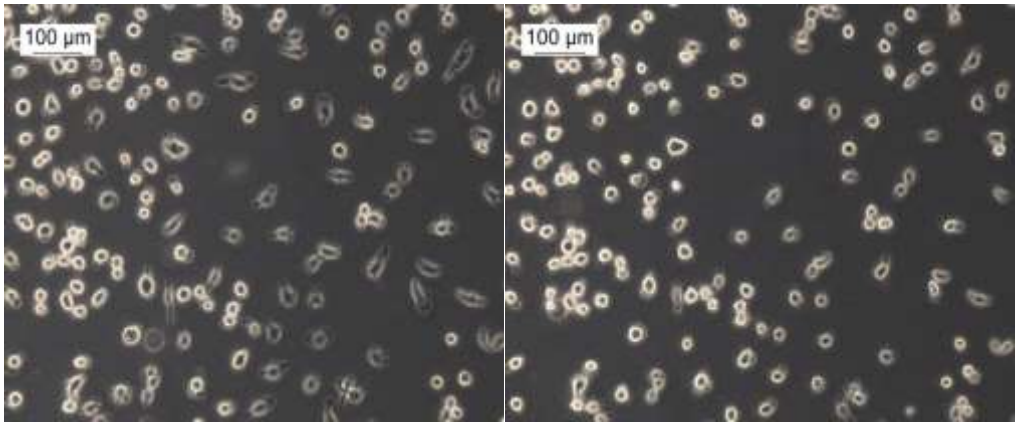

Figure 2. 2 *Trypsinization. Left image: cells in culture prior to addition of trypsin. Right image: after the addition of trypsin.*

As observed under the microscope, cells are detached from the bottom of the flasks and become round in shape, enabling them to flow in the trypsin. 3ml (6-10ml) of culture medium is then added into the flask to stop the trypsinization. All of the cells are extracted into a centrifuge tube with the culture medium, and then the tube is centrifuged at 1500 rpm for 5mins. The cells remain at the bottom of the centrifuge tube after centrifuge. The supernatant is then replaced by 5ml (10ml) PBS, and peptide gum used to mix the PBS with the cells for deep washing prior to the tube being centrifuged for 5mins at 1500 rpm for a second time. Once again, all the supernatant is removed, leaving all the cells inside the tube. 1ml of culture medium is added into the tube to enable cell number counting. The cells are then cultured at a density of 5000 cells/ml in a new flask as a new passage in the incubator. The culture medium is changed every 2-3 days, as before.

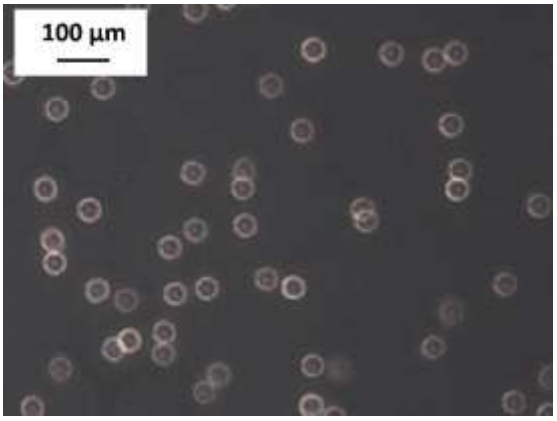

Figure 2. 3 *Microscope image for HUVECs in passage 7 after 10 mins of sub-culture.*

2.2 Cryopreservation and reawakening of HUVECs

For future usage and financial reasons, HUVECs are preserved in liquid nitrogen in flasks when they reach the desired confluence. Cells are usually frozen slowly and thawed quickly to support maximal survival.

Firstly, the cell suspension is centrifuged at 1500rpm for 5mins so that the cell pellets remain at the bottom of the tube. 10ml dimethyl sulfoxide (DMSO) is filtered into a tube with a laminar flow hood. DMSO is a harmful substance and can penetrate latex gloves, so double gloves are needed for this procedure. 1ml DMSO is added to 2ml FBS with 7ml culture medium, then the three are mixed together. Secondly, the supernatant is removed from the centrifuge tube, leaving the cells inside the tube. 1ml of a solution containing 20% FBS, 70% HUVECs culture medium and 10% DMSO is carefully added to create a cell suspension which is then removed into a cryovial. Thirdly, this cryovial can be stored at -20°C for a few hours, transferred to a low temperature freezer at -86°C overnight, then transferred into liquid nitrogen for long term storage.

In summary, after the cells are trypsinized, they are centrifuged, resuspended at a concentration of $5 \times 10^5 – 2 \times 10^6$ cells/ml in 1ml freezing medium in each cryovial, then placed into freezer at -86°C overnight then transferred into liquid nitrogen.

Before the HUVECs are thawed, the culture medium is warmed through a water bath and 10 ml is pipetted into a centrifuge tube. The vial is removed from the liquid nitrogen and warmed through a water bath, maintaining 37°C as soon as possible, until the ice is completely gone. The cells are placed into the tube and centrifuged with warm medium at 1500rpm for 5min to remove the DMSO. Then the supernatant is removed from the tube in order to resuspend the pellet cells in fresh medium. A cell count is performed before the cells are transferred into a flask with warm culture medium. Finally, the cells are cultured in the incubator at 37°C at 5% CO_2.

2.3 Immuno-fluorescent staining of HUVECs

HUVECs are cultured on glass cover slips. After immuno-fluorescent staining through the reagents shown in table 2.5, the HUVECs are prepared for immunofluorescent observations.

Dyes	Company	Stock solution	Dilution
FITC conjugated wheat germ agglutinin from *Triticum vulgaris*	Sigma	1mg/ml	1:150
4',6-Diamidino-2-Phenylindole, Dilactate (DAPI)	Invitrogen	5mg/ml	1:400
CellTrackerTM Red CMTPX	Invitrogen	10mM	1:50
CellTraceTM Far Red DDAO-SE	Invitrogen	10mM	1:100

Table2. 5 *The staining reagents for HUVECs.*

Table 2.6 shows the targeting areas on HUVECs for different dyes.

Dyes	Targeting
FITC conjugated wheat germ agglutinin from *Triticum vulgaris*	β-(1-4)-N-acetyl-D-glucosamine & N-acetylneuraminic acid
4',6-Diamidino-2-Phenylindole,Dilactate (DAPI)	Nucleus
CellTrackerTM Red CMTPX	Cytoplasm
CellTraceTM Far Red DDAO-SE	Cytoplasm

Table2. 6 *The targeting elements corresponding to different staining reagents.*

Before immunofluorescent observation, the sample (cells cultured on glass slide) is washed twice with serum free medium. Then 0.2ml of Wheat Germ Agglutinin (WGA) and Cell Tracker Red CMTPX working solution is applied for 20mins at room temperature. After washing 3 times with warm serum free medium, 0.2ml of DAPI working solution is added for 10mins at room temperature. Finally, the samples are washed again 3 times with warm serum free medium then kept in 10% serum culture medium, completing the preparation for immunofluorescent observation.

2.4 Enzyme treatment of glycocalyx

The technique for enzyme treatment has been well developed in the last 10-12 years (Barker, Konopatskaya et al. 2004, Pahakis, Kosky et al. 2007, Singh, Van Hamme et al. 2007). The components of the endothelial glycocalyx may be degraded by different GAG enzymes; the types of enzyme used in this project are shown below:

Enzymes	Targeted component	Company	Stock solution	Dilution
Neuraminidase from Clostridium perfringens	N-acetyl neuraminic acid	Sigma	10U/ml	1:10
Heparinase III from Flavobacterium heparinum	1-4 linkages between hexosamine and glucuronic acid residues in heparan sulphate	Sigma	10U/ml	1:50

Table2. 7 *The types of enzymes.*

Neuraminidase (sialidases) is a group of glycoside hydrolase enzymes that can cleave the glycosidic linkages of neuraminic acids. Viral neuraminidase is the best-known neuraminidase in the world, responsible for influenza virus release and spreading.

Figure 2. 4 *Neuraminidase of influenza virus (Colman 1994).*

Figure 2.4 shows the structure of neuraminidase as a 3D mode, simplifying the complicated protein structure of viral neuraminidase by representing the various proteins as differently coloured ribbons, as presented by Universitat Autònoma de Barcelona (UAB). The arrow regions represent segments of neuraminidase inhibitor compound which is located on the neuraminidase enzyme surface. Every type of neuraminidase has the same cave-like structure.

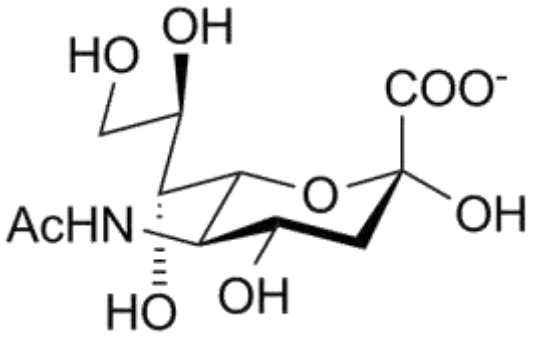

Figure 2. 5 *The chemical structure of N-Acetylneuraminic acid.*

The figure above shows the chemical structure of N-Acetylneuraminic acid. In an earlier project in our laboratory, neuraminidase was used to target the sialic acid residues and N-acetyl-D-glucosaminyl residues of glycoproteins. Barker et al provided the method for neuraminidase treatment (Barker, Konopatskaya et al.

2004). In preparation, samples are washed twice in warm serum free medium then kept inside the incubator with 1U/ml neuraminidase for 10 minutes. The experiment also works with a control group where the HUVECs remain in culture medium with no neuraminidase treatment.

Heparinase is another enzyme that targets the degradation of heparin substrates. There are three heparinase types: heparinase I, II and III. Various studies have outlined the distinguishing substrate specificities of these three heparinase types (Nader, Dietrich et al. 1987, Linhardt, Turnbull et al. 1990, Nader, Porcionatto et al. 1990).

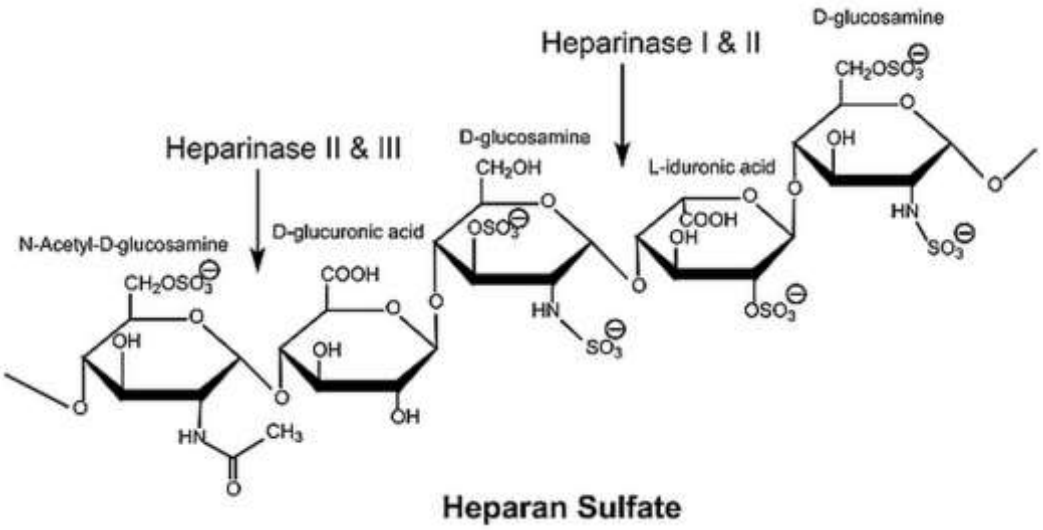

Figure 2. 6 *The chemical structure of heparan sulphate.*

Heparan sulphate and heparin are very complex heterogeneous mixtures which include numbers of disaccharide repeat units. These disaccharide units are composed of a uronic acid (D-glucuronic or L-iduronic acid) and a D-glucosamine or N-acetyl-D-glucosamine structure. Zero to tri-sulphation takes place (at O and/or N) on each monosaccharide unit. We can differentiate between heparan sulphate and heparin via the degree and numbers of sulphation: heparin is more sulphated than heparan.

Hep-III from Flavobacterium heparinum cleaves 1-4 linkages between hexosamine and glucuronic acid residues in heparan sulphate (Thi, Tarbell et al. 2004). Hep-III

is not active with heparin or any low molecular weight heparins (Silva and Dietrich 1974).

For heparinase treatment, the sample is washed twice with warm serum free medium first, then 1ml of warm serum free medium containing 0.2U/ml Hep-III is added into the sample for 2 hours in the incubator. The sample is washed twice with the experimental medium through the monolayer, then retained inside the experimental medium and the sample is ready. As in the neuraminidase study, the control group is not treated and is kept inside the culture medium.

3. Mechanical properties of the endothelial cell glycocalyx *in vitro*

3.1 Introduction

Cell mechanical properties are deeply connected with a number of the cell functions: many researchers have found linkages between cell mechanical properties and cell morphology, adhesion, migration etc. (Sheetz 1995, Guck, Schinkinger et al. 2005, Yamazaki, Kurisu et al. 2005). Familiar approaches to cell mechanical property determination include micropipette aspiration, cytoindentation, magnetic or optical tweezers and atomic force microscopy (AFM) (Svoboda and Block 1994, Guilak, Jones et al. 1999, Shin and Athanasiou 1999). Drake et al. started to use AFM to investigate the different properties of biological cells in the 20th Century, and Henderson conducted research through AFM as well (Drake, Prater et al. 1989, Henderson 1994). AFM has excellent capabilities for topographic characterization at a molecular level, due to its sensitive response to pic-newton force (Fisher, Marszalek et al. 2000, Chaudhuri, Parekh et al. 2009). It can also be used to analyse changes in elastic properties of cells: Sato *et al*. is a good example of a team that has investigated the relationship between changes in the Young's modulus and increasing culture time of HUVECs through AFM (Sato, Katano et al. 2001, Sato, Kataoka et al. 2004). Their work shows there are different Young's modulus values in different regions of the cell; the thinner region has lower elasticity. Comparing cell regions with thickness of 0.418 μm and 1.51 μm, the measured Young's modulus increases from 5 ± 0.2 kPa to 49 ± 1.4 kPa. This suggests further study is worthwhile to evaluate the changes in mechanical properties of the cells within stimulations of endovascular interaction. Kataoka *et al* obtained measurements for decreases in the Young's modulus in the apical region of the HUVECs from 2.7 ± 1.8 kPa to 1.6 ± 0.6 kPa after 2 hours' monocyte application. In other words, the endothelial cell softened as a result of the monocyte interaction (Kataoka, Iwaki et al. 2002).

Many studies have measured the elasticity of various types of cells. Guilak et al. measured the Young's modulus of enzymatically-isolated human cartilage chondrocytes at around 0.66kpa (Guilak, Jones et al. 1999); the Young's modulus of BALB 3T3 fibroblasts has been measured at 1.01± 0.4 kPa (Park, Koch et al. 2005); human chondrosarcoma cells have a Young's modulus of apx. 2kPa (this measurement varies considerably depending on the aggressiveness of the cell line used) (Darling, Zauscher et al. 2007). However, research into the mechanical properties (especially the elastic modulus) of the glycocalyx itself has not been not a popular area until around 2010 onwards. In this very specialized field of relevance to the study presented here, the Young's modulus for bovine lung microvascular endothelial cells (BLMVECs) glycocalyx has been calculated by O'Callaghan *et al* at 0.26±0.03 kPa (O'Callaghan, Job et al. 2011). Bai *et al.* are thought to have been the first to evaluate changes to the Young's modulus of glycocalyx of endothelial cells over culture time, using HUVECs (Bai and Wang 2012). In their study, Bai et al. measure a decrease in the Young's modulus from 2.93±1.16 kPa (3 culture days) to 1.20 ±0.51 kPa (7 culture days), a further decrease to 0.35±0.15 kPa (14 culture days) but no further significant change between 14 and 21 culture days, when the Young's modulus was measured at 0.33±0.19 kPa (Bai and Wang 2012).

Glycocalyx is the inner layer of endothelium, in directly contact with the circulating blood system; it plays an important role in shear stress mediation between the blood flow and endothelial cells. More knowledge is needed about the mechanical properties of the glycocalyx layer in order to understand these processes. In this chapter, the Young's modulus of endothelial cells is evaluated by AFM indentation experiments. The Young's modulus of the glycocalyx layer is determined via the value of the Young's modulus of the HUVECs membrane a) with the glycocalyx layer intact and b) following the removal of the glycocalyx layer through cleavage.

3.2 AFM and cantilever

Atomic force microscopy is used to determine the morphology of HUVECs by imaging. Figure 3.1 shows the AFM cantilever scanning process. The cantilever tip contacts or taps the surface of the sample, causing the angle of the back of the cantilever to change in response to movement up or down. In tapping mode, the tip is vertically oscillated. A laser spot is reflected off the angled back of the flexible cantilever structure onto a photodetector, translating the micro scale movements of the tip to macro scale displacements of the laser spot. This allows the height features of the surface to be measured.

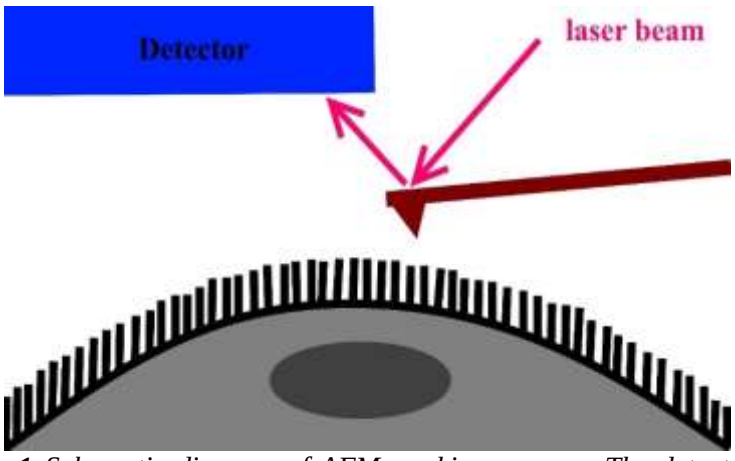

Figure 3. 1 *Schematic diagram of AFM working process. The detector receives the reflected laser signal from the cantilever tip pushing on the HUVECs membrane.*

HUVECs are cultured on round shaped cover glass slips (d = 13mm) and then placed on a microscopic liquid sample platform. The different parts of the atomic force microscope (NT-MDT Ntegra System) are shown in the figure below. A specialist hybrid probe head is used, developed for high resolution imaging in liquid experimental environments (Appnano HYDRA6R-200NG). The equipment is connected to a computer which controls the sample platform, and determines and saves the data from the experiment. A microscope is connected to the AFM to enhance images of the cantilever as it moves across the sample and ensure the laser point is correctly located on the back of the cantilever tip. A Halcyonics anti-vibration table keeps the sample platform steady and movements smooth throughout the process.

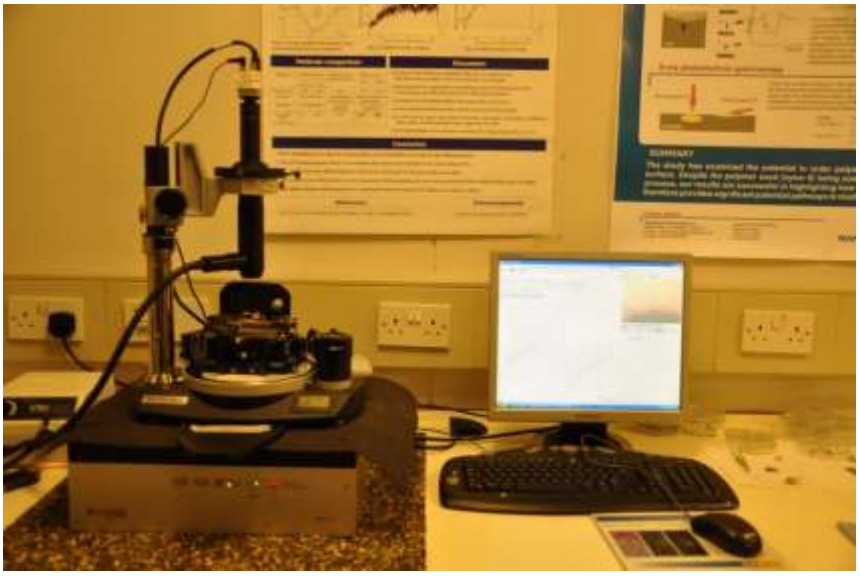

Figure 3. 2 *The complete system for AFM*

The figure below shows the sample platform of the AFM. The circular plate contains liquid in the sample holder, which has a magnet at the bottom to keep the sample steady and a piezo adjuster to raise or lower the sample platform. The sample platform also has a position adjusting screw on each side which can move the sample laterally on the X- and Y-axes. There are three support points which correspond to the three feet of the scanning measure head.

Figure 3. 3 *The sample platform is mounted on top of the specific z-piezo element, which enables the operator to make tiny adjustments to move the sample up or down into position.*

The AFM scanning head is placed above the HUVECs sample. The positioning of the sample, is very carefully calibrated using the z-piezo element underneath the sample platform, to locate the tip in the sample medium but slightly above the level of contact with the cells, to prevent any cell or tip damage from contact force. The laser beam is carefully located to reflect off the tip of the cantilever, at a position 80% along its length (20% distance from the end). The morphology of the sample is mapped using the laser light reflections from the cantilever tip. The maximum size of the image is 160µm x 160µm. Once the morphology of the sample has been determined, giving an image of the sample, a further indentation test is carried out to give measurements for the calculation of the Young's modulus.

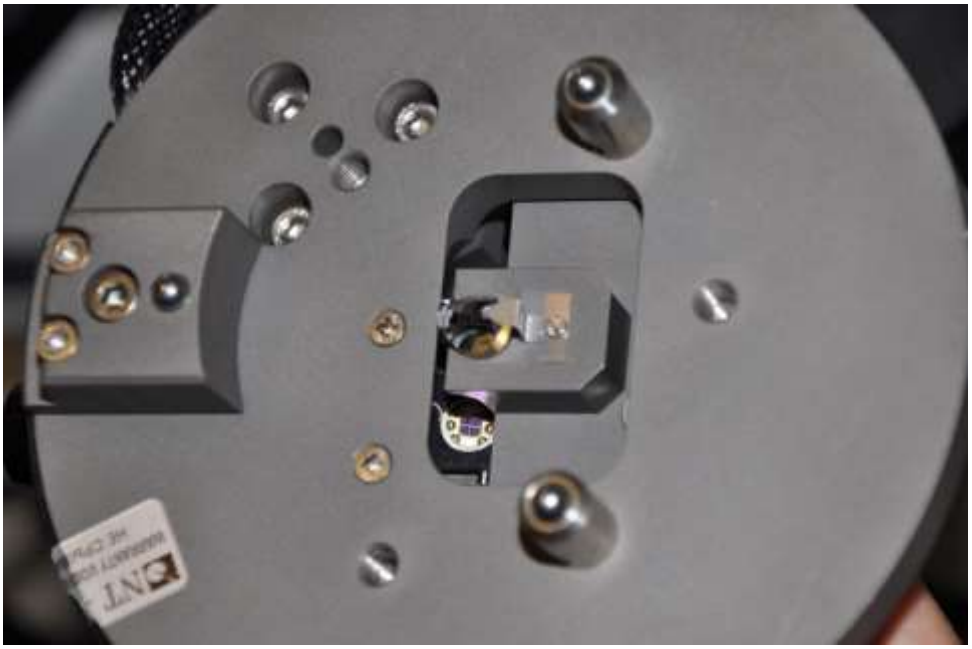

Figure 3. 4 *The specialist scanning sensor head for liquid state work.*

A very specialist probe is used to enable force-distance measurements and give high quality images in either air or liquid environment. The Appnano HYDRA6R-200NG probe has a low stress silicon nitride cantilever with a single crystal silicon tip. The sharp point of the tip is pyramidal shaped with a radius of 6nm. The reflex side is coated with gold, which ensures that electrostatic forces will not apply between the sample and the sensor, which could affect the accuracy of measurements.

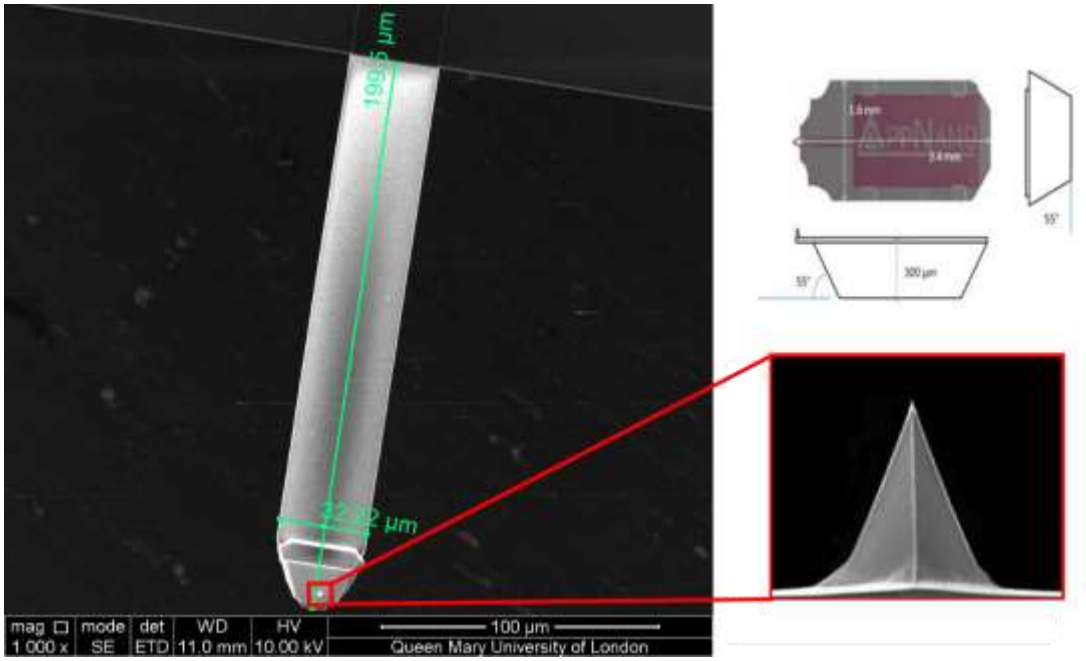

Figure 3. 5 *SEM image of cantilever.*

Figure 3.5 above shows a Scanning Electron Microscope (SEM) image of the HYDRA6R200-NG cantilever. The red box on the left hand image shows the position of the cantilever tip. The close-up image in the red box on the right is a sideways view of the cantilever tip showing its pyramidal shape. The tip, which is the only part in contact with the cell sample, is located at the far end of the cantilever. The base length of the pyramidal tip is 4.2 µm and its height is 6 µm. The half-opening angle of the tip is approximately 20 degrees.

The probe is supplied with a rectangular cantilever of nominal length (l) 200µm, but according to the manufacturer's specifications this value may vary from (minimum) 190µm to (maximum) 200µm. Similarly, the nominal width of the cantilever is 35µm but this may vary from (minimum) 30µm to (maximum) 40µm. The spring constant of the cantilever is uniform and can be calculated from the length and width of the cantilever in use. The measurements given in green on the left hand image above for the cantilever in use are (l) 195.5µm, (w) 32.22µm.

Once the spring constant value for the particular cantilever in use has been calculated, this can then be used to calculate the force applied, and thence the Young's modulus, by an equation given below in .

3.2.1 Two AFM scanning modes used for imaging and mechanical property examination

There are three different AFM scanning modes: contact mode, non-contact mode and tapping mode. Two of them are used for this experiment, tapping mode which is used to determine the morphology of HUVECs, giving an image, and contact mode which is used to measure the Young's modulus through indentation testing. The figure below shows the principle of these two different modes.

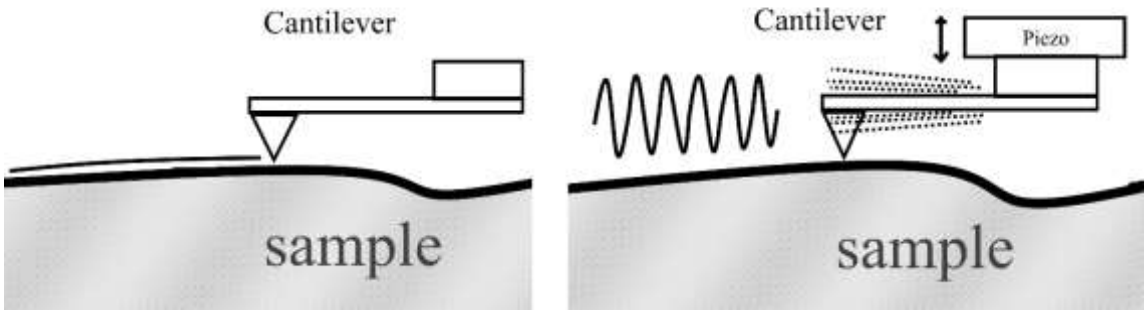

Figure 3. 6 *Contact mode(left) and tapping mode (right) of AFM.*

In tapping mode, the piezo-electric element oscillates the cantilever head vertically at high frequency. The cantilever's movement will be stopped as soon as the tip of the cantilever reaches the surface of the sample, as a result of the loss of energy through contact between two materials. As the cantilever moves along the X or Y axis over the bumpy surface of the material, the amplitude of the oscillating movement will be increased when the tip moves around a down fold, or decreased while the tip moves around a bump region. Very delicate details of sample morphology can be traced in tapping mode in this way, because the cantilever moves very gently and no damage is done to the cells in the sample.

In contact mode, the amplitude of the cantilever movement is fixed without oscillation, so that it exerts a force on contact with the surface of the sample. This setting is widely used to obtain mechanical properties for various types of materials.

3.2.2 Cell morphology imaging

AFM observations are made using cells with exactly the same culture time as those observed with the confocal microscope: 8 days. Samples are kept in the culture medium throughout the AFM process. 2 hours out of the incubator is the maximum time cells can be used without their state degrading, so all AFM procedures must be completed within this time. The sensor head is set in tapping mode to take measurements across an area of the sample defined on the x and y axis. AFM gives a phase image of the cell while also calculating cell height, as discussed above. Figure 3.6 shows these two types of image for HUVECs, taken in tapping mode. The dimensions of the HUVECs are around 50μm×80μm.

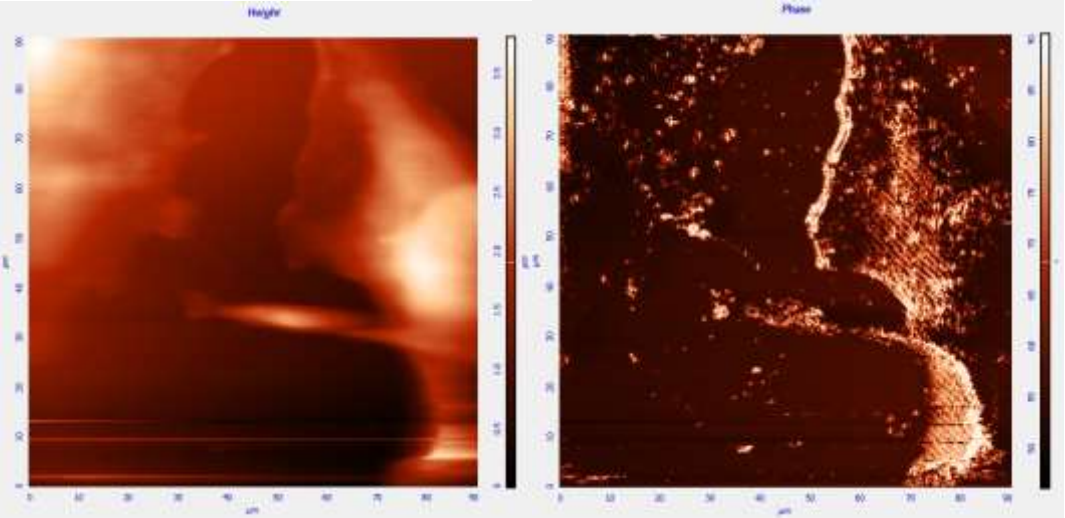

Figure 3. 7 *AFM height image (left) and phase image (right) for HUVECs after 8-day cell culture.*

The left image shows the different height at various locations within the sample. The brightest areas show the highest region of the cell, where the nucleus is located. Darker areas show material nearer the height of the glass slide, where the cell's basal membrane is. There is a sharp distinction between the cells and glass slide. The phase image, on the right, clearly shows a distinct boundary at the edge of the cells. This phase image is helpful to identify the location of the cell for the indentation test which follows. It also reveals impurities, whereas the height image cannot distinguish between cell and impurity. This is a significant advantage of a method which can produce two types of image at the same time: comparison between the two is very helpful for accurate cell boundary screening.

After the tapping-mode scan determines the sample's morphology, the next step is the indentation test, with the probe in contact mode. The data determined via AFM is used to calculate the Young's modulus of HUVECs in different areas on the membrane of a cell.

3.2.3 Calibration of the cantilever

The cantilever is 200μm in length, 35μm in width, with a uniform spring constant of approximately 0.035N/m (this can be used to calculate the force applied, by an equation given below). The tip, which is the only part in contact with the cell sample, is located at the far end of the cantilever. The base length of the pyramidal tip is 4.2 μm and its height is 6 μm. The half-opening angle of the tip is approximately 20 degrees.

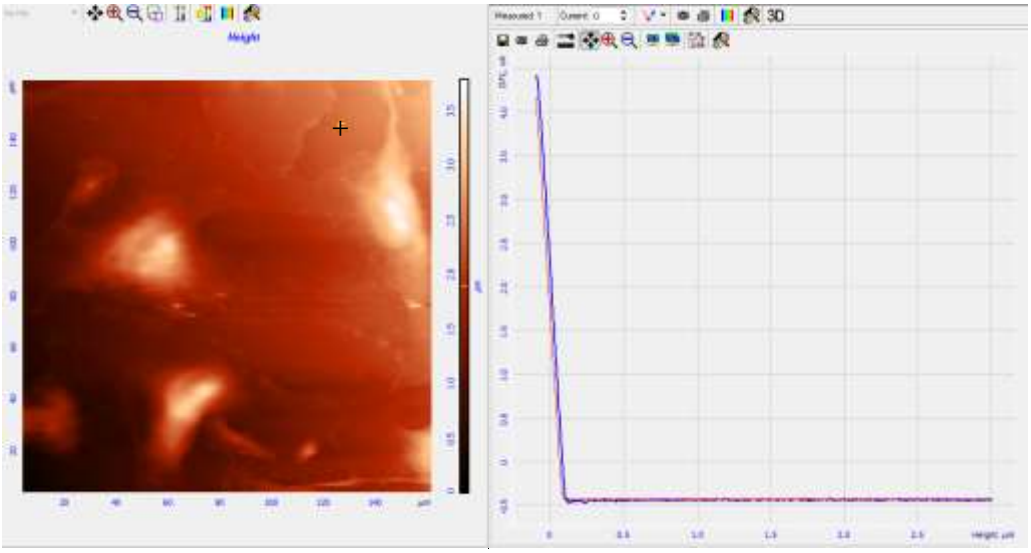

Figure 3. 8 *Cantilever calibration process.*

The left hand image shows the location of indentations on top of the sample (darker image: lower areas of the sample), the right hand image shows the deflection-piezo displacement curves, each of which is made up of thousands of pieces of data measured by the indentation experiment.

Firstly, the cantilever must be calibrated. Using the image generated from the tapping-mode scan, an empty point on the glass slide is selected, where no cell

culture is present. Calibration was here undertaken at the spot marked by the black + markeron the left-hand image within Figure 3.7: the dark colour on the height image at this point demonstrates that no cell culture is present. The deflection-piezo displacement curves generated by the calibrating contact-mode scan for this area of empty glass, with no sample under the sensor, are shown on the right-hand image in Fig. 3.7. In this right-hand image, the x axis shows the vertical height between the cantilever and the sample surface, in μm (the calculation for this is discussed below). The y axis shows the value for the vertical deflection of the cantilever, produced by the contact force. This is measured on the AFM by means of the vertical optical registration system, converted into electrical signal DFL (deflection value), and recorded in nA. There is a linear relationship between the DFL value and the force applied to the sample.

The sloped area of the graph, to the left where values on the x axis are <0.1μm approx., plots the data during contact with the sample. The flat area of the graph, to the right where x axis values are >0.1μm, plots data where there is no contact between tip and sample.

The red and blue curves show two groups of indentation data: a) in red, the loading indentation data from the cantilever as the tip approaches the sample; b) in blue, the unloading data as the tip retracts from the sample surface. The cantilever setting appropriate for working with HUVECs applies a very low level of force to the tip. For glass, a very stiff substance, the tip presses, or indents, almost no distance into the surface: therefore there is an almost total overlap between the red and the blue graph at the low level of force applied to the tip. The slope of the graph, showing the relationship between the height from sample to cantilever (μm, x axis) and the cantilever deflection value (nA, y axis), can then be used to calibrate conversion calculations on the measurements obtained from the sample.

To calculate the Young's modulus, we need to determine the applied loading force (F). Cappella & Dietler detemined the applied loading force in an AFM indentation test by the equation as follows (Cappella and Dietler 1999):

$$F = k * \alpha * V$$

where

- F is the force between the AFM tip and cell sample (F, Newton)
- k is the cantilever's spring constant (k, Newton / metre)
- α is the cantilever deflection sensitivity (α, metre / volt)
- V is the cantilever deflection voltage (V, volt).

Two vertical measurements are relevant to the calculation of the indentation depth:

a) The vertical distance moved by the sample as it is raised/lowered by the z-piezo adjuster (shown on the x-axis of the graph as h)
b) The vertical displacement of the sensor tip under cantilever displacement, as it is pushed upwards by contact with the sample (this is calculated from the displacement value plotted on the graph).

The moment of contact between sensor tip and sample is shown on the graph at the point the red and blue graphs diverge.

The next step is to calculate the pure indentation depth, i.e. the distance the sensor tip has pushed into the sample, using the measurements above and the method as explained below in figure 3.9.

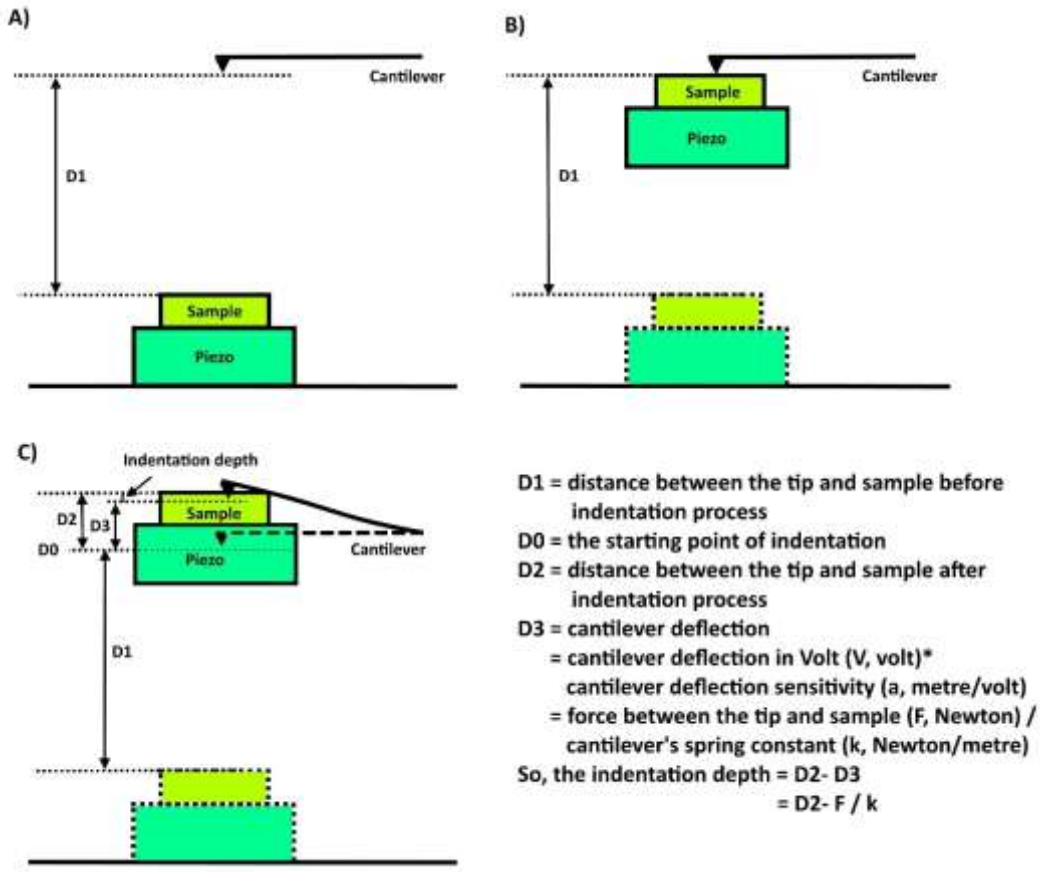

Figure 3. 9 *Diagrams to show the pure indentation depth calculation process.*

This set of diagrams illustrates the calculation of the pure indentation depth. From the position shown in diagram a), the sample platform is moved smoothly upwards under control of the piezo electric platform until contact is made with the sensor tip, as shown in diagram b). As already noted, the moment of contact between the sample and the sensor tip is shown by the divergence of the red and blue graphs.

As the sample continues to move upwards in contact with the sensor tip, the sample exerts an upward force on the sensor tip, and the resistance generated by the cantilever exerts a downward force on the sample. This is what produces the indentation of the sensor tip into the sample as shown in diagram c). The pure indentation depth is calculated by subtracting D3, the displacement of the sensor tip, from D0, the vertical distance moved by the platform.

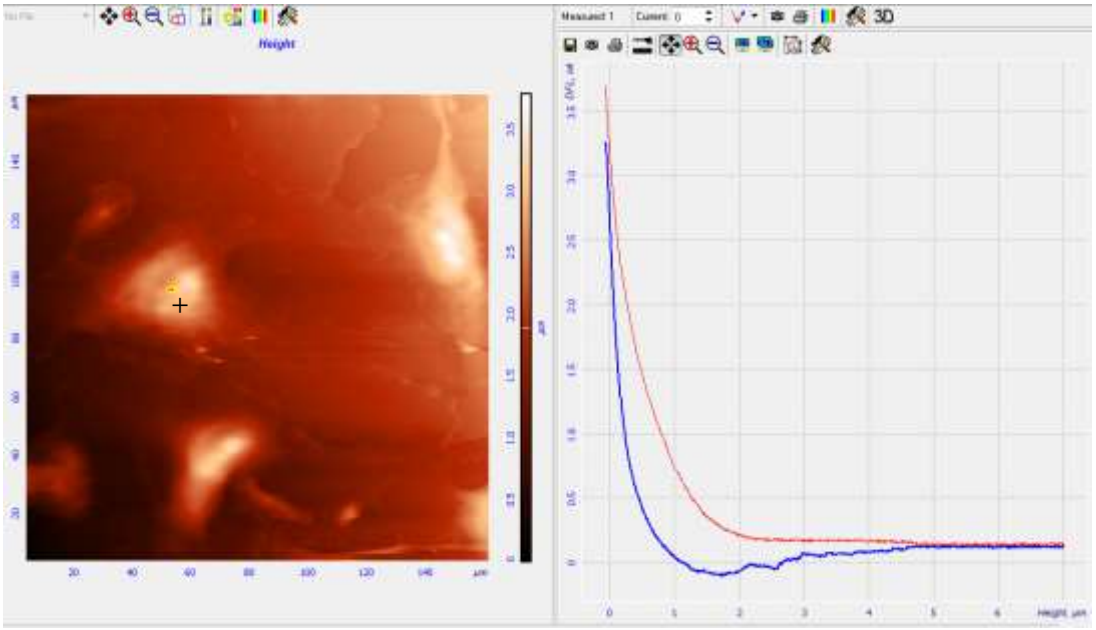

Figure 3. 10 *Image from indentation test on HUVECs with deflection-piezo displacement curves.*

Note that the piezo displacement height is not the displacement of the tip against the testing sample, but the vertical distance moved by the sample surface under the z-piezo adjuster.

Figure 3.10 above shows the image and the data observed from an AFM experiment. The left hand image shows the morphology of the sample: the + sign shows the point chosen for the indentation test. The indentation point is located on the brightest area on the cell, which is the apical region above the nucleus.

The right hand image shows the deflection-piezo displacement curves for the sample, with red showing the loading or approach motion and blue showing the unloading or retracting motion, as in the calibration graph. The straight line area, on the right of the graph, is data from before contact is made between the sensor tip and the sample surface: there is no deflection force at all. When the tip of cantilever makes contact with the cell surface, the red and blue curves diverge. The slight rise in the red curve shows the cantilever spring bending slightly on initial contact with the sample. The curve then rises up sharply at the moment of hard contact with the cell surface, showing the repelling force applied by the cell.

The blue curve is not smooth because as the sensor tip retracts from the sample, it experiences adhesive forces from chemical affinity, surface coatings etc. in the cell membrane which surrounds it. As the tip continues to retract, the molecules stretch and connections are broken: these tiny sudden changes in the adhesive force acting on the tip result in a jagged line on the graph. The tip of the cantilever then moves rapidly away at the moment the tip detaches from the membrane of the cell.

The deflection-piezo displacement curve for indentation on a cell sample shows no overlap between the red and blue curve for the whole time the sensor tip is in contact with the sample, in total contrast with the curve for glass. The reason for this result is the viscoelastic property of HUVECs: the curve shows the cell membrane responding very shortly after the indentation force is applied, i.e. the cell is deforming.

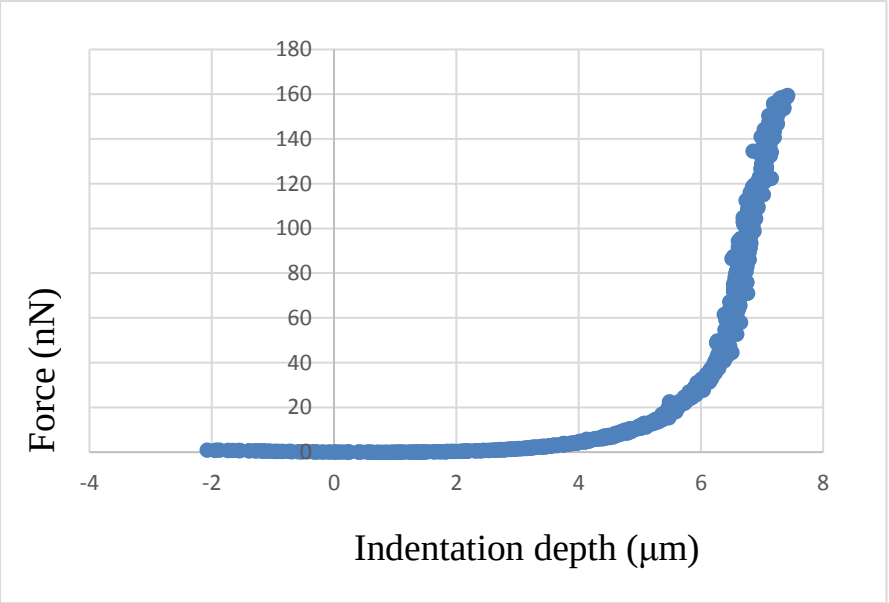

Figure 3. 11 *Force-distance curve for HUVECs with 8 culture days.*

Figure 3.11 shows an example of force-distance curve for indentation on HUVECs cultured for 8 days. The indentation is carried out in the apical area where the nucleus shows up. At the very beginning of the indentation process, the tip of cantilever is far away from the sample surface so the deflection force is constant at 0nN. The value of the deflection force increases when the tip of cantilever makes contact with the cell

membrane. The force-distance curve presents the relationship between the force and the indentation depth.

3.2.4 Calculation of the Young's modulus

The Hertz model for indentation on a homogeneous soft sample by a stiff cone is used to analyze the force-distance curve and Young's modulus (Hertz 1882, Sato, Kataoka et al. 2004):

$$F = \frac{\delta^2 * 2 * E}{\pi * (1 - \vartheta^2)} \tan \alpha$$

Where

- F is the applied loading force,
- δ is the indentation distance, described above as the pure indentation depth,
- ϑ is the Poisson ratio of the tissue sample and is assumed to be 0.5 as cells are considered to be incompressible,
- α is the half opening angle of the tip of the AFM cantilever,
- E is the Young's modulus.

Because the force-distance relationship is a curve, the Young's modulus is not a constant value throughout the whole of the indentation process. The experiment is concerned only with the initial period of the indentation, from the first moment of contact between sensor tip and sample to a pure indentation depth of <200 nm. This is because the glycocalyx is considered as a simple isotropic, homogeneous and incompressible layer of a maximum 200 nm in depth. The cell membrane lying below the glycocalyx is considered as a deformable flat surface. In order to minimize possible influence of the cytoplasm and cytoskeleton on the results, therefore, only raw data from the first 200 nm of indentation depth are used in all the calculations.

The slope of the part of the force-distance curve that relates only to the first 200nm of indentation depth is calculated. According to the equation the slope of the curve at this point equates to

$$\frac{2 * E * \tan \alpha}{\pi * (1 - \vartheta^2)}$$

Since all other values in the equation are known, this therefore allows a value to be derived for E, the Young's modulus of the glycocalyx.

Because the Young's modulus is not a constant value, the experimental methodology involved taking measurements for Young's modulus of the glycocalyx in three different areas of the cell membrane in order to show the distribution of the glycocalyx across the cell membrane.

3.3 Results

According to the research of Potter et al., the hydrodynamically relevant thickness of glycocalyx will not increase after seven culture days, assuming the healthy passage of cells and 80% confluence (Potter, Jiang et al. 2009). This is the reason for the samples in this experiment being cultured for 8 days before imaging.

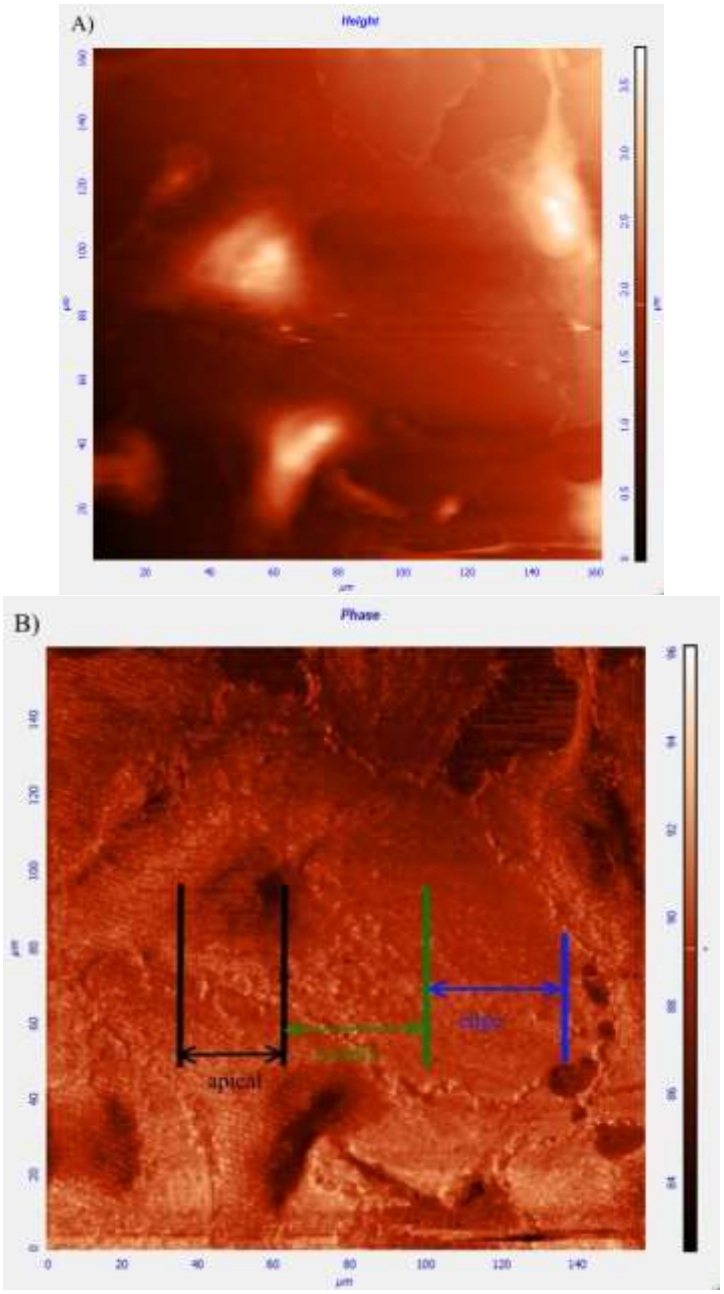

Figure 3. 12 *AFM images of HUVECs.*

A) Height image to show the morphology details of HUVECs cultured on glass slide; B) Phase image to show the location of each indentation area (apical, middle and edge) on HUVECs.

The height and phase image show morphology information about the HUVECs surface. Both images are obtained simultaneously while the tip scans the samples of cells. The brightness in the height image (Figure 3.12 A) shows the different heights within the cell sample with the brightest colour equating to the highest area. The

phase image (Figure 3.12 B) also shows a contrast between different heights and also shows more details in the edge of the cells. In figure 3.12 B, the highest area of cells is considered to be the apical region, shown by the brightest area of the image (labelled between the black lines): this area includes the endothelial cell nucleus inside. The remaining area can be divided into two regions following Bai and Wang's description: the 'middle' region (showing between green and black lines) and the 'edge' region (showing between the green and blue lines) (Bai and Wang 2012). These three regions are used as the standard descriptions for distinguishing the Young's modulus in different locations on cell surface.

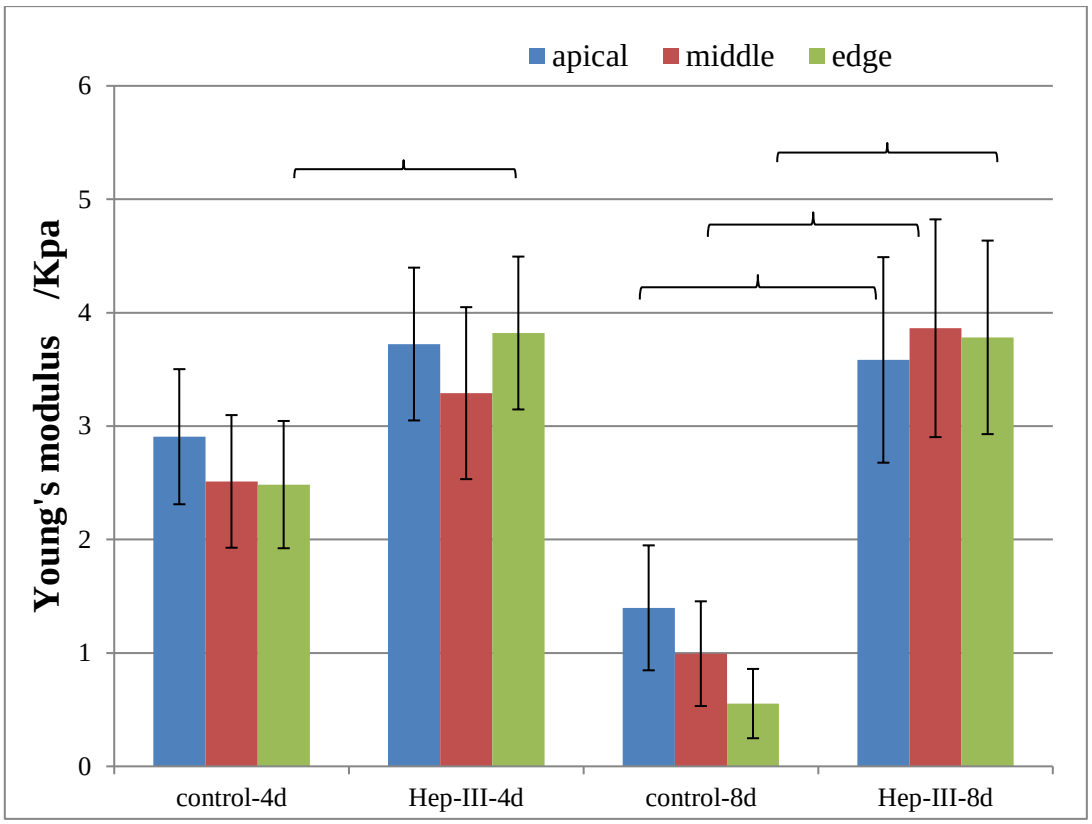

Figure 3. 13 *The Young's modulus of HUVECs membrane in vitro for untreated and Hep-III treated HUVECs cultured for 4 days (control) and 8 days.*

The indentation test is applied on the cell membrane by AFM in apical, middle and edge regions of the cell.

In the figure 3.13, the Young's modulus of the cell membrane in three different regions is determined by an AFM indentation test. The cell samples were cultured

for 4 and 8 days before being tested. A comparison was made between samples with an intact glycocalyx layer, and with glycocalyx layer damaged through cleavage with Hep-III treatment.

The Young's modulus of the cell membrane decreased with culture time, from approximately 2.91 ± 0.6 KPa (n= 51) at day 4 to 1.4 ± 0.55 KPa (n=51) at day 8, at the end of culture time.

After Hep-III treatment, the Young's modulus is clearly larger than in either of the control groups, showing an increased elasticity under indentation for the cell membrane without glycocalyx, as compared to the cell membrane when coated with soft glycocalyx.

At 4 days' culture, our results show a small difference in Young's modulus of each of the three regions of the cell between the untreated (control) and Hep-III treated samples. The largest differential is shown in the edge region.

At 8 days' culture, the Young's modulus of the cell membrane in the untreated (control) group is significantly lower than that of any of the other samples. In the 8-day control sample, there is also a huge difference between the Young's modulus for the apical region (1.4 ±0.55 KPa, n=17) and the edge region (0.55±0.31 KPa, n=17).

Comparing the untreated control sample and the Hep-III treated sample at 8 days' culture, the stiffness of the cell membrane increased almost 7-fold, which is a change from 0.55 KPa to 3.78 KPa after Hep-III treatment. Again, the largest differential for one region is shown in the edge region of the cell. These results show that the glycocalyx is particularly well developed in the edge region after 8 days' culture.

Even though the glycocalyx layer is not 100 percent cleaved away after Hep-III treatment, we take it that the Young's modulus of the glycocalyx layer can be calculated with reasonable accuracy from the values of the Young's modulus in cell membrane with, and without, glycocalyx. The glycocalyx layer and the remaining

part of the cell membrane may be considered as two connected springs in a series system. The spring constant of the whole series system can be defined as follows:

$$K = \frac{K_0 K_1}{K_1 - K_0}$$

where

- K is the Young's modulus of glycocalyx,
- K_0 is the Young's modulus of cell membrane in the control group,
- K_1 is the Young's modulus of cell membrane after Hep-III treatment.

For this project, the Young's modulus of the cell membrane with glycocalyx layer is 0.55 KPa, and taking the sample with the same culture time, the Young's modulus of cell membrane without glycocalyx layer is 3.78 KPa. Working through the equation, the Young's modulus given for the pure glycocalyx layer is 0.64 KPa.

3.4 Discussion

There were a limited number of projects focused on the mechanical properties of the endothelial glycocalyx layer until O'Callaghan *et al* presented their research on bovine lung microvascular endothelial cells (O'Callaghan, Job et al. 2011). O'Callaghan *et al* measure the Young's modulus value for the bovine glycocalyx at 0.26±0.03 kPa.

Bai & Wang also obtain results similar to the present study, using neuraminidase as the cleaving agent to show the Young's modulus of glycocalyx on HUVECs is approximately 0.39kPa (Bai and Wang 2012).

The basis for the Young's modulus calculation is based on the equation reported by Hertz in 1882 (Hertz 1882). This theory refers to testing with contact mechanics on a curved surface. It is a well-established method for determining the Young's modulus through an AFM indentation test. In this project the Young's modulus was shown to be significantly different between the edge region and apical region on the HUVECs

membrane, cultured for 8 days to examine glycocalyx regeneration following cleaving. The results demonstrate that the growth of the glycocalyx is not equal across the whole cell membrane. The glycocalyx always develops from the edge region and then spreads out to the apical region of the HUVECs.

Some researchers have reported that the elastic properties of the cell were largely dependent on their thickness, including the cell thickness and the indentation depth, as well as the type of cantilever used. All of these research studies were based on the Hertz theory and assumed the glycocalyx is presented as an isotropic, homogeneous and linear elastic material (Bilodeau 1992, Dimitriadis, Horkay et al. 2002, Rico, Roca-Cusachs et al. 2005). At small depth of indentation compared to the total height of the cell, there will be an increasing possibility of error in the calculation of the elastic properties: this is because very small indentation depths imply a large strain on the tip of the cantilever as it is pushed upwards by the sample. To avoid this, the sensor should be carefully calibrated to apply an adequate constant force, sufficient to produce a useful indentation depth without rupturing the cell membrane.

Computational modelling would be one method for improving the Young's modulus calculation in future studies. The force-displacement curve can be reproduced by simulating the AFM indentation test using finite deformation models. The process of indentation could be recorded and re-presented through finite deformation modelling to provide corrections and empirical formulae, allowing much more accuracy in results for mechanical properties of the cell (Dimitriadis, Horkay et al. 2002, Kang, Wen et al. 2009).

This study investigates the distribution of the glycocalyx layer in vitro for different locations across time. It also provides some verification of the changes between healthy cells and those with damaged glycocalyx, elements of the results are directly relevant to research on vascular pathophysiology.

4. Effect of oscillatory flow on morphological change of endothelial cells

4.1. Introduction

It is established that the morphology and functions of endothelial cells are regulated by shear stress from blood flow and therefore, shear stress plays an important part in vascular regulation, remodelling and disease. The shear stress response of the endothelial cytoskeleton has been recognized as an important focus for research. MJ Levesque and RM Nerem demonstrated that endothelial cells elongate, then orient with the shear flow direction; that they become more elongated under higher shear stress; and that there is a strong correlation between the degree of alignment and the shape of the cell (Levesque and Nerem 1985). Merks *et al*. demonstrated that this elongation of the cell during remodelling is a key step in vasculogenesis towards stable vascular network growth (Merks, Brodsky et al. 2006). In a study by Arras *et al* using vasodilators or ligation of the femoral artery, it was demonstrated that increased shear stress for a period of 7–14 days could result in the formation of mature collateral vessels (Arras, Ito et al. 1998). However, very little research has examined the behaviour of endothelial cells under turbulent stress such as oscillatory shear flows.

Yao et al. demonstrated that intact glycocalyx was essential for cell alignment over 24h under shear stress stimulation (Yao, Rabodzey et al. 2007). Enzyme cleaving was therefore not undertaken for this part of the study.

4.2 Methodology

4.2.1 Design of the flow experiment

The schematic image in Figure 4.1 shows luminal (steady flow) shear stress stimulation via a parallel flow chamber. Hydrostatic pressure is created through the height difference between the two reservoirs which creates the flow of medium over the chamber from the high to the low reservoir. The flow circuit is completed by the peristaltic pump which pumps the experimental medium from the low to the high reservoir. A heater and thermostat (not shown in the schematic) maintain the culture medium and sample at a constant temperature of 37°C. As a closed loop system entirely under the hood for the whole duration, the experimental setup gives greater reliability for sterile conditions being maintained as compared to the AFM contact mode and tapping mode tests and this, together with the ability to maintain the sample temperature at 37°C, enables a longer duration for the experiment.

A control sample is kept in the incubator for the duration of the experiment.

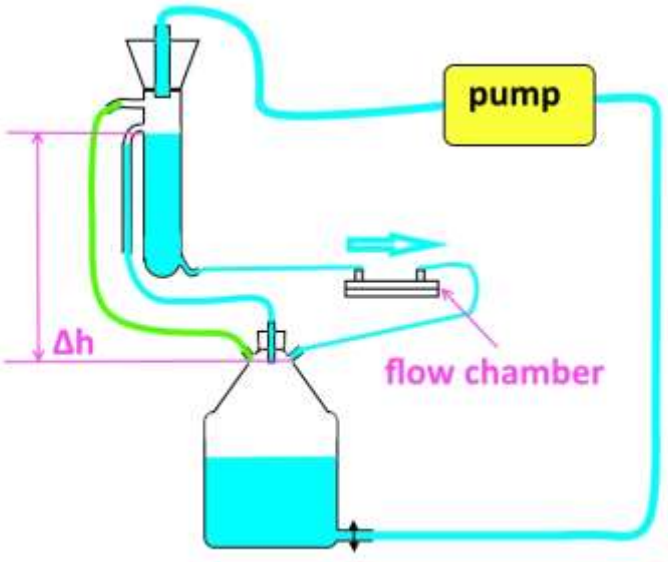

Figure 4. 1 *Schematic for steady flow stimulation.*

As shown in Figure 4.2, the custom made flow chamber is secured by rectangular aluminum rings, secured together with 6 screw fixings. The rings hold a 'sandwich' structure containing two slides of polymethylmethacrylate (PMMA), vertically spaced by a silicon gasket which creates a 0.2mm x 70mm x 20mm chamber that houses the cell culture in the flowing medium. A central depression in the lower PMMA plate houses two glass slides holding the HUVECs culture samples; the top of the sample slides sits flush with the level of the surface of the lower PMMA plate. The upper PMMA plate has two protrusions that extend into the empty space inside the upper aluminium ring to connect with rubber pipes that convey the medium from the upper reservoir, across the flow chamber and out to travel down to the lower reservoir.

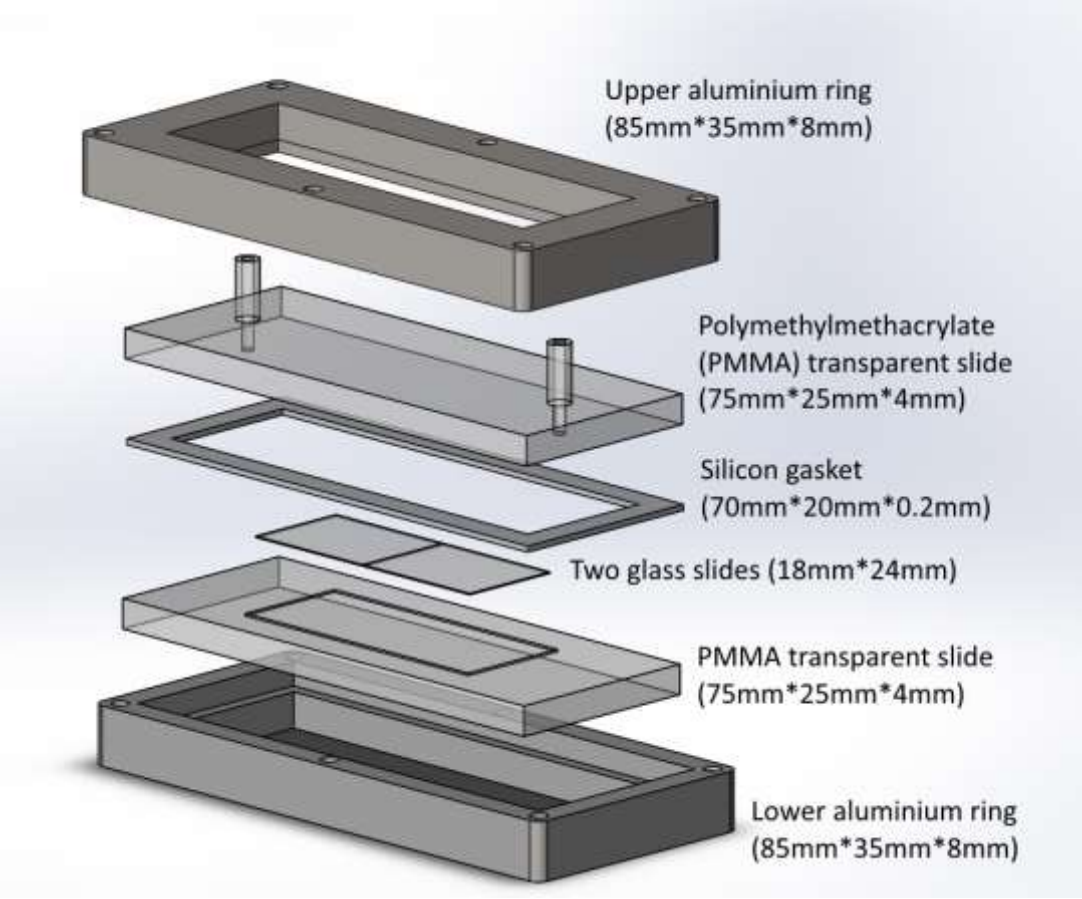

Figure 4. 2 *Structure of the flow chamber (expanded view).*

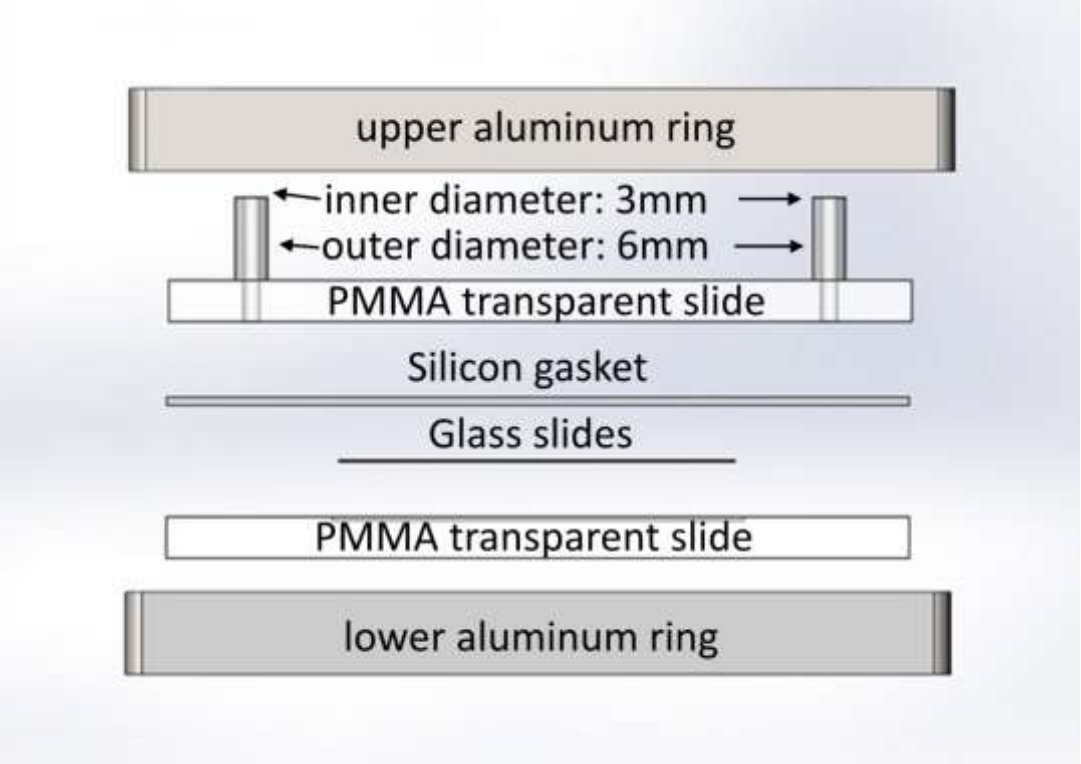

Figure 4. 3 *Structure of the flow chamber assembly (side view).*

The figure 4.3 shows a side view of the structure of the flow chamber assembly. The grey rectangle at the top is the upper aluminum ring, the clear rectangle below it is the upper PMMA transparent slide, next is the silicon gasket ring, two 18mm x 24mm glass slides with cultured HUVECs (cell sample facing up), the next item is the lower PMMA slide with a depression to house the glass slides, and at the base is the lower aluminum plate.

The fluid delivery system is set up as a closed loop using two reservoirs and a peristaltic pump. Culture medium in a medium reservoir is pumped out into a cylinder reservoir at a constant rate. The equilibrium between influx and efflux maintains a constant volume of medium in the cylinder reservoir, which results in a steady flow passing through the flow chamber. Finally, the medium is drained back into the media reservoir and recycled for the whole duration of the shear stress stimulation. As the dimensions of flow chamber are fixed, the flow rate (Q) across the flow chamber is determined by the height of the medium in the cylinder reservoir.

For the oscillatory shear stress stimulation part of the experiment, two syringe pumps are used, one on each side of the flow chamber and positioned at the same height. The flow chamber is exactly the same as that used in the steady flow stimulation. Since the syringes are connected in a closed system, this maintains an equal amount of experimental medium pumped in and out of the flow chamber. A heater and thermostat ensures the sample and medium is kept at a constant temperature of 37°C. As before, a control sample is maintained in the incubator for the duration of the experimental procedure. Again, as a closed loop system entirely under the hood for the whole duration, the experimental setup gives greater reliability for sterile conditions being maintained as compared to the AFM contact mode and tapping mode tests and this, together with the ability to maintain the sample temperature at 37°C, enables a longer duration for the experiment.

The process of oscillatory flow stimulation is shown schematically below (figure 4.4).

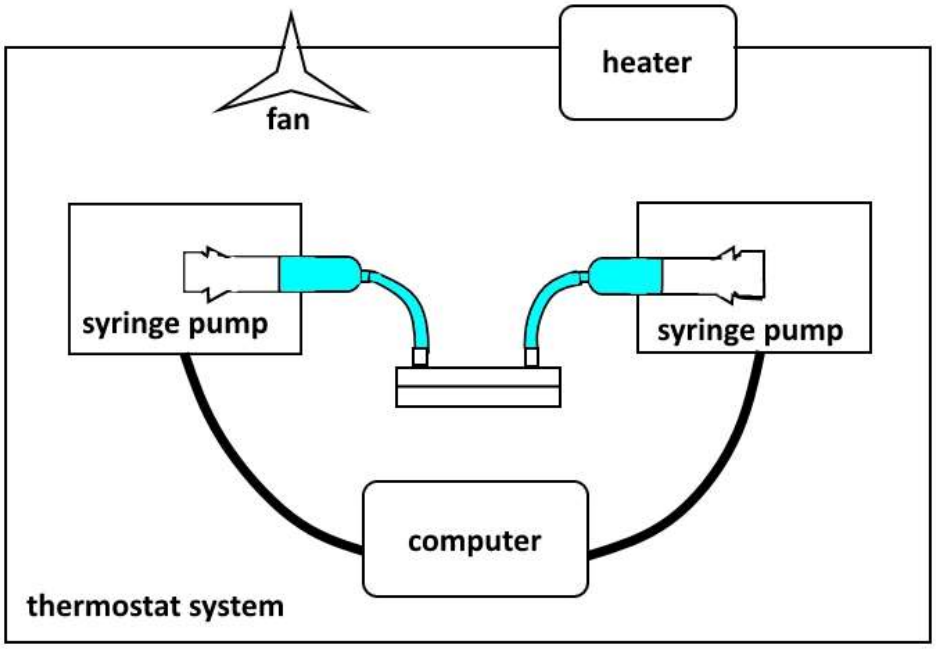

Figure 4. 4 *Schematic diagram for oscillatory flow stimulation.*

4.2.2 Preparation of experiment

Table 4.1 shows the components for the flow chamber experiment assembly.

Product	Company
Polymethylmethacrylate (PMMA) Sheet	Goodfellow
Cellulose Acetate Film	Goodfellow
Masterflex® Variable-speed drive	Cole Parmer
Masterflex® Pump Head	Cole Parmer
Masterflex® platinum-cured silicone tubing (L/S 16)	Cole Parmer
Polytetrafluoroethylene (PTFE) plate	RS
Silicone Grease	RS
Platinum electrode wire (0.2mm thick)	Fisher Scientific
Stainless steel plates	SEMS-QMUL
Acrylonitrile butadiene styrene (ABS) bridge	SEMS-QMUL
Glass reservoirs	SEMS-QMUL
Syringe pump	Next Advance
BD™ Hypodermic Syringe only	BD

Table 4. 1 *Equipment and materials for the flow chamber experiment assembly.*

The plate used to construct the flow chamber is made of Poly (methyl methacrylate) (PMMA). PMMA is a transparent thermoplastic so it has a low melting point (160 °C) and high transparency (95%). The glass transition temperature of PMMA has a range from 85 °C to 165 °C. In summary, a high temperature environment will deform the PMMA so sterilization is undertaken via exposure to UV light for 1 hour. The glass reservoirs, silicone tubing and stainless steel plates are autoclaved for 20 mins at 121 °C in order to achieve sterilization.

4.2.3 Calculation of the shear stress

Depaola et al. provide an equation to determine the shear stress between parallel plates (DePaola, Gimbrone et al. 1992).

$$\tau = \frac{6\mu Q}{Wh^2}$$

where

- τ is the shear stress (dyn/cm^2),
- μ is the viscosity of experimental culture medium, in this case 0.0084 (Pa*s) in 37°C,
- Q is the flow rate (ml/s),
- W is the channel width, 20mm for the custom-made chamber (mm),
- h is the height of the channel, 0.2mm for this silicon gasket (mm).

The height differential between the reservoirs corresponds to the flow rate, Table 4.2 shows shear stresses calculated from different height differentials.

Height differential, H (cm)	Flow rate, Q (cm^3/s)	Shear stress, τ (dyn/cm^2)
5	0.038	2.394
10	0.088	5.544
15	0.132	8.316
20	0.185	11.655
25	0.227	14.301

Table 4. 2 *Shear stress calculations for the steady flow section of the experiment.*

The linear plotting in Figure 4.5 shows the relationship between the height difference for two reservoirs and the shear stresses.

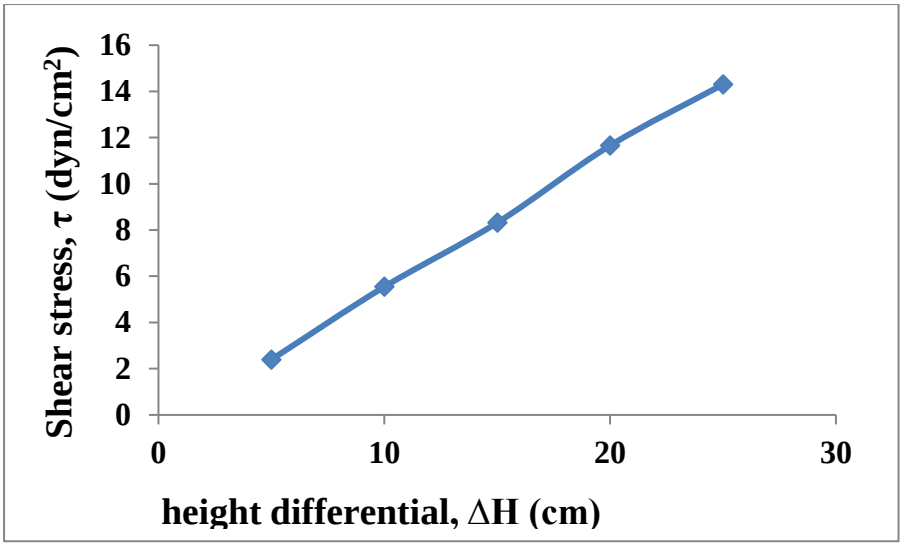

Figure 4. 5 *The relationship between height differential for two reservoirs and shear stress.*

The flow rate for oscillatory stimulation is given by the size of the syringe and the velocity of pumping of the medium. In this experimental setup, the flow rate for oscillatory stimulation is 0.2 ml/s, giving a shear stress of 12.6 dyn/cm2. Therefore, in the steady flow stimulation experiment, the equipment is set to give a matching shear stress of 12.6 dyn/cm2, i.e. the height differential of 22cm between the two reservoirs.

4.2.4 Shear stimulation of HUVECs

HUVECs are cultured on glass cover slips for 8 days then exposed to a shear stress of 12.6 dyn/cm^2. The base culture medium used in the experiment is buffered with Sodium Phosphate dibasic (Na_2HPO_4-$7H_2O$) and Potassium Phosphate monobasic (KH_2PO_4) for pH maintenance. This means that 5% CO_2 is not required for the process.

4.3 Results

Images were acquired at the outset of the experiment and after 5h of shear stress application (constant or oscillatory), with images also taken of control samples at the same times. ImageJ software was used to trace around the perimeter of each cell in the samples, and the software then automatically calculated the:

- area
- perimeter length
- angle of orientation
- aspect ratio

for each cell.

4.3.1 Steady flow stimulation

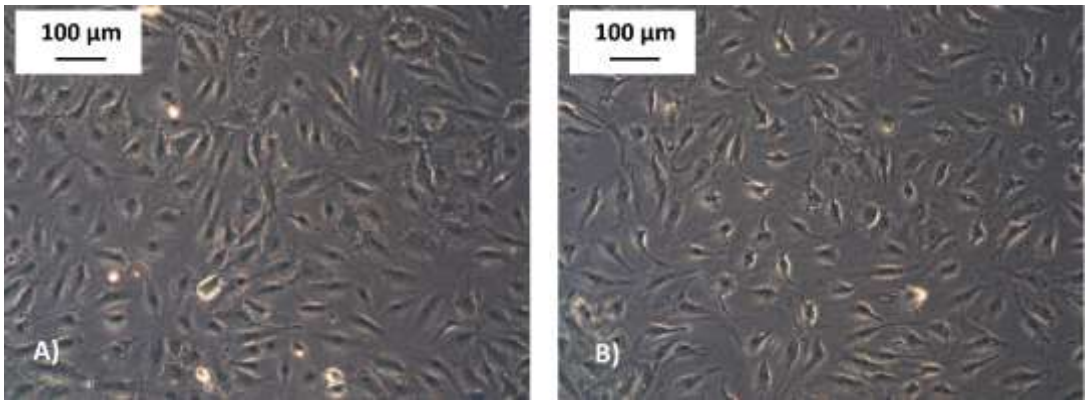

Figure 4. 6 *Microscope images for 5 hrs' luminal flow stimulation.*

A) Control: HUVECs cultured on glass cover slides in static medium (no flow applied). B) HUVECs cultured on glass cover slides with steady flow (luminal) shear stress applied.

Unidirectional shear stress may be experienced in straight blood vessels, but in areas of complexity such as branching regions, turbulent and oscillatory shear stress occurs and these areas are known to be important to an understanding of angiogenesis as well as pathology. Oscillatory shear stress is characterized by significant changes in direction, as well as magnitude.

The Figure 4.6 shows a comparison between cells' location in a control sample under static medium and a sample under application of 5hrs' luminal (steady flow) shear stress. There is no significant change between them. However, Figure 4.7 (below) shows a clear change between the control cells in static medium and the sample under luminal flow for 24 hours. All the cells have elongated along the axis of luminal flow.

As noted in the Review of Literature, cells elongate and orient along the axis of shear flow, whereas in static medium they orient randomly. This reorientation reduces the intracellular stresses resulting from the change in morphology under hydrodynamic stress: in a computational fluid dynamics simulation conducted by Barbee *et al*., peak surface stress and stress gradients were demonstrated to be reduced by cellular alignment with the direction of flow (Barbee 2002).

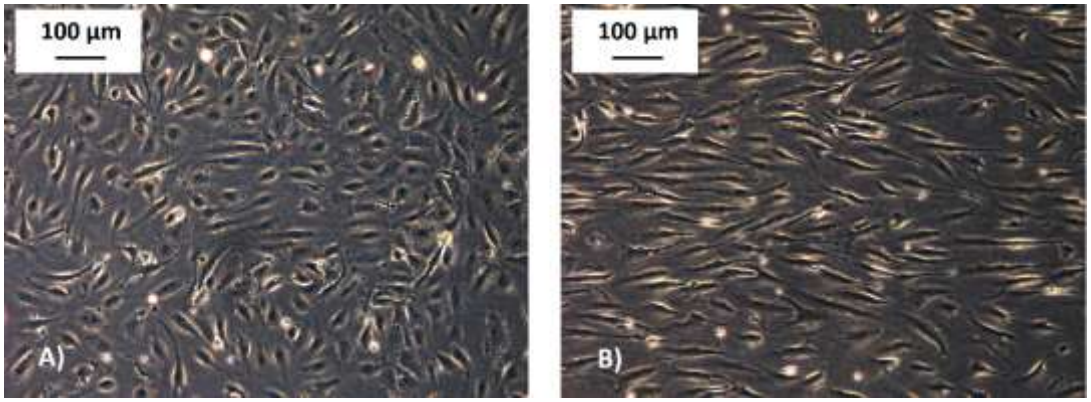

Figure 4. 7 *Microscope images for 24 hrs' luminal flow stimulation.*

A) Control: HUVECs cultured on glass cover slides in static medium (no flow applied). B) HUVECs cultured on glass cover slides with steady flow (luminal) shear stress applied.

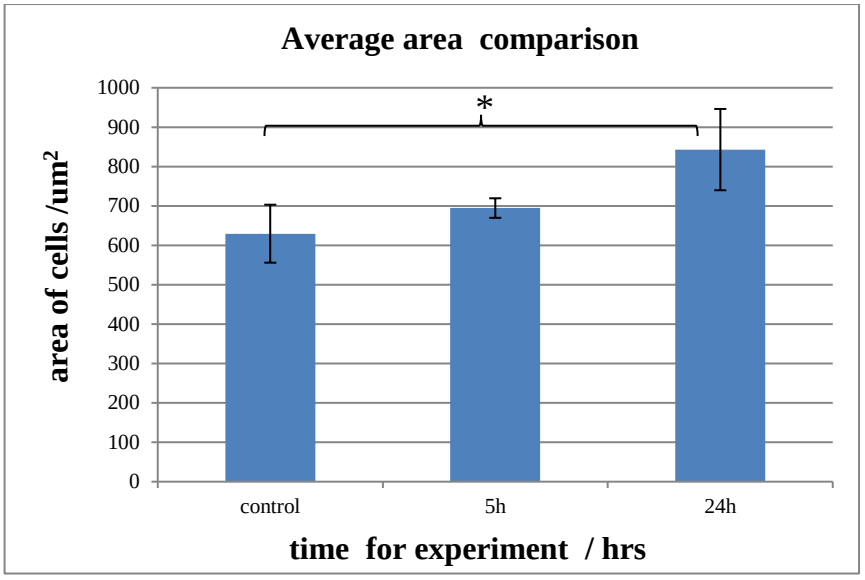

Figure 4. 8 *Chart showing average cell areas, analyzed using ImageJ for different timescales of luminal shear stress application.*

Data analysis of the HUVECs samples using ImageJ shows the difference between samples. The average area of the cells increased significantly over 5hrs' duration and then increased significantly again over 24hrs' duration of shear stress, from 630µm² for the control sample of cells (in static medium) to 695µm² for the sample with 5hrs' luminal flow applied, then to 843µm² for the sample with 24 hrs' luminal flow applied.

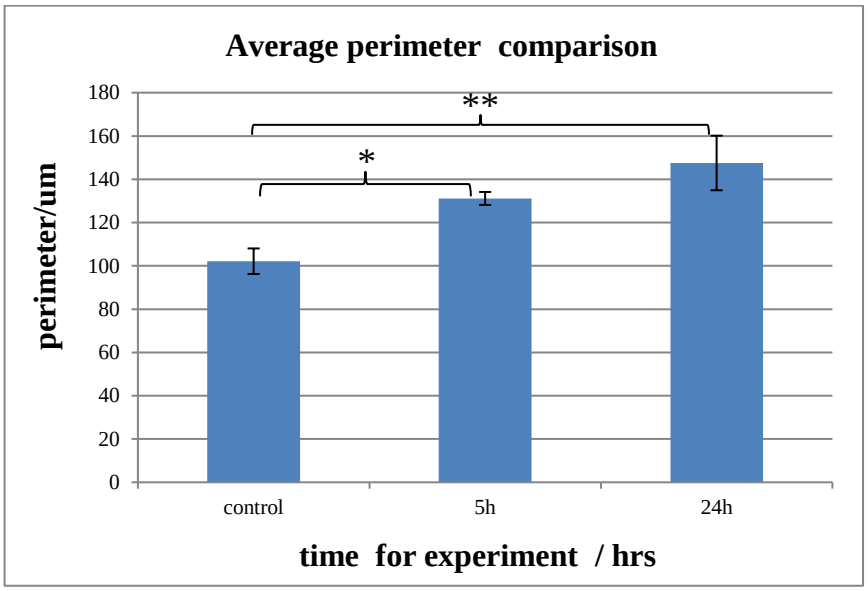

Figure 4. 9 *Chart showing average cell perimeters, analyzed using ImageJ for different timescales of luminal shear stress application.*

Data analysis of the HUVECs samples using ImageJ demonstrates a progressive increase in average perimeter, from 102µm for the control sample cells (static flow applied) to 131µm for the cells with 5 hours' luminal flow applied, reaching 147µm for the cells with 24 hours' luminal flow applied.

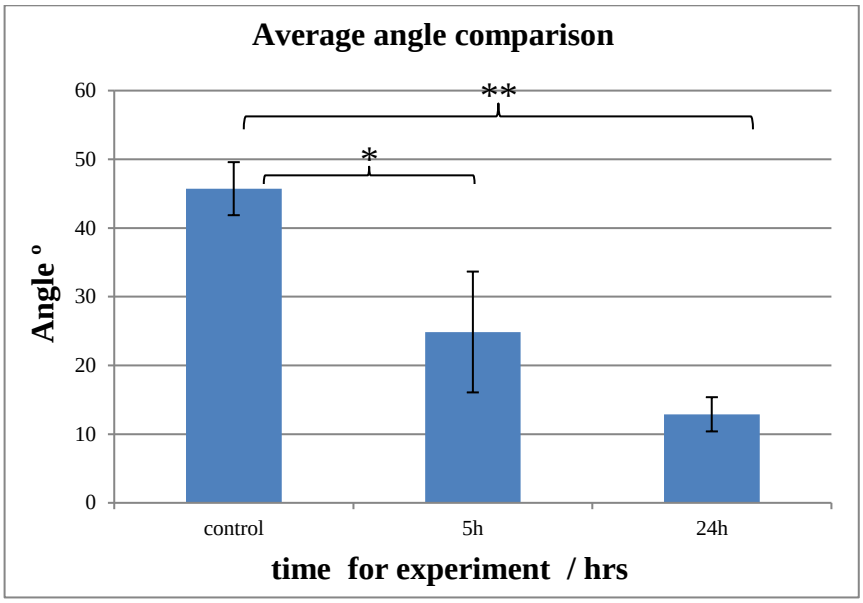

Figure 4. 10 *Chart showing average change in angle of orientation of the cell, analyzed using ImageJ for different timescales of luminal shear stress application*

ImageJ calculates the angle between the orientation of the cell's longitudinal axis and the direction of flow. The smaller the angle, the more nearly parallel the cells are to the direction of flow. Any angles computed by the software at >90% are reduced by a value of 90%, so that no obtuse angles are reported.

The change in the average angle demonstrates the average change in orientation of the cells over the period of the experiment. In this luminal flow experiment, the average angle decreased over time from a control of 46◦ (static medium) to 25◦ (5 hours' luminal flow applied), and subsequently to 13◦ (24 hours' luminal flow applied). That is, the cells were observed to orient themselves towards the direction of flow.

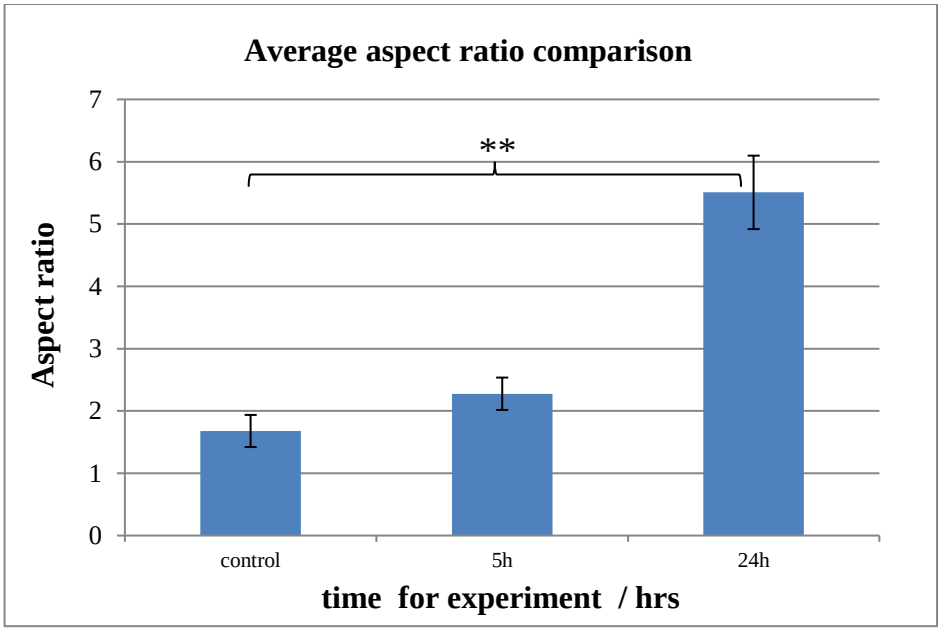

Figure 4. 11 *Chart showing average change in aspect ratio of the cell, analyzed using ImageJ for different timescales of luminal shear stress application*

The aspect ratio is the ratio of length to width of the cell. The value of the average aspect ratio in this experiment increased slightly from 1.68 (control sample in static medium) to 2.28 (sample with 5 hours' luminal flow applied) and continued to increase substantially to 5.51 (sample with 24 hours' luminal flow applied). The change after 5hrs is not considered to be significant whereas after 24hrs' stimulation there is a significant increase in the elongation of the cell, a measure which has been shown to be a key factor in cell remodeling and vasculogenesis.

4.3.2 Oscillatory flow stimulation

It is known that oscillatory shear stress is associated with atherogenesis and its negative effects on the vascular system, as well as with angiogenesis (the formation of new vessels). This part of the study attempts to build on existing research by providing a comparative study for cell morphology and reorientation under oscillatory shear stress, with a control sample being maintained under static conditions.

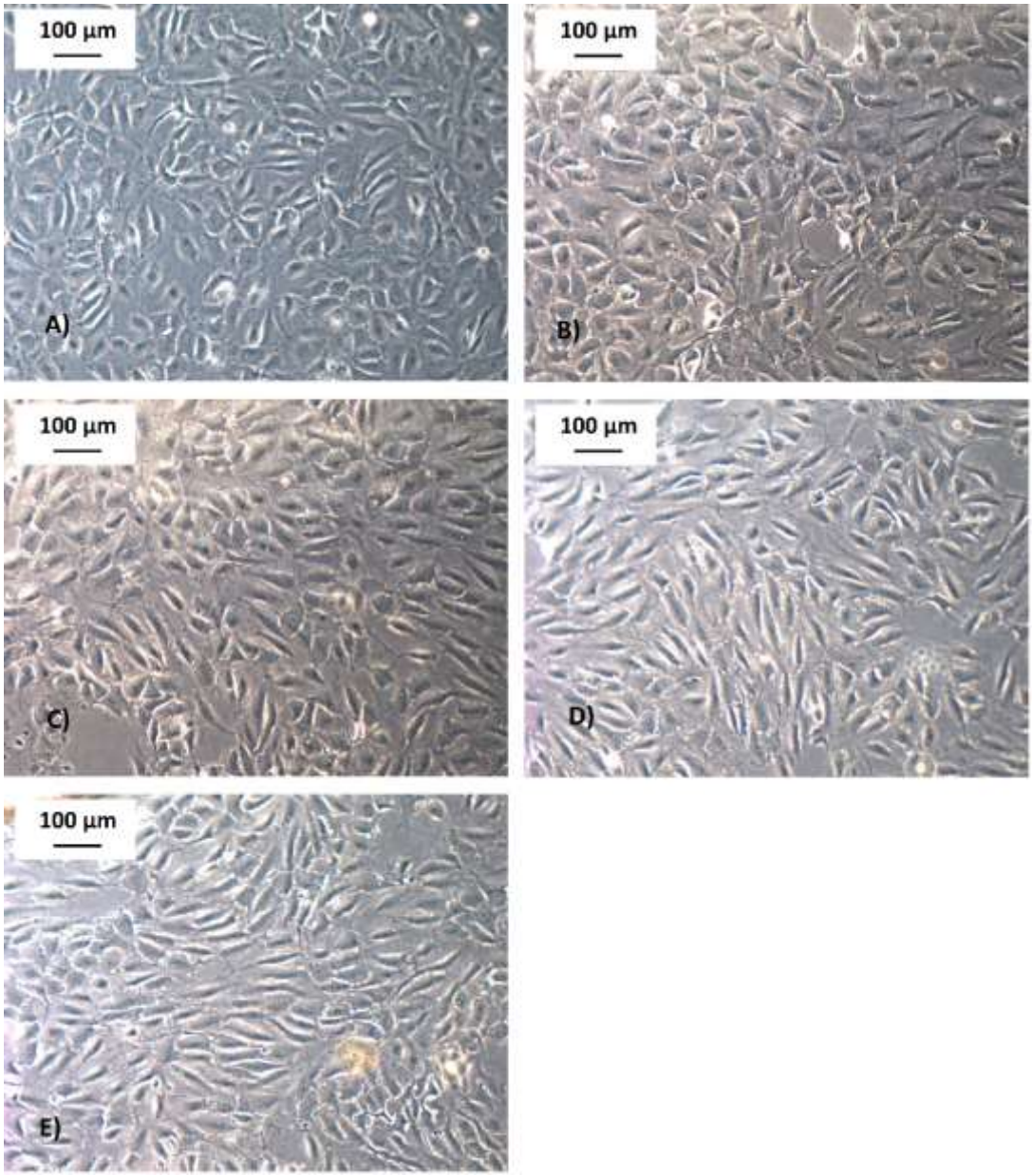

Figure 4. 12 *Microscope images for 5 hrs' oscillating flow stimulation experiment.*

A) Control sample: HUVECs cultured on glass slides in static medium (no flow applied). B), C), D), E): HUVECs cultured on glass slides with 5 hours' oscillatory shear stress applied, at B) oscillatory reversal time 5s, C) oscillatory reversal time 10s. D) oscillatory reversal time 15s, E) oscillatory reversal time 20s.

The figure above shows the morphology of HUVECs with, and without, oscillatory shear stress applied for 5 hrs' duration. The experimental control group sample of cells from the same culture batch is kept in the incubator in medium (i.e. static, no flow). The images show limited changes between the control group and the samples that have been exposed to oscillatory flows at increasing reversal times.

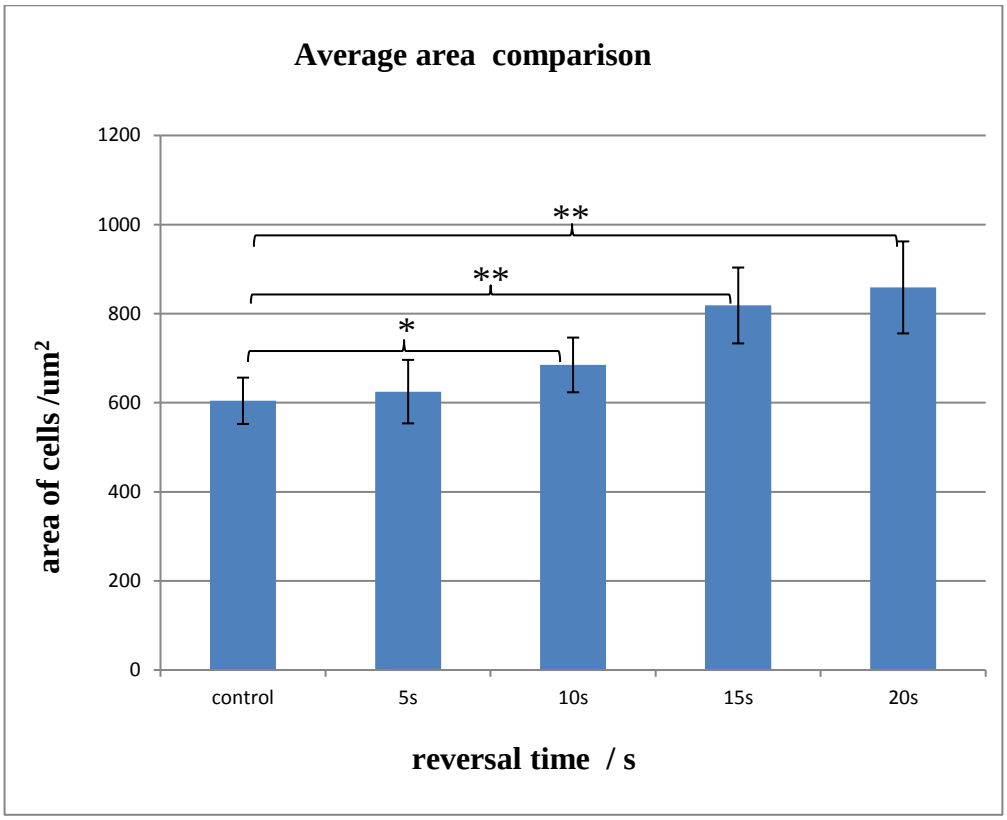

Figure 4. 13 *Chart showing change in average area of the cell, analyzed using ImageJ for different reversal timescales of oscillatory shear stress (5 hrs' experimental duration).*

The average area values calculated by the ImageJ software are 604µm² (control sample incubated in static medium for 5h), 625µm² (sample exposed to oscillatory shear stress for 5hrs at a 5s reversal time), 685µm² (10s reversal time), 818µm² (15s reversal time) and 859µm² (20s reversal time). There is a linear relationship between the increase in average area and the increase in reversal time of the oscillatory flow. The larger size of the cells results from the longer time of the reversal time for the experiment. The shear stress is 12.6 dyn/cm^2, the force applied by the shear is hypothesized to push the cell cytoplasmic spread out and increase the size of cells.

At 20 seconds' flow reversal time, no significant change was observed as compared to the samples exposed to 15 seconds' flow reversal time.

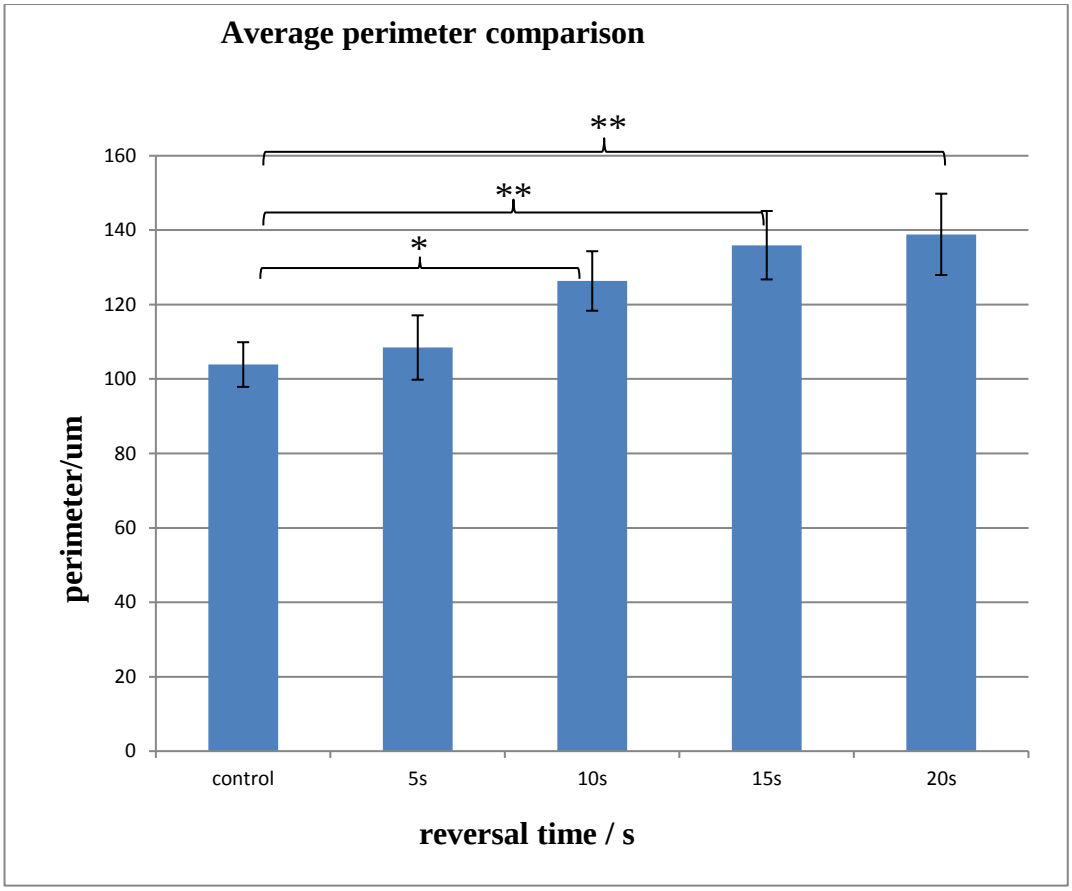

Figure 4. 14 *Chart showing change in average perimeter of the cell, analyzed using ImageJ for different reversal timescales of oscillatory shear stress (5 hrs' experimental duration).*

The average perimeter increases from 104µm (control sample incubated in static medium for 5hrs), 108µm (sample exposed to oscillatory shear stress for 5hrs at a 5s reversal time), 126µm (10s reversal time), 136µm (15s reversal time) and 139µm (20s reversal time). These values clearly demonstrate the morphological limit of the cell perimeter, because the perimeter increases with the reversal time for the oscillatory shear stress, but in the increase between 15s and 20s of reverse time is insignificant: it may be considered that this is the limit of the perimeter of the cells under oscillatory shear stress.

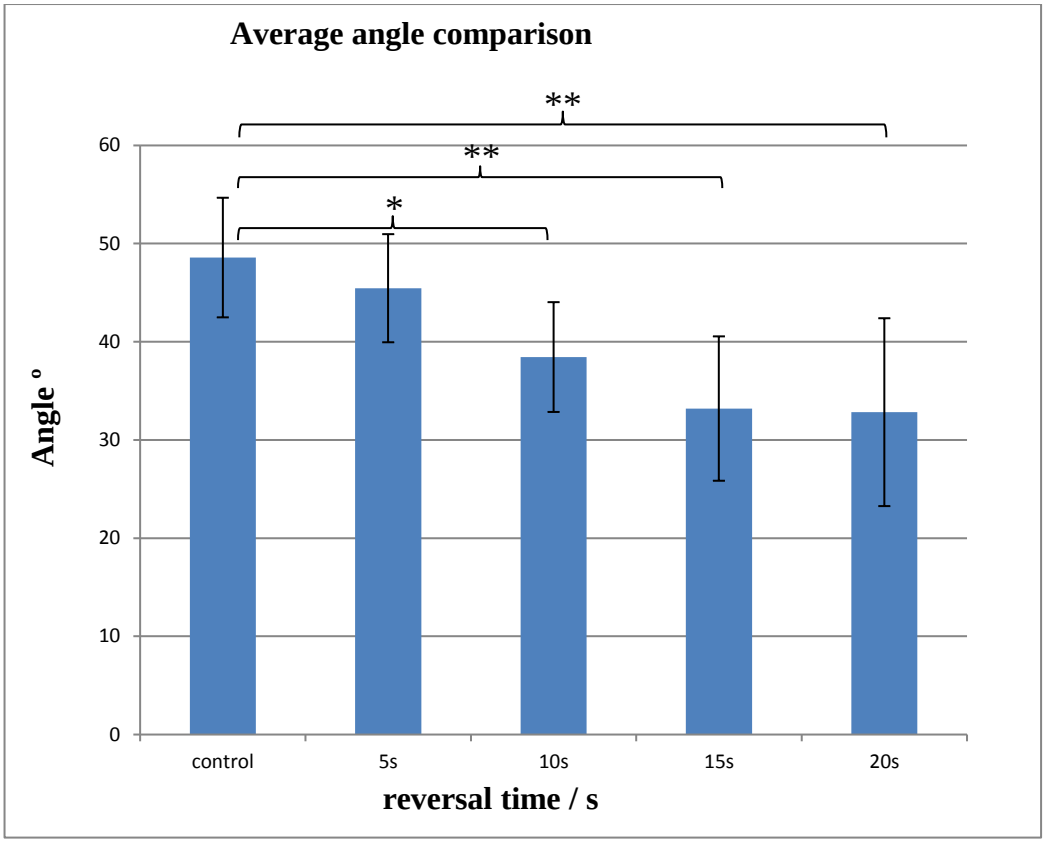

Figure 4. 15 *Chart showing change in average angle of cell orientation, analyzed using ImageJ for different reversal timescales of oscillatory shear stress (5 hrs' experimental duration).*

ImageJ calculates the angle between the orientation of the cell's longitudinal axis and the direction of flow. The smaller the angle, the more nearly parallel the cells are to the direction of flow. Any angles computed by the software at >90% are reduced by a value of 90%, so that no obtuse angles are reported.

The change in the average angle demonstrates the average change in orientation of the cells over the period of the experiment. The values calculated for the average angle of orientation of the cells decrease from 48.6° (control sample incubated in static medium), 45.5° (sample exposed to oscillatory shear stress for 5hrs at a 5s reversal time), 38.4° (10s reversal time), 33.2° (15s reversal time) and 32.8° (20s reversal time). These cells all orient closer to the oscillating flow direction, as shown by decreasing values for the angle, the as reversal time increases. However, the effect produced under oscillatory flow was smaller than in the steady flow

experiment where cells realigned from an average angle in the control sample of 46° (static medium) to 25° (5 hours' laminar flow applied),

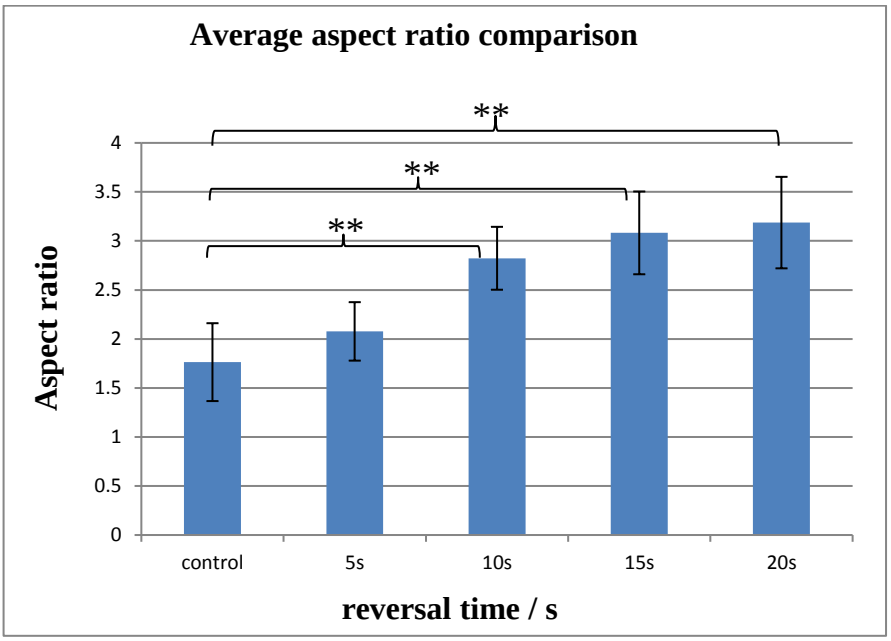

Figure 4. 16 *Chart showing change in average aspect ratio of cell, analyzed using ImageJ for different reversal timescales of oscillatory shear stress (5 hrs' experimental duration).*

From the data analysis through ImageJ, the values of the aspect ratio changes from 1.76 (control sample incubated in static medium), to 2.08 (sample exposed to oscillatory shear stress for 5hrs at a 5s reversal time), 2.82 (10s reversal time), 3.08 (15s reversal time) and 3.19 (20s reversal time). All the values show the elongation of the cells after oscillatory shear stress is applied. The shear stress operating from two opposite directions does not pull the cells together, as might be hypothesized; the cytoplasm is not compressed by the oscillating flow. The opposite effect is observed: the cells elongate through the flow direction with the increased reversal time of oscillatory shear stress. The observed change in aspect ratio is greater under 5 hrs' oscillatory flows of 10s, 15s and 20s reversal times than the previous experiment under 5 hrs' steady (luminal) flow, where the average aspect ratio value increased only slightly from 1.68 (control sample in static medium) to 2.28 (sample with 5 hours' luminal flow applied). In the very turbulent flows with 5s reversal time, the change in aspect ratio actually decreased as compared to the luminal flow experiment.

The experiment under oscillatory flow conditions for 5 hrs' duration clearly shows changes in cell morphology as compared to luminal (steady) flow conditions for 5 hrs, where changes were not significant compared to the control in static medium. As the reversal time of the oscillatory flow increases, the changes – increase in area; increase in perimeter; orientation towards the direction of the flow; and increase in aspect ratio as the cell elongates - become more pronounced up to 15s reversal time. Between 15s and 20s, no significant change was observed.

The reason is hypothesized to be the difference between the types of flow. Comparable shear stress is applied in both cases, but under oscillatory flow conditions, where flows act from different directions in a more turbulent manner, it is believed that the cytoskeletal structures are more likely to be broken, and temporary or permanent structures formed to stabilize the cell against the shear stress. As the protein structures in the cytoskeleton break and new stress fibres are formed, this gives rise to more movement.

Relevantly for this research, the Thi *et al*. team observed that endothelial cells in regions of high shear stress gradient experience more significant junctional disruption than those in regions under uniform shear stress (Thi, Tarbell et al. 2004). This may be as a result of cell–cell inability to stabilize and establish steady-state adhesion, and permanent contact inhibition, under high shear stress gradients, as discussed in section 1.4.3, Mechanotransduction.

The next focus of the experiment is to extend the time under oscillatory shear stress stimulation from 5hrs to 24hrs. Here the experiment compared 5s, 10s and 15s reversal times, since the change between 15s and 20s in the previous experiment was not judged to be significant.

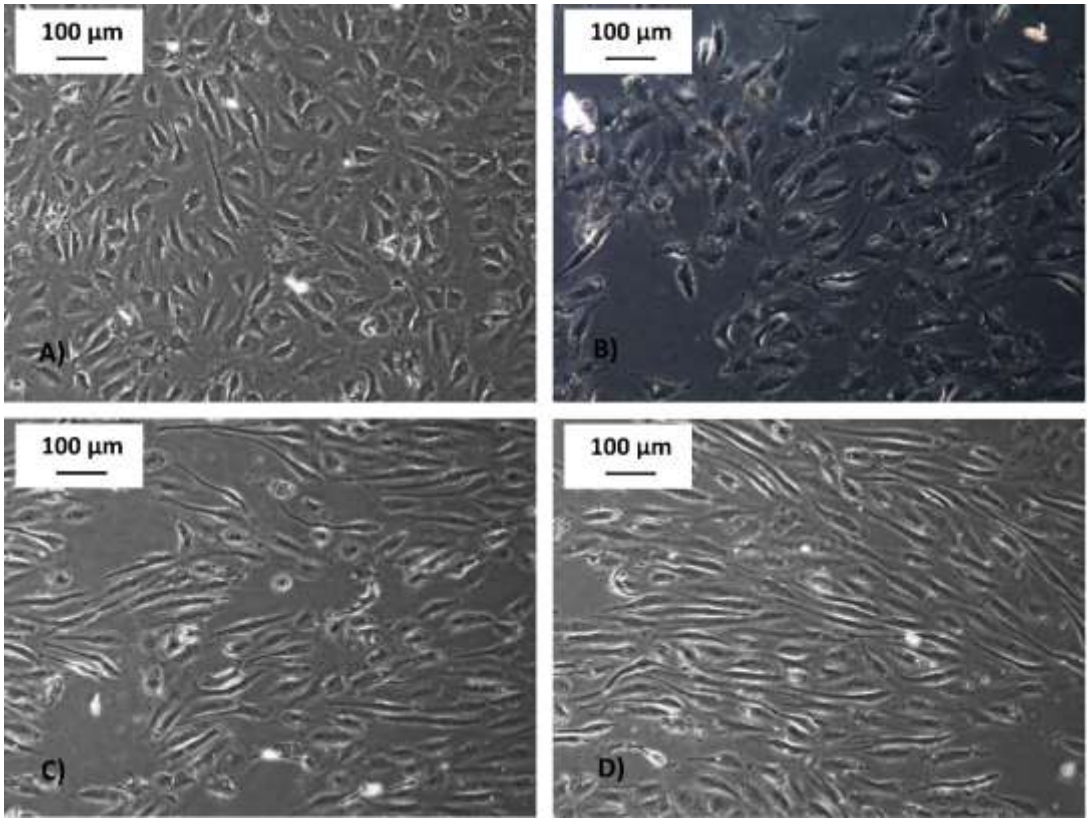

Figure 4. 17 *Microscope images for 24 hrs' oscillating flow stimulation experiment.*
A) Control sample: HUVECs cultured on glass slides in static medium (no flow applied). B), C), D): HUVECs cultured on glass slides with 5 hours' oscillatory shear stress applied, at B) oscillatory reversal time 5s, C) oscillatory reversal time 10s. D) oscillatory reversal time 15s.

The figure above shows the microscope image for cells exposed to oscillating flow for 24 hours with different reversal times of 5s, 10s, and 15s, against a control maintained in the incubator in static medium for the same duration. The results show significant evidence of change compared with the control group in static medium. Particularly in the image from experiments with 10s and 15s reverse time, the cells elongate with the flow direction, similar to the experiment under luminal flow applied for 24 hrs. This demonstrates that over a 24 hour duration, oscillating flow conditions have an effect on cells similar to that of luminal flow conditions. The percentage of dying or dead cells under oscillatory flows is higher than under luminal flow, as observed from the size and number of empty areas on the images.

Endothelial realignment under shear stress also gives rise to decreases in cell membrane elasticity, i.e. increased resistance to deformation (Sato, Katano et al.

2001). This will be demonstrable from measurements of the Young's modulus of cells following shear stress stimulation. A study by Kemeny *et al.* demonstrated that the loss of elasticity arose from a rigid realignment of the cortical cytoskeleton beneath the surface cell membrane, and observed longitudinal ridge features under AFM (Kemeny, Figueroa et al. 2011).

The results of ImageJ computations for the 24 hrs oscillatory flow experiment are presented below.

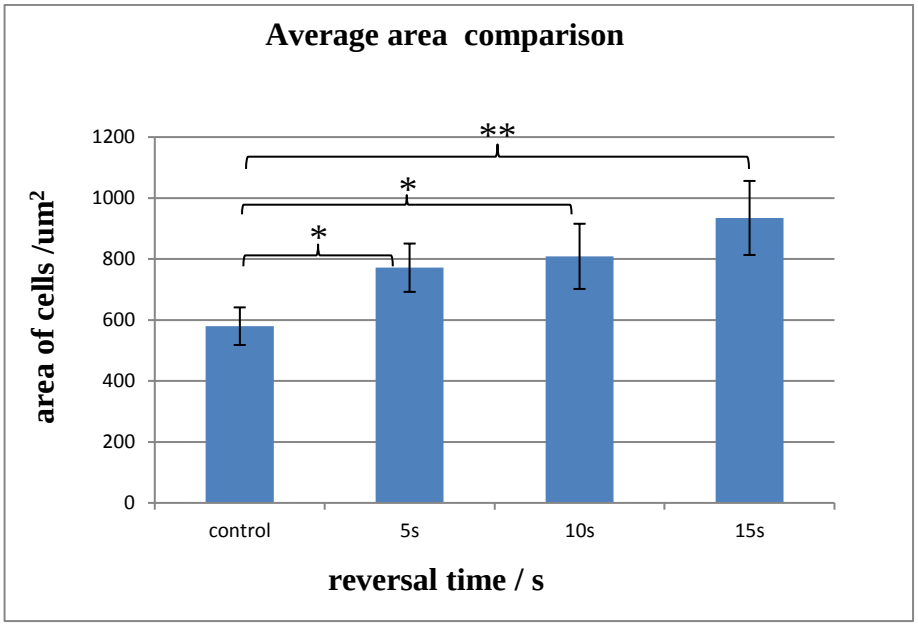

Figure 4. 18 *Chart showing change in average area of the cell.*

Analyzed using ImageJ for different reversal timescales of oscillatory shear stress (24 hrs' experimental duration).

Data analysis through ImageJ, as shown in Figure 4.18, shows that the average cell area value increases under oscillatory shear stress from 580µm² (control in static conditions for 24h) to 772µm² (sample exposed to oscillatory shear stress for 24hrs at a 5s reversal time), 809µm² (10s reversal time), and 935µm² (15s reversal time). The average area increase grows as the reverse time of the oscillatory shear stress increases. The values are also larger than the experiment under the same conditions but for the shorter duration of 5 hours.

Under a shear stress of 12.6 dyn/cm^2, the force applied by the shear on the cell induces the cytoplasm to spread out and increase the cell size. With increasing experimental time, increased force is exerted on the cells producing a larger increase in the cell area.

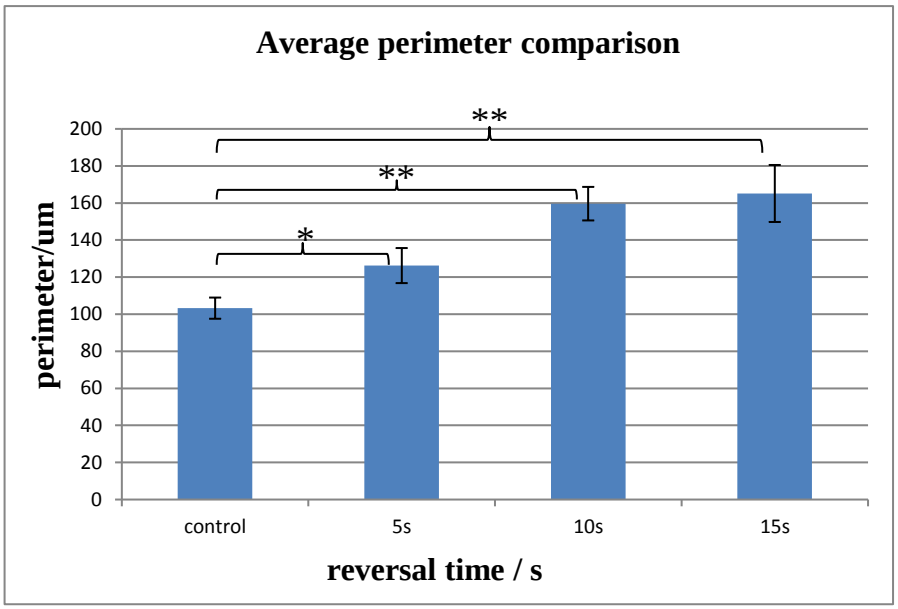

Figure 4. 19 *Chart showing change in average perimeter of the cell.*

Analyzed using ImageJ for different reversal timescales of oscillatory shear stress (24 hrs' experimental duration).

Data analysis through ImageJ, as shown in Figure 4.19, shows that the average perimeter value for the cells increases under oscillatory shear stress from 103µm (control sample under static conditions for 24h) to 126µm (sample exposed to oscillatory shear stress for 24hrs at a 5s reversal time), 160µm (10s reversal time) and 165µm (15s reversal time). There is a significant increase to the perimeter between static flow conditions and 5s reversal time, and another significant increase between 5s and 10s. No further significant change to the perimeter takes place between reversal times of 10s and 15s.

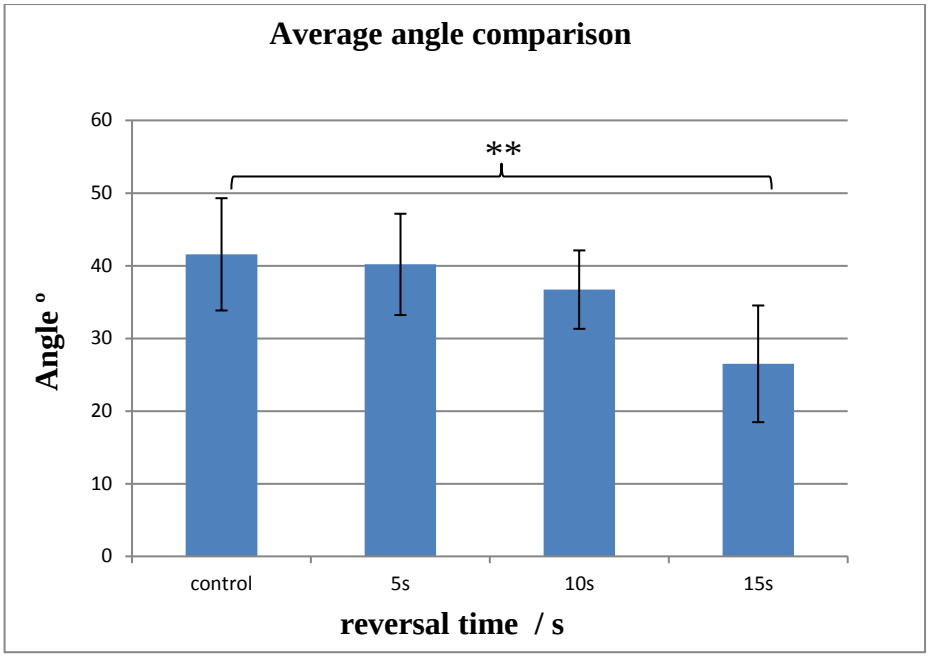

Figure 4. 20 *Chart showing change in average angle of orientation of the cell.*

Analyzed using ImageJ for different reversal timescales of oscillatory shear stress (24 hrs' experimental duration).

ImageJ calculates the angle between the orientation of the cell's longitudinal axis and the direction of flow. The smaller the angle, the more nearly parallel the cells are to the direction of flow. Any angles computed by the software at >90% are reduced by a value of 90%, so that no obtuse angles are reported.

The change in the average angle demonstrates the average change in orientation of the cells over the period of the experiment. The values calculated for the average angle of orientation of the cells are 41.6° (control sample under static conditions for 24h), 40.2° (sample exposed to oscillatory shear stress for 24hrs at a 5s reversal time), 36.7° (10s reversal time) and 26.5° (15s reversal time). Comparing this with the strength of the reorientation observed under 5hrs' oscillatory flow, from 48.6° (control sample incubated in static medium), 45.5° (sample exposed to oscillatory shear stress for 5hrs at a 5s reversal time), 38.4° (10s reversal time), and 33.2° (15s reversal time) it is clear that the reorientation process has increased over time from 5hrs to 24hrs.

It is demonstrated that the alignment of the cells towards the direction of flow continues in oscillating flows: and that the alignment motion increases as the oscillatory reversal time rises. The realignment under oscillatory flow of either duration is weaker than that seen previously in the steady flow experiment, where the cells exposed to luminal flow for 24 hrs realigned from an average angle of 46° to 13°.

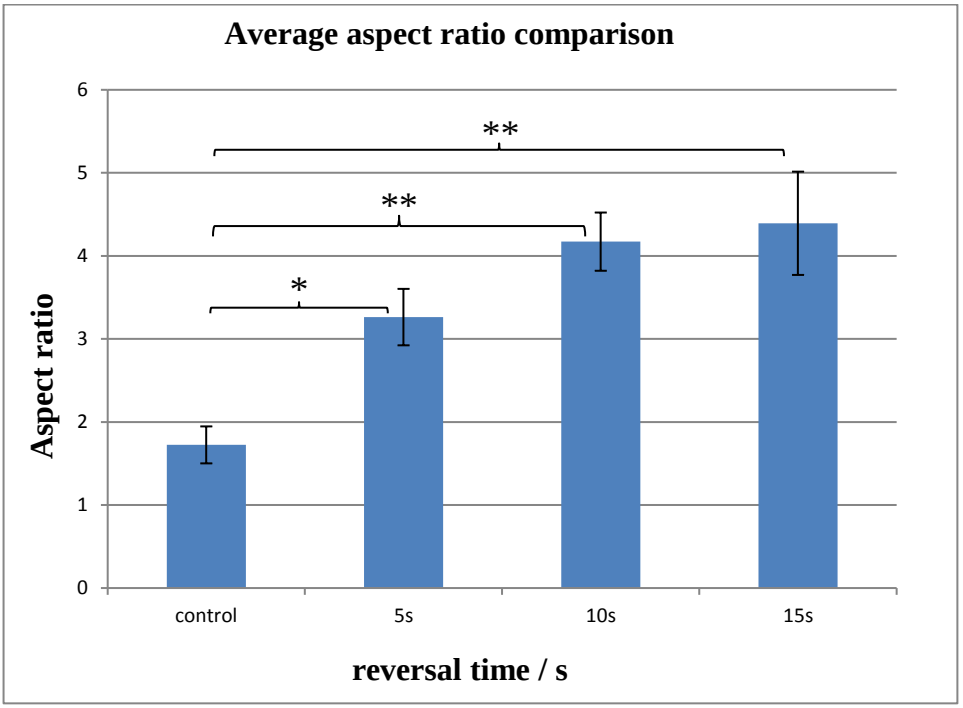

Figure 4. 21 *Chart showing change in average aspect ratio of the cell.*

Analyzed using ImageJ for different reversal timescales of oscillatory shear stress (24 hrs' experimental duration).

From the data analysis through ImageJ, the values of the aspect ratio are 1.72 (control sample under static conditions for 24h), 3.26 (sample exposed to oscillatory shear stress for 24hrs at a 5s reversal time), 4.17 (10s reversal time) and 4.39 (15s reversal time). All the cells elongate significantly after oscillatory shear stress is applied for 24 hours: even those in the very turbulent flows with 5s reversal time. The elongation is greater than that shown in the 5hrs oscillatory flow experiment, where the values of the aspect ratio changed from 1.76 (control sample incubated in static medium), 2.08 (sample exposed to oscillatory shear stress for 5hrs at a 5s

reversal time), 2.82 (10s reversal time), 3.08 (15s reversal time). However, none of the aspect ratio changes under oscillatory shear stress, of any duration, matched the size of the change seen under steady (luminal) flow, where an aspect ratio of 5.51 was seen after 24 hrs.

An increase in flow reversal time means that the shear stress acts in a laminar manner on the cells for a longer timeframe (in each of the two directions) after the initial severe turbulence at the change of direction has reduced. Technically, as the reversal time increases, the mode of force approaches more closely to laminar flow: note that if the period of reversal time is infinity, then the oscillatory flow becomes a laminar flow. Under the conditions tested, however, the cell samples are exposed to turbulence and to two laminar flows from opposing directions, rather than to unidirectional flow. The oscillatory shear stimulation part of the experiment demonstrates that these conditions give rise to some distinct changes when compared to cells under unidirectional laminar flow. This difference is understood to be potentially significant, since *in vivo* this type of turbulence in flow is experienced particularly in vascular sites which are most at risk of arterial disease.

A change to the elasticity of the cell membrane is hypothesized alongside the change in aspect ratio after 24 hrs' oscillatory shear stress. In a further test, indentation via AFM is used to determine the Young's modulus for cells after 24 hrs' oscillatory shear stress. Differences in the Young's modulus of HUVECs samples were measured in response to an oscillatory shear stress of varying reversal time, for 24 hours at 12.6 dyn/cm^2. Due to the growth and recovery of the glycocalyx layer, glycocalyx removal is not considered necessary for this project.

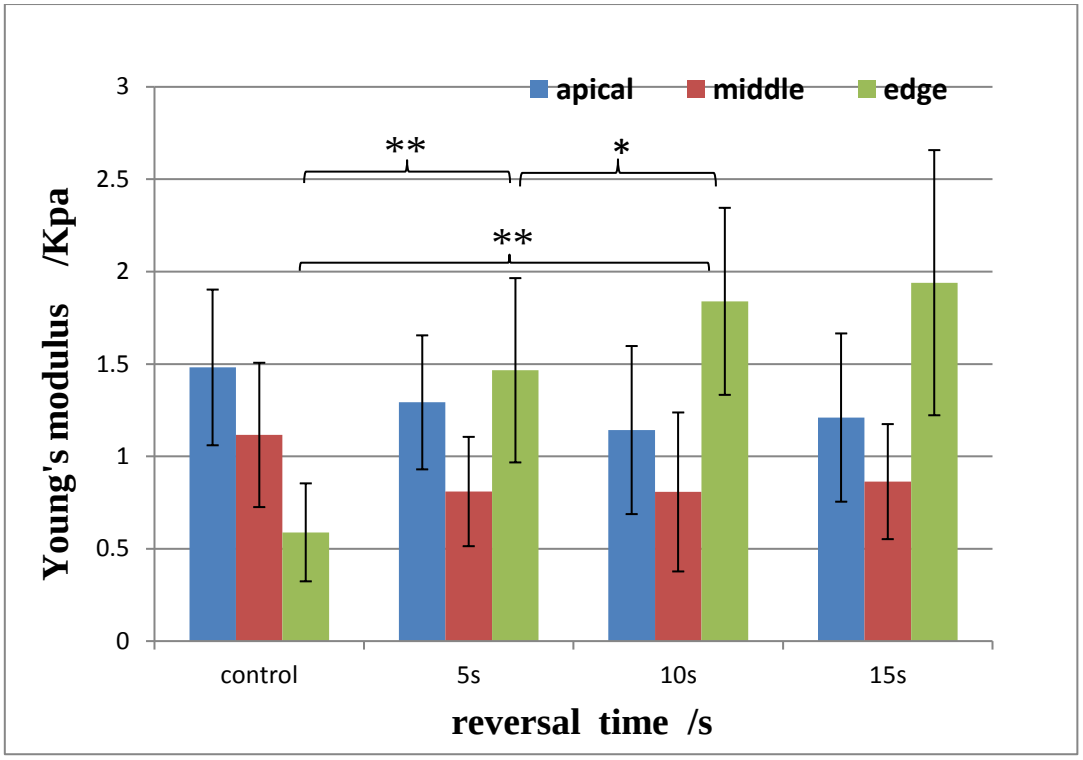

Figure 4. 22 *The Young's modulus of HUVECs at different regions of the cell membrane, in vitro.*

HUVECs are cultured for 7 days then 24 hours' oscillatory shear flow is applied. The indentation test via AFM is then carried out in apical, middle and edge regions on the cell membrane. The control group is maintained in static conditions.

The figure above shows the Young's modulus of cell membrane at three different regions, after oscillating shear stress of various reversal times and for a control group of cells which are maintained in the incubator in static medium (no flow applied). Samples are tested after 24 hrs' exposure to oscillatory shear stress with reversal times for the oscillating flow direction of 5s, 10s and 15s, as previously. The cell samples were cultured for 7 days then used for a 24h experiment, giving a total timeframe of 8 days' culture. The Young's modulus of the cell membrane in the apical region decreases from 1.48 ± 0.42 KPa (n= 30) for the control group, to 1.29 ± 0.36 KPa (n=30) for the sample exposed to 24 hrs' oscillatory shear stress with a 5s reversal time, then continues to decrease to 1.14 ± 0.45 KPa (n=30) for the sample with a 10s reversal time. The Young's modulus shows a slight increase, i.e. the membrane becomes slightly stiffer, with 15s reverse time of oscillating flow in apical region which is 1.21 ± 0.86 KPa (n= 3). As in the apical region, the Young's

modulus in the ‘middle’ region is decreases from 1.12 ± 0.39 KPa (n= 30) in the control sample to 0.81 ± 0.30 KPa (n=30) for the sample exposed to 24 hrs’ oscillatory shear stress with a 5s reversal time: the Young’s modulus of the membrane in ‘middle’ region under 10s and 15s reversal time of oscillatory shear flow is 0.81 ± 0.43 KPa (n= 30) (10s reversal time) and 0.86 ± 0.31 KPa (n= 3) (15s reversal time).

As the region where the glycocalyx growth occurs first, the edge region is well developed with glycocalyx so the Young’s modulus is 0.59 ± 0.27 KPa (n= 30) in the control group. Then the Young’s modulus increases as oscillating flow is applied for 24 hours. The value of Young’s modulus for the three experimental samples under 24hrs’ oscillatory flow is 1.47 ± 0.50 KPa (n= 30) (5s reversal time), 1.84 ± 0.51 KPa (n= 30) (10s reversal time) and 1.94 ± 0.72 KPa (n= 3) (15s reversal time). These increases are significantly changed from 5s reversal time ($p<0.01$, denoted by **), and significant change is still observed from the 10s reversal time experiment ($p<0.01$, denoted by **), however, the experiment for 15s reversal time was not repeated enough times for a reliable demonstration of a significant difference with the control group($p=0.08$). There is also a difference between the 5s and 10s reversal time ($p<0.05$, denoted by *).

This increase in value may be hypothesized to derive from the decrease in the concentration of glycocalyx, as the glycocalyx is distributed away from the edge region in response to the oscillatory shear stress, and is also distributed across a wider cell area following the increase in the average cell area and periphery length. Compared with the glycocalyx removal experiment, a larger volume of glycocalyx remains in the edge region and the HUVECs membrane becomes stiffer after 24 hours’ oscillatory shear flow. In addition, however, Thi *et al*. demonstrated in 2004 that F actin fibres are distributed at the peripheries of cells as DPABS with a small number of stress fibres: exposure to shear stress promoted the formation of increased numbers of stress fibres around the border to the cell (Thi, Tarbell et al. 2004). This is likely also to contribute to changes in the elastic properties of the cell membrane in this region.

5. Effect of oscillatory flows on the distribution of the glycocalyx

5.1 Introduction

Yao *et al.* demonstrated the redistribution of HS proteoglycans (glycocalyx components) to the cell junctional regions, away from the nucleus, after 24h of shear flow application (Yao, Rabodzey et al. 2007). This was hypothesized to be an adaptive mechanism by the cell, to decrease the shear stress gradient acting on the apical surface.

Bai and Wang demonstrated that the glycocalyx distribution recovered 24h after the removal of shear stress (Bai and Wang 2014). In Zeng and Tarbell's study, it was further observed that if shear flow was sustained for 24h, the increased concentration of HS glycocalyx structures at the cell boundary remained, but in addition, all four components return to a much more even distribution across the cell apical region, restoring apical glycocalyx to close to the baseline measurement. This suggests that the glycocalyx adaptively synthesises new HS under ongoing shear stress to restore levels in the apical region, while the original HS continues to be deployed to the protein structures in the edge region.

The impact on mechanotransduction functions may be relevant to underlying causes of pathologies including stroke, diabetes and hypertension as well as other endothelial functions such as selective permeability and leucocyte adhesion.

Again, these studies were conducted under laminar shear flow, whereas the research presented here considers the redistribution of the glycocalyx under oscillatory shear flows which are considered to model more closely the conditions at branches and high stress regions of the vasculature *in vivo*.

5.2 Results

5.2.1 Confocal images

Confocal laser scanning microscopy (CLSM) gives the user the ability to control the depth of field of image for samples up to 100μm in thickness, and therefore provide a high quality image (Corle and Kino 1996, Sheppard 1997). All confocal microscopes can operate in transmission, reflection or fluorescence mode. In this project, fluorescence mode will be used. The laser system emits light continuously. The light travels through a pinhole aperture before passing through the sample, and is then focused to pass through a second pinhole aperture, thus eliminating out-of-focus light, which is scattered around the pinhole and does not reach the receptor. In traditional microscopy, the light illuminates the whole specimen at once, the aim being to excite fluorescence emissions or reflections through the total depth of the specimen. By comparison, CLSM provides images of increased contrast and sharpness because the whole system (fluorescence emissions or reflections due to illumination) can be geared to a focal plane (Pawley 1995, Davidson, Truman et al. 2007).

The CLSM can be used to provide data for a 3-dimensional simulation of the structure of the sample, as follows. The CLSM data recorder scans 2-dimensional images of the sample on the x-y axes, while altering the depth of the scan on the z axis at small intervals, controlled by a computer-controlled fine-step motor. Working its way from top to bottom of the sample, the recorder builds up a bank of data which can them be combined to generate an image for a complete in-focus projection of the sample in three dimensions (Pawley 1995, Davidson, Truman et al. 2007). The glycocalyx is stained green using wheat germ agglutinin (WGA-FITC) treatment, a flurophore which binds to sialic acid; the cytoplasm of HUVECs is stained red using Cell Tracker Red CMTPX treatment; and the nucleus is stained blue using 4',6-Diamidino-2-Phenylindole, Dilactate (DAPI) treatment. Ar-ion (488 nm, 514 nm) and He-Ne laser (543 nm) beams are used in the CLSM, wavelengths appropriate to the excitation spectrum of the three fluorophores in use (Masters 2006). Figure 5.1 (following) shows CLSM images of glycocalyx on live HUVECs under static (no flow) conditions: A) in cross section, B) the x-y sectional images, C) individual and merged images.

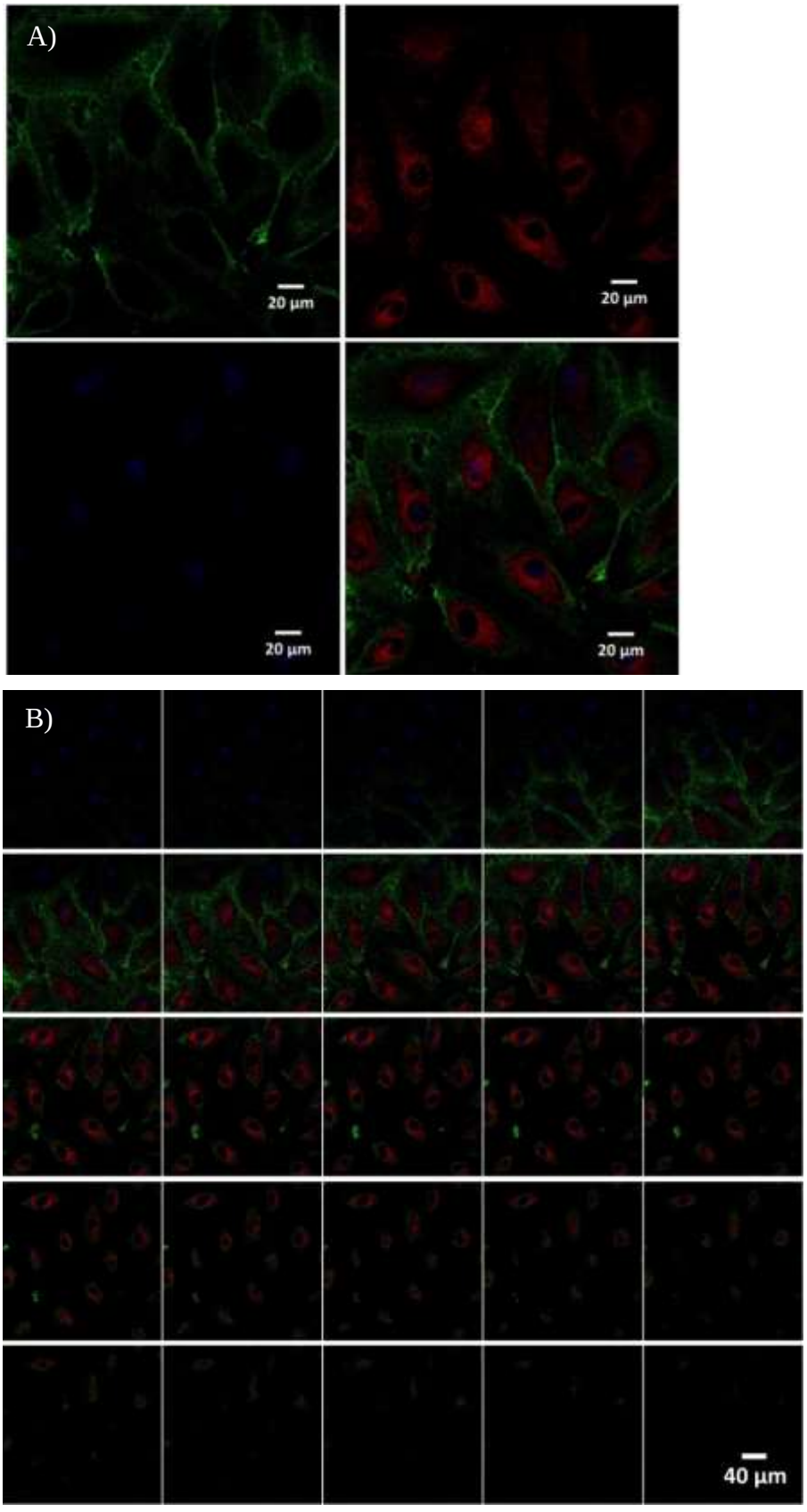

Figure 5. 1 *CLSM images of glycocalyx on live HUVECs under static (no flow) conditions. Green marks glycocalyx on the cell membrane; red marks the cytoplasm; blue marks the nucleus. A) The individual and merged images of HUVECs. B) the x-y sectional images of*

HUVECs shown at different depths on the z axis, from bottom to top of the sample. Δz = 300nm.

In Figure 5.1, HUVECs are cultured for 8 days and stained with three different fluorescents. The figure above shows the glycocalyx located on the cell membrane of the HUVECs. CLSM imaging is one of the methods used to determine the distribution of the glycocalyx across the cell membrane. CLSM gives a clear image of each x-y axis cross section of HUVECs in a 2D plate view. The 3D reconstruction is based on these individual cross sections, either from top to bottom or from bottom to top of the HUVECs culture sample on the glass slides. There are 300nm intervals between these cross sections along the z-axis. Figure 5.1 B) shows 25 sequential x-y cross-sectional images, taken from bottom to top with 300nm spaces between images: the scale bar is 40μm. The nucleus, stained blue, is clearly shown in most of the images. The glycocalyx, stained green, is visible mostly at the bottom of the HUVECs even though there is no cytoplasm visible in the cross-section images at this depth. As the CLSM moves up the z-axis, the cytoplasm, stained red. is increasingly visible and the glycocalyx forms a ring surrounding the nucleus. Finally, the area of visible glycocalyx and cytoplasm decreases until the sectional images approach the top of the HUVECs. Figure 5.1 C) shows the glycocalyx, cytoplasm and nucleus treated by WGA-FITC, CTR CMTPX and DAPI respectively. The top left panel is the sialic acid stained with green, the top right panel is the cytoplasm stained with red, the bottom left panel is the nucleus stained with blue, and the bottom right panel is the merged image from the first three panels which clearly shows the distribution of the glycocalyx, visible across the whole membrane of the HUVECs.

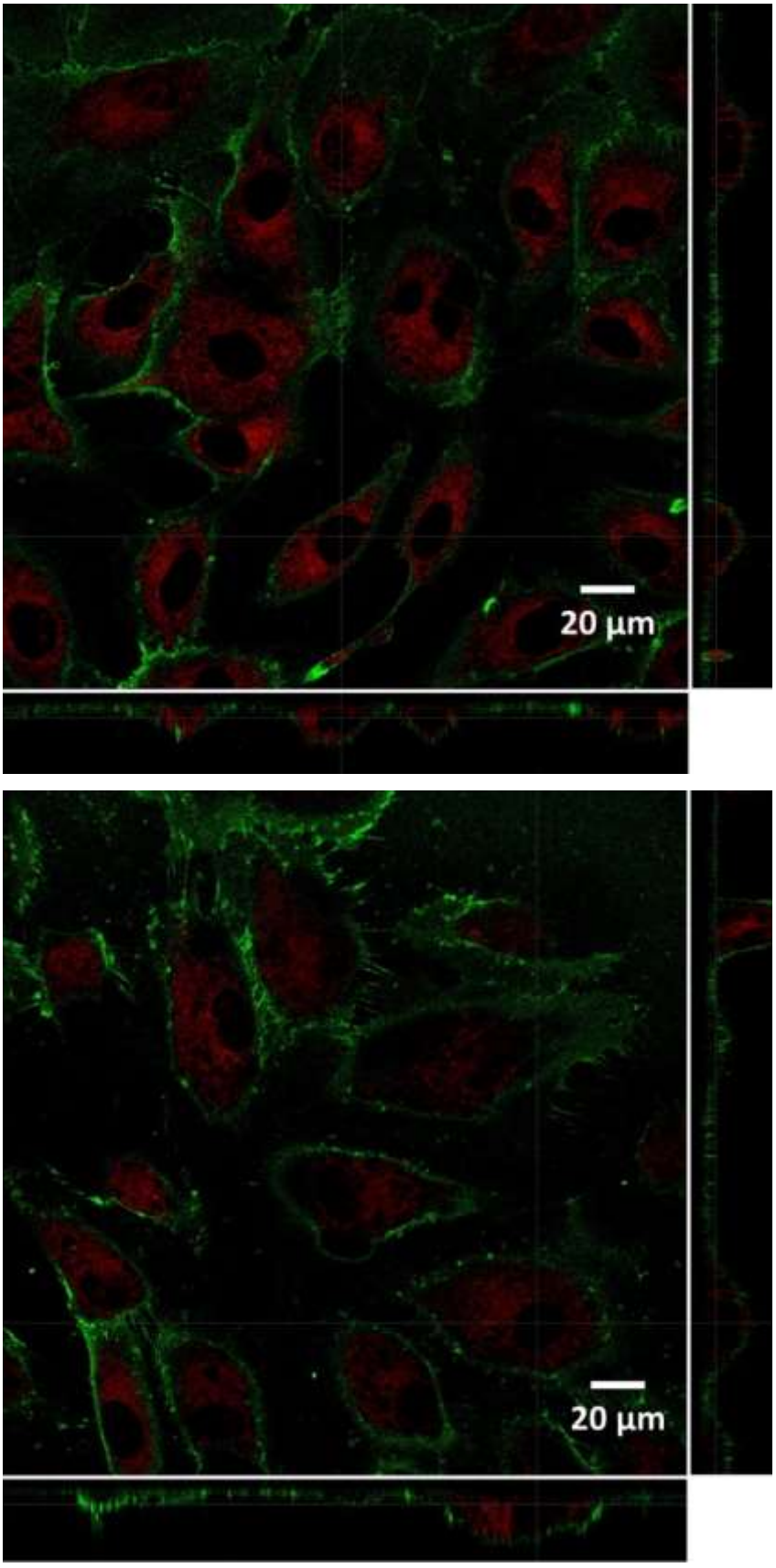

Figure 5. 2 *the formatted sequential images for samples of HUVECs under oscillatory shear stress, with a control group cultured for the same time in static no-flow) conditions.*

A) control group with 8 days' culture. B) HUVECs sample cultured for 7 days on glass slides then exposed to 24 hours' oscillating shear flow with 5s reversal time for direction of flow. Scale bar = 20μm.

Both the experimental sample and the control group in these two sequential images use the same cell passage line of the HUVECs and are cultured for the same length of time. The two images focus entirely on the apical section just across the nucleus. The nucleus in the control group is located in the top area of the cell as a whole: the nucleus in the experimental sample has moved slightly to one side. In other words, the apical area with nucleus has moved some distance following exposure to the oscillatory shear stress. The height of the cells was also observed to have increased in the experimental group: there is an increased number of x-y sectional images for this sample, giving an increase in the average cell height from 7.2-8.7μm (25-30 frames) for the control to 8.4-10.2μm (29-35 frames) as given by the uniform space between images (300nm). The cytoplasm region, visible in red, demonstrates that the size of the cells has increased as a result of the oscillating flow applied.

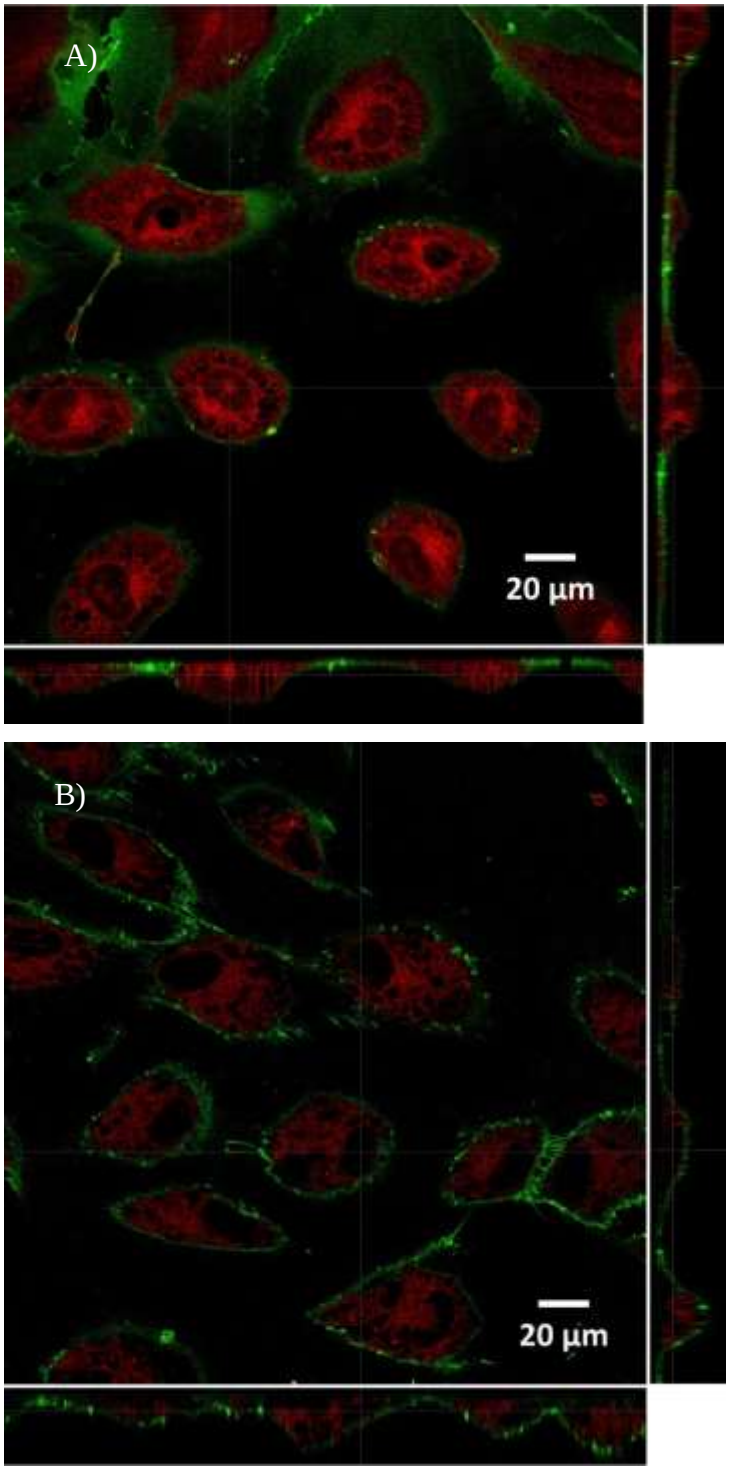

Figure 5. 3 *Formatted sequential images for samples of HUVECs under oscillatory shear stress, with a control sample incubated in static medium (no flow).*

A) control group with 8 days' culture. B) HUVECs cultured for 7 days on glass slides then exposed to 24 hours' oscillating shear flow with 10s reversal time for direction of flow. Scale bar = 20µm.

Figure 5.3 above shows the sequential image for HUVECs with and without oscillatory shear flow for 24 hours, with an oscillatory reversal time of 10 seconds. Similar results are seen to those for the 5 seconds' reversal time experiment: both the area and the height of the cells both increase after exposure to oscillatory shear stress, as compared to the sample. The vertical cross-section slices at the bottom and right hand side of the image demonstrate clearly that the shape of the cells changes, from gently sloping sides from the perimeter to apical region in the control sample (which could be described as a 'hill-like' morphology), to a steeper gradient in the experimental sample (which could be described as a more 'mountain-like' morphology). This 3-D imaging increases our understanding of how oscillatory shear stress acts on the cell to change the distribution of the cytoplasm, increasing the cytoplasm depth in the apical area and also increasing the area and perimeter of the cell (as observed in section 4.3.2, where cells exposed to shear flow were viewed under AFM and the results analyzed with ImageJ). This rearrangement of cytoplasm on the z-axis may also explain the changes to the area, perimeter and aspect ratio of the cells as viewed on a 2-dimensional plane via AFM.

As previously observed in the indentation tests in section 4.3.2, the brightest green staining is seen at the peripheral or 'edge' region of the membrane rather than the apical or 'middle' area: this signifies that the majority of the glycocalyx is in the peripheral region of the cells. This supports previous experimental findings which demonstrated the redistribution of the glycocalyx to the cell membrane periphery under shear stress, with the hypothesis that the redistribution acts to reduce stress on the cell from the shear flow (Thi et al., 2004). The vertical cross-section slices at bottom and right hand side of the image also reveal green stained glycocalyx covering the apical region of the membrane over the nucleus, suggesting that the glycocalyx has already begun to regenerate in this region and potentially contribute to the increase in height observed. The passage of the cell line, the culture time, the time and concentration for the staining, and the wavelength of the sources are maintained as equal conditions between the experimental and control group, so the brightness of the colour may be considered as another piece of evidential data to show the changes in the glycocalyx.

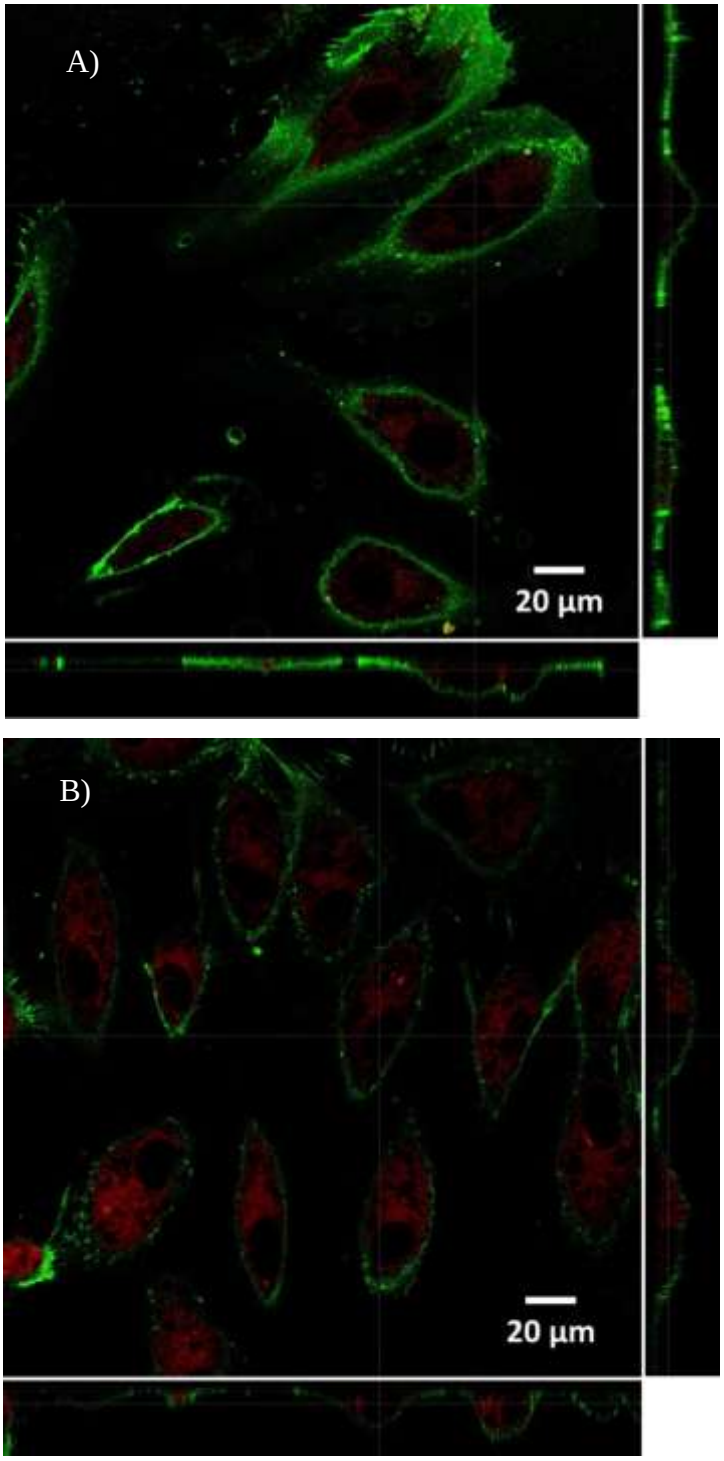

Figure 5. 4 *Formatted sequential images for samples of HUVECs under oscillatory stress, with a control sample incubated in static medium (no flow).*

A) control group with 8 days' culture. B) HUVECs cultured for 7 days on glass slides then exposed to 24 hours' oscillating shear flow with 15s reversal time for direction of flow. Scale bar = 20µm.

Figure 5.4 shows the different shapes of cells after 24 hours' oscillating flow experiment with a flow reversal time of 15 seconds. It is notable that a high number of cells die during and after the experiment. The rubber on the syringe which assists with the piston motion required to reverse the flow direction has an increasing chance of fatigue with a risk that cracks may develop. Contamination, or the leaking of medium through the syringe and its replacement with air, are likely reasons for the death of cells.

In this experiment, the size and the perimeter of the cell membrane is increased, and the morphology of the cells continues to change from oval to fusiform (elongated) as well as distinct changes towards a "mountain" shaped morphology on the z axis previously observed in the sample exposed to oscillating shear stress at 10 seconds' reversal time. This group of images clearly show the angle of orientation of the cells is almost in the same direction: as would be expected, therefore it is observable that the amount of glycocalyx is decreased in the edge region of the cells.

5.2.2 Super-resolution images

Even the highest-performance light microscope has limited resolution: 200nm in the lateral (XY) and 500nm in the axial (Z) direction. Light microscopes cannot image objects with a distance of <0.5x the light used for observation: this is known as the diffraction limit. Super-resolution microscopy is now a well-established technique to exceed the diffraction limit and double both the axial and lateral resolution of light microscopes to determine high quality images of extremely small samples/objects. The figures below show examples of the image quality that can be achieved using super-resolution microscopy (Mikliaev and Asselborn 2007, Moerner 2015).

This study uses the wide-field structured-illumination (SI) approach or SIM (structured illumination microscopy). SIM is capable of collecting information from frequencies outside the observable region and using them to enhance spatial resolution. Combined data from the observable region and reciprocal space is put through a Fourier transformation, mapped and analysed in frequency space, generating a computationally reconstructed FT image with a high level of resolution

information. This is then reverse Fourier transformed to give the eventual super-resolution image (Gustafsson 2005).

Structured illumination is a widefield technique that generates a grid pattern through interference between diffraction orders. The grid pattern is then superimposed onto the specimen. In between the taking of each image data set, the grid pattern is shifted or rotated in steps. An image set is composed of a number of individual subsets, each captured after rotating the grid by (for example) 60 degrees. After it has been processed with a highly specialized algorithm, the raw data yields high-frequency information to allow a reconstructed image to be produced with a lateral resolution roughly double that of diffraction-limited instruments and a 150 to 300 nanometer range of axial resolution (Gustafsson 2005, Reymann, Baddeley et al. 2008).

SIM can be used with all common types of organic dyes usually bound to antibodies or fluorescent proteins. A highly specific labelling is required, with low background, to ensure a good signal to noise ratio. For multicoloured samples, the fluorophores should be selected to minimise overlap in the spectrum so that results can be clearly interpreted (Gustafsson 2005).

This study uses filter sets for ELYRA PS.1 optimized for the available laser lines: 405, 488, 561 and 642 nm. As with the confocal experiment, glycocalyx is stained green using wheat germ agglutinin (WGA-FITC) treatment; the cytoplasm of HUVECs is stained red using Cell Tracker Red CMTPX treatment; and the nucleus is stained blue using 4',6-Diamidino-2-Phenylindole, Dilactate (DAPI) treatment.

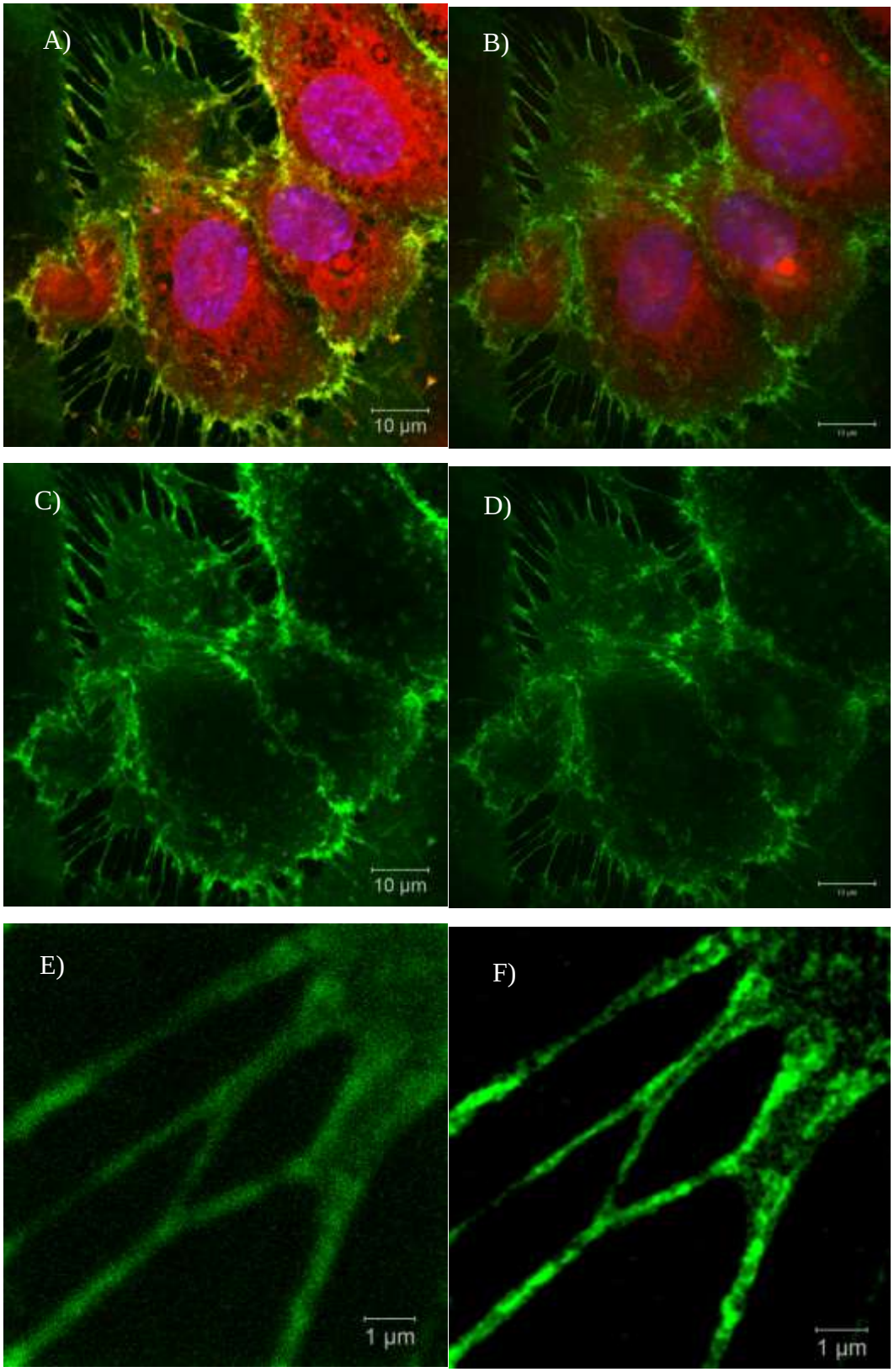

Figure 5. 5 *Comparison of CLSM images and super-resolution images to show overview and detail of various locations within the sample.*

Scale bar = 10µm (ABCD), scale bar = 1µm (EF). The left column shows the confocal images for cultured cells: the right column, super-resolution images for the same cultured cells.

Viewing comparative images side by side gives a very clear demonstration of the advantages of SIM. The first two images show an overview of the HUVECs cultured on the glass slide: the left is a confocal image; the right uses super-resolution technique. The samples have been treated with multiple immunofluorescents that the image in each case shows three different colours: green, red and blue. At this resolution there is not a significant difference between the confocal and SIM images, although the colour of the confocal image was more intense and brighter than the super-resolution image. The reason may be lie in the process of merging these three panels into one image. For the second panel, it is not necessary to combine images to create a merged picture: these two images, in the green panel, show the glycocalyx layer distributed across the cell membrane. No significant difference is visible between these two images, but at a higher zoom (apx. 10 greater) to examine them in greater detail, in the third pair of images, the difference is starkly apparent. The boundary of the edge area of the membrane in the confocal images is blurry even when the red and blue elements of the image data are removed to make the image as clean as possible. Thousands of noisy dots appeared on confocal images, which is strong evidence to demonstrate the superiority of super-resolution image compared with the confocal image.

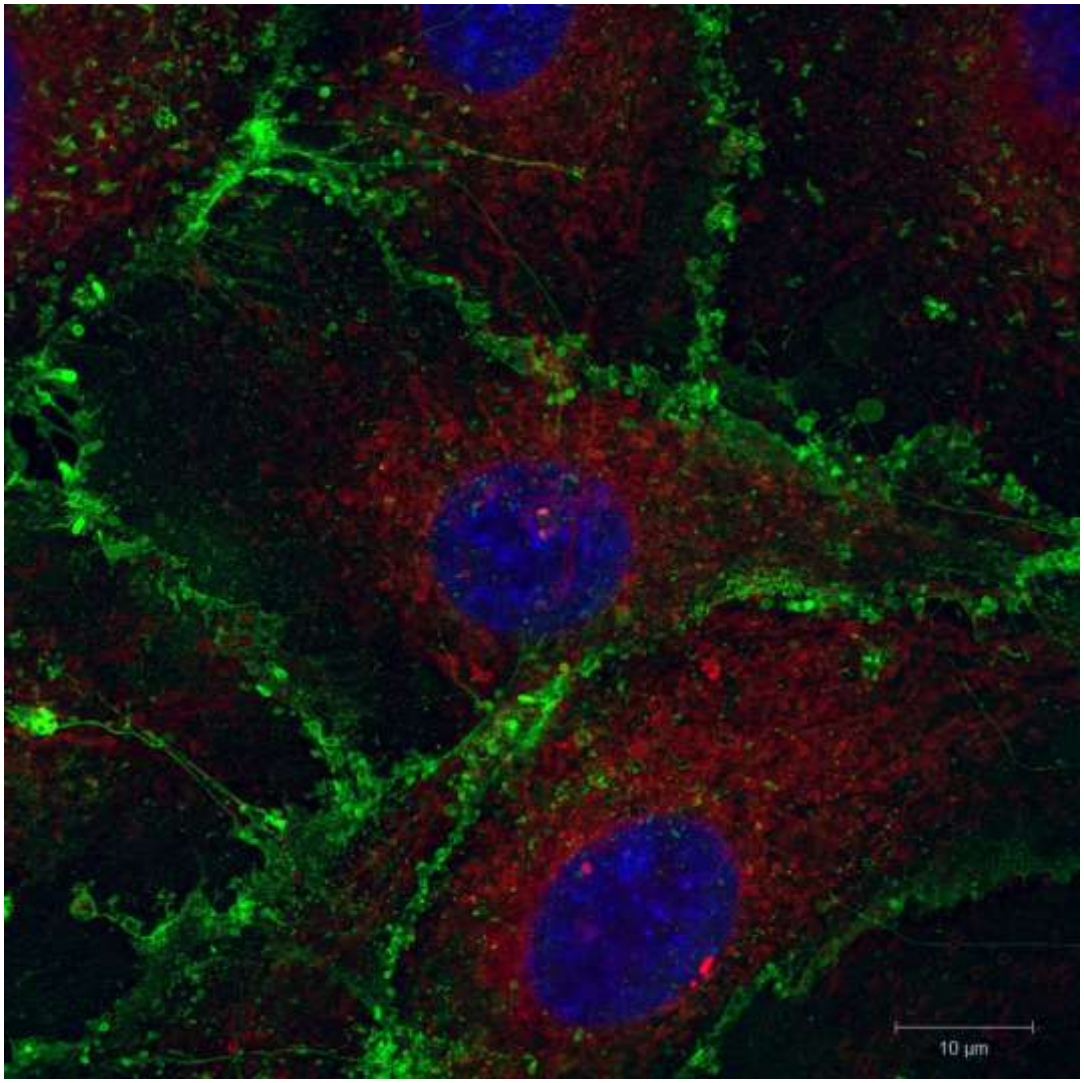

Figure 5. 6 *2D super-resolution image for control sample of HUVECs cultured for 8 days. Scale bar=10µm.*

The super-resolution image shows a high image quality of the details across the entire cell. Figure 5.6 is a 2D image showing the junctions between cells in high resolution: the HUVECs are at 80-90% confluence with the cells strongly bound to each other. The shape of the nucleus (blue staining) is mostly circular or oval on a 2D sectional image in the cytoplasm: the nucleus is always in the middle of the cells if they are not influenced by any external force, which may cause them to move anywhere inside the cells, as seen previously with the sample exposed to shear stress and imaged using confocal microscopy.

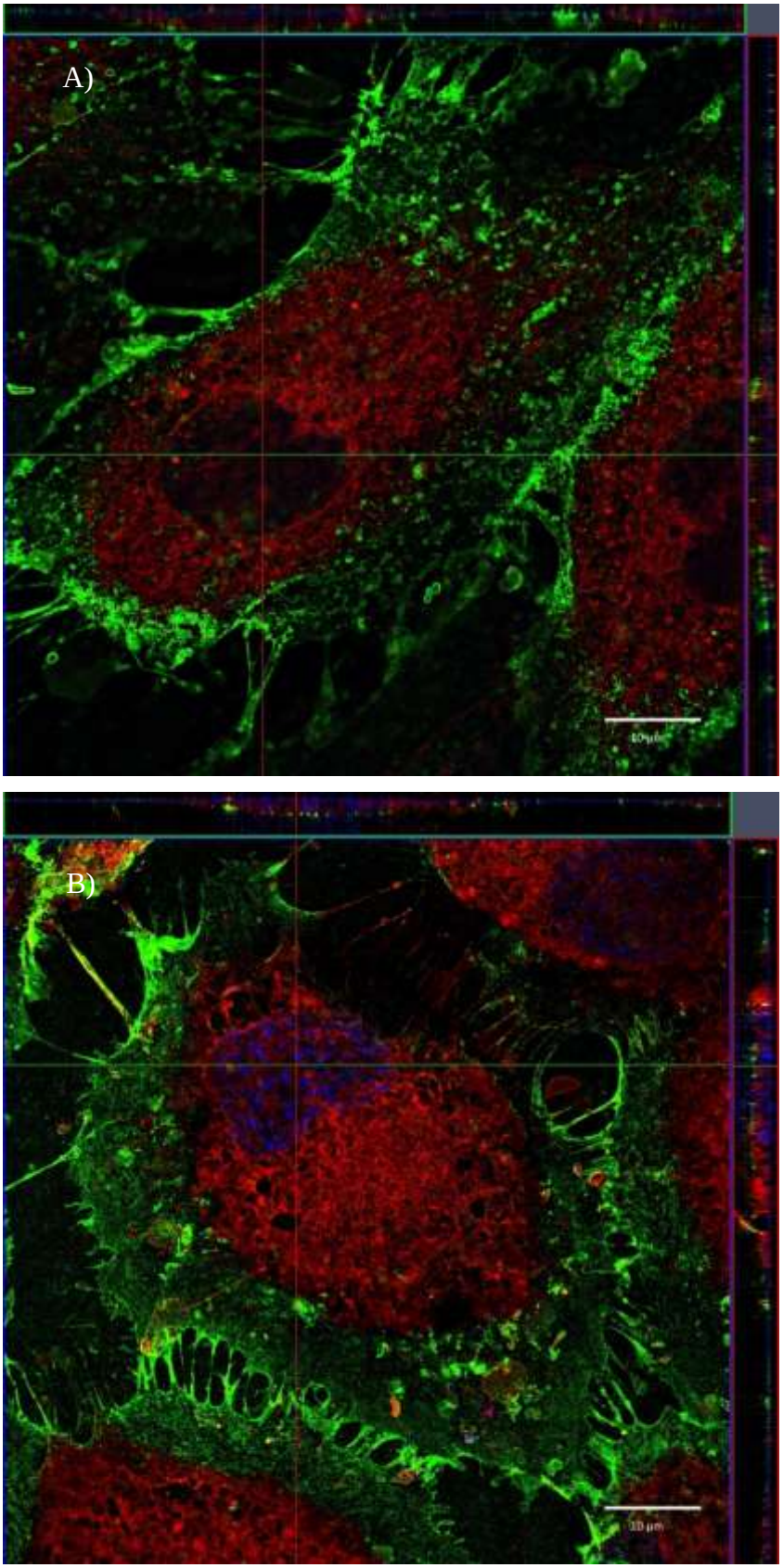

Figure 5. 7 *Formatted super-resolution images.*

A) control sample of HUVECs cultured for 8 days in static medium; B) HUVECs experimental sample cultured for 7 days and then exposed to 24 hours' oscillatory flow at a 5 second reversal time. Scale bar=10μm.

Comparing the control sample to experimental samples in the images above, not a great deal of change is seen. The control sample HUVECs still have a large volume of glycocalyx on the edge region of the cells and the cytoplasm is fully spread inside the cells. Compared with the control group, in the sample exposed to oscillatory shear stress reversing every 5 seconds for 24 hours, a significantly larger number of stress fibre structures is seen between the cells, as predicted in Thi *et al.*: however, the glycocalyx is distributed around the whole cell periphery after oscillatory flow, not distributed towards one end as theorized in the Thi *et al.* model for unidirectional shear flow (Thi, Tarbell et al. 2004).

The region of cytoplasm appears to be squeezed towards the nucleus. There is some growth in both the area and the perimeter of the cells. It is hard to determine if there is a change in the angle of orientation, because both two groups show random directions among the cells in the sample. The nucleus in the experimental group appears to be moved towards one side of the cells, possibly as a result of the force of the oscillatory shear stress. The oscillatory shear stress applies a force from two opposing sides along the flow direction, but can be considered as a laminar flow until the direction of the flow changes. In addition, the force is steady and uniform up until the change in flow direction. In other words, it is analogous to a simple model of a beach structure. The waves scour the sand on the shoreline, but the in and out motion is an oscillating laminar flow, while the sea tide rises and ebbs over a certain period of time. An oscillatory flow might be conceptualized as one piece of land experiencing two tidal water forces randomly. In these turbulent conditions, if the glycocalyx can enable the cell membrane to grip the cover glass tightly, the fluid cytoplasm would move towards the nucleus and the edge of the cell should mostly be glycocalyx.

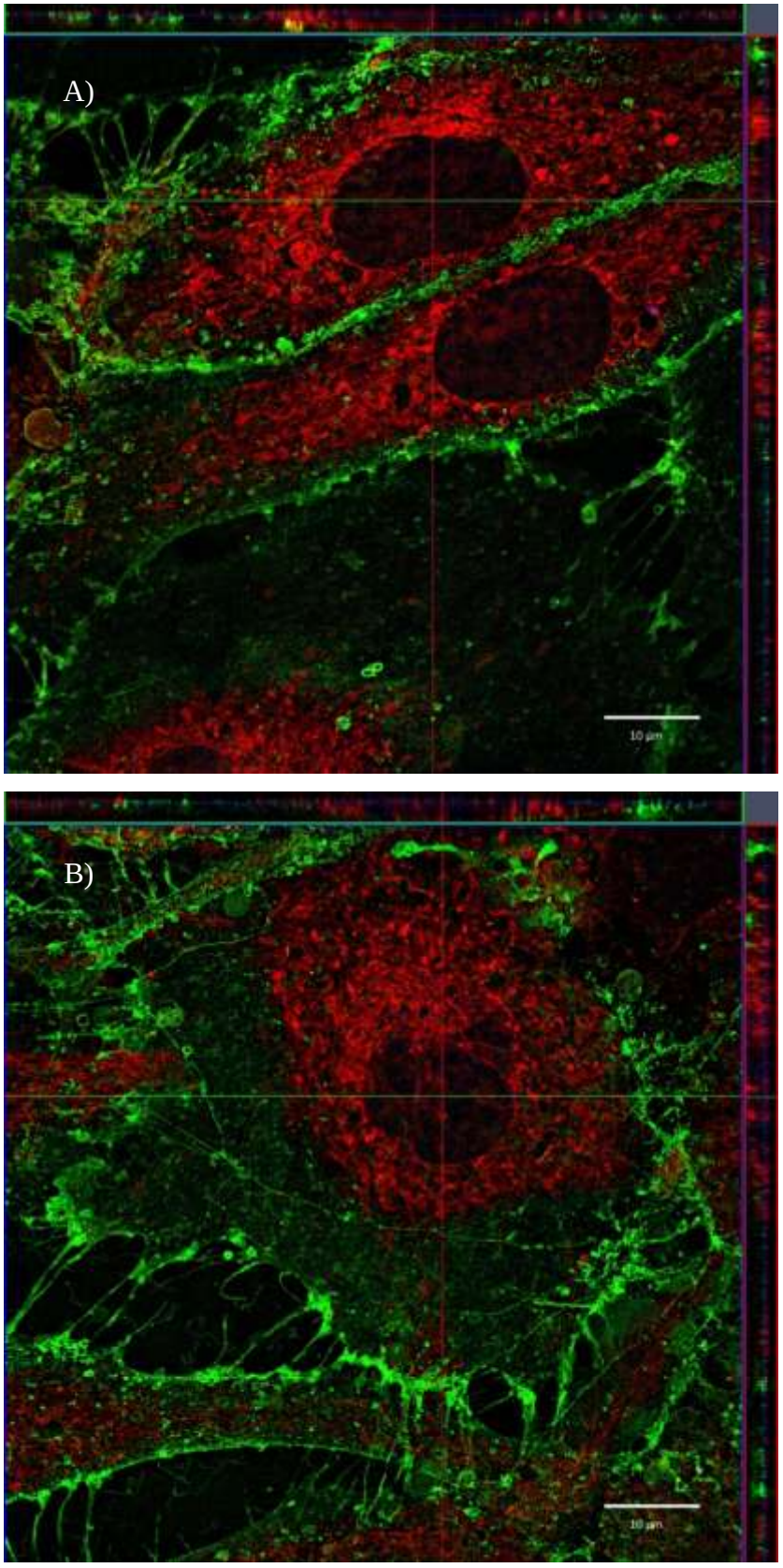

Figure 5. 8 Formatted super-resolution images.

A) control sample of HUVECs cultured in incubator for 8 days; B) experimental sample of HUVECs incubated for 7 days then exposed to 24 hours' oscillatory flow with a 10s reversal time. Scale bar=10μm.

Figure 5.8 is a 2D image of a control group of HUVECs cultured for 8 days in static medium, compared to an image of an experimental sample of HUVECs cultured for 7 days in the incubator then exposed to 24 hours' oscillatory shear stress with a flow reversal time of 10s. The upper image shows a range in morphology of the normal cells, from irregular shapes to an approximate circle (50% seen in image), and also oval like structures. As seen with the other control groups, this control group had a distribution of glycocalyx covering the whole structure of its cells. The lower image for the experimental sample demonstrates that the cells are forced to adapt to the assault that comes from the shear stress flow (natural, or experimentally applied). The cell size and perimeter are clearly increased in the experimental group. There are more numerous junctions between cells. The oscillatory flow may be conceptualized as a mudslide-like event, with the cell recruiting the grass-like glycocalyx to provide a structure similar to a root network, that stabilizes the subsoil to ensure it is not washed away by force. The shape of the cells is always distorted by the force from the flow, due to the low resistance of the fluid cytoplasm to the force of the shear stress. The density of cytoplasm near the nucleus has demonstrably increased, giving a brighter red colouring in this area of the image, as the cell morphology has changed to a more 'mountain-like' shape.

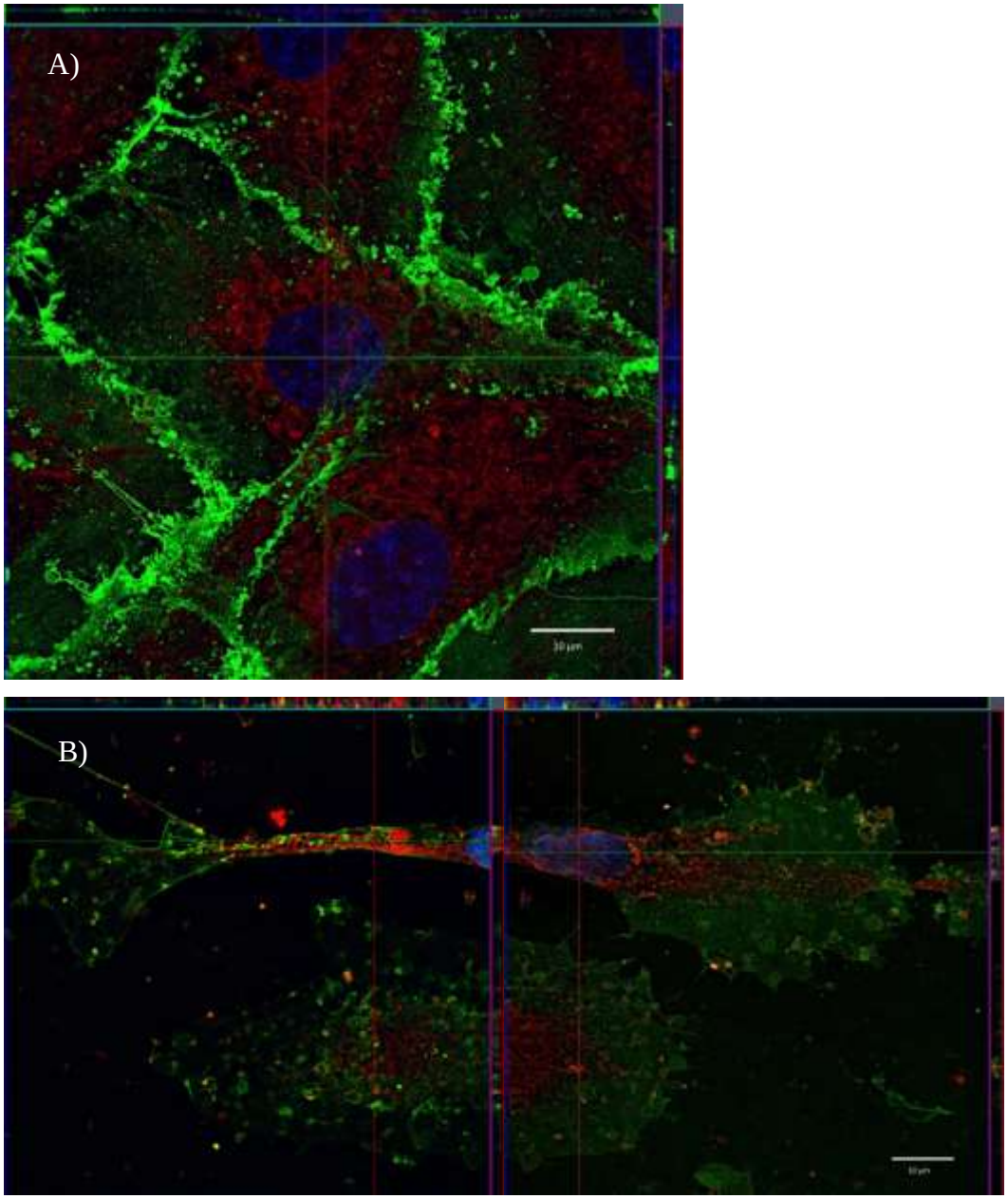

Figure 5. 9 *Formatted super-resolution images.*

A) control sample of HUVECs cultured in incubator for 8 days; B) experimental sample of HUVECs incubated for 7 days then exposed to 24 hours' oscillatory flow with a 15s reversal time. Scale bar=10μm.

This is the third comparison between a control group in static medium and an experimental group exposed to oscillatory shear flow. In this experiment, the only change of condition is the time for the reversal of flow direction, which is tested at 15 seconds to compare with the 5s and 10s reversal time experiments. As seen from the data analysis of the oscillatory flow stimulation experiment in 4.3.2, the increase

in flow reversal time means that the shear stress acts in a laminar manner on the cells for a longer timeframe (in each of the two directions) after the initial period of severe turbulence at the change of direction has died down. This is hypothesized to be a useful simulation of some of the conditions present *in vivo* at vascular junctions, where turbulent flows cause the blood to curl around and travel in opposing directions, similar to the flow seen in a fountain or volcano.

Significant differences are observed between the control group and the experimental group. The morphology of the cells elongates to a long shuttle or fusiform shape, the aspect ratio shows a huge increase compared with the control group, and the cells' angle of orientation clearly changes.

The Figure 5.9 B) demonstrates one weak point of super-resolution imaging: the maximum size of sample that can be imaged is around 80μm x 80μm. Where cells have spread across a wide area, as in this case and others in the experiment, this may not be enough to capture an image of an entire cell. Also it shows a typical cell deformation after exposure to oscillatory flow for 24 hours with reversal of flow direction every 15 seconds. There is a significantly higher aspect ratio as compared with the cells in the control group.

The cell junctions are not so clearly observed in the experimental sample image, as compared with the samples exposed to shorter reversal times. It is known that the changes in orientation and morphology that are observed reduce the stress on the cell from the shear flow. The reduction in stress fibre structures may also indicate that the flow longer reversal time creates a more settled flow pattern with a longer duration of more laminar flow: and that the actin stress fibres initially formed to stabilize the cell in turbulent regions are quickly broken back down, with their proteins adopted for more permanent structures such as tight junctions as the cell migrates into a new position. A third reason for the reduction in stress fibre structures observed, however, may be the increased number of dead cells in this sample, which leave blank spaces within the sample where junctions cannot be formed.

6. Discussion and future work

The endothelial glycocalyx is composed of a wide variety of membrane-bound macromolecules, which lie as a thin layer on the luminal side of endothelial cells in the vasculature. Research has established the sensitivity of this layer to its hemodynamic environment, such as shear stresses originating in the blood flow: these affect its structure, distribution and functions including mechanotransduction, its important contribution to the endothelium's role as a permeability barrier allowing substances carried in the blood stream to be filtered and absorbed, and its role in the body's immune responses. A number of researchers have identified that degradation of the glycocalyx results in the reduction of protective and anti-adhesive properties of the endothelium. Because the endothelium plays such a critical role in a large number of human pathologies including atherosclerosis and cardiovascular disease, it is anticipated that these experimental results may make an important contribution to research aiming to increase understanding in this area.

Recent research continues to identify important differences in the function of the endothelium and glycocalyx. This PhD project tests a method of producing oscillatory shear stress stimulation in vitro, and measures the development of glycocalyx in response to this complex set of stresses. The Young's modulus of the cell membrane is used as a way to analyze the establishment of the glycocalyx. The change in the value of the Young's modulus of the cell membranes with, and without the glycocalyx presents information for the calculation of the Young's modulus of the glycocalyx itself. Using this approach, we have estimated the Young's modulus of the endothelial glycocalyx to ~0.64 kPa, i.e. 6 fold softer than that of the endothelial cell membrane, which is ~3.78 kPa.

The Young's modulus of the cell membrane decreased with culture time, from approximately 2.91 ± 0.6 KPa (n= 51) at day 4 to 1.4 ± 0.55 KPa (n=51) at day 8, at the end of culture time. These results are similar to those shown in Bai and Wang's research measuring the Young's modulus of the cell membrane at 3, 7, 14 and 21 days of cell culture, which demonstrate the Young's modulus reducing significantly between days 3 and 7, a less striking reduction between days 7 and 14, and then no significant change after day 14. We hypothesize that the lower elasticity of the cell

membrane is caused by growth of the soft glycocalyx layer on the surface during cell culture (Bai and Wang 2012). As previously stated, a culture time of 8 days was selected for this experiment following Potter et al. who demonstrated that the glycocalyx on cell membrane can be well developed with one-week culture (Potter, Jiang et al. 2009).

This PhD project introduces either laminar flow or oscillatory flow to cultured endothelial cells, and investigates changes to the cell morphology and orientation. In a development of the study, the distribution of the glycocalyx is observed following exposure to 24h oscillatory flow at various lengths of reversal time, and the results are compared with a control group in static medium.

The study results confirmed that the distribution of the endothelial glycocalyx varies between the apical and edge areas of the endothelial cell membrane. Sialic acid staining reveals the glycocalyx to be located mainly at the cell-cell junction areas, as expected.

Data from the AFM indentation following 24h oscillatory shear stress show decreased distribution of the glycocalyx in the edge of cells, as measured by an increase of the local Young's modulus. This is hypothesized to be due partly to the glycocalyx redistributing towards the apical area of the cell, and partly to the increase in area of the cell on the x-y plane.

The changes that are observed suggest a likely change to the functionality of the glycocalyx under these conditions as a) prior to exposure to shear flow, the existing glycocalyx is distributed towards the 'edge' region of cells, b) under the stress of oscillatory flows, there is a slight decrease in the amount of glycocalyx present, and c) additional glycocalyx is generated in the apical region of the cell under oscillatory flows. All of these effects are likely to have impacts on the functions of the glycocalyx, for instance its role in mechanotransduction of NO which mediates vasodilation and regulates blood pressure, and its effect on the permeability of the endothelium to large molecules.

The study employs AFM nano-indentation on the cell membrane to evaluate its mechanical properties. The Young's modulus of the HUVEC membrane treated with Hep-III is approximately 3.78 kPa, which is almost six-fold greater than that of the untreated cells, at ~ 0.55kPa. The Young's modulus of the endothelial glycocalyx layer is evaluated from the above results as being approximately 0.64 kPa. This study used a different cleavage component to that used in Bai and Wang (Bai and Wang 2012) for this calculation, but the similar results obtained support the method and direction of their study: their measurement for the Young's modulus of the glycocalyx layer was approximately 0.39kPa. The difference between the results of the two studies is assumed to derive from the different cleavage component used, generating a break in the glycocalyx at a different point in its structure.

Having tested the method from the Bai and Wang study with a different cleavage component, this study was then extended, from a comparison of shear stress against a control under static flow conditions, to include oscillatory flow conditions which were intended to replicate the turbulent flows that might be experienced by endothelial cells in vivo at sites of vascular branching and/or damage, and may be contributory causes of atherosclerosis. Turbulent flows of various oscillatory reversal times were tested to try to recreate conditions within blood vessels of a variety of dimensions. Following this exposure, cell morphology and orientation were examined. Significant change was observed in both the steady flow (shear stress) and oscillatory flow experiments, including increasing alignment of the cells in the direction of flow and changes to the aspect ratio. Cells under laminar flow are observed to undergo greater elongation, as measured by their aspect ratio, and greater reorientation in the flow direction, than those under oscillatory flows.

Increases in the reversal time of the oscillatory flow result in increased cell area, perimeter and aspect ratio as well as reorientation in the flow direction. Only under oscillatory flows were cells observed to undergo morphological changes from a "hill-like" to a more "mountain-like" morphology. Future studies could usefully

replicate this methodology to minimize the possibility of error.

The Young's modulus of HUVEC membrane shows a significant difference between the edge and centre regions of the cell. This is consistent with the confocal imaging results, which show uneven spatial distribution of the glycocalyx layer on the cell membrane. Measurement of the regrowth of the glycocalyx after cleavage demonstrates that regrowth begins at the edge region of the cell and the glycocalyx in the apical region of the cell regrows more gradually.

When both reversal time and experiment duration are increased, cell survival rate decreases. This may be a result of the cells' lack of ability to adapt to long periods of stress, or of the longer experimental duration introducing greater risk of contamination.

Changes in the glycocalyx structure at the cell perimeter viewed under super-resolution microscopy appear to support the theoretical framework of Thi et al. who describe the formation of additional stress fibres to support the cell when tight junctions and DPAB membrane structures are broken under high shear forces, returning to a more stable structure when turbulence reduces (Thi, Tarbell et al. 2004).

There are a number of areas that future work could focus on to extend the understanding of glycocalyx responses to flow stress gained in this study.

Cleaving of the glycocalyx can be undertaken at different points to validate the value of the Young's modulus of the glycocalyx, e.g. SA using neuraminidase, or other GAG chains using HA or CS cleavage: or several components could be used simultaneously to cleave the glycocalyx structure in a number of places at once, simulating extensive damage to the glycocalyx. Studies should investigate the effects on cell morphology and on the glycocalyx's ability to regenerate. These experiments can be combined together to observe remodelling of the endothelial cells under shear stress for various periods of time after glycocalyx cleavage to

determine the distribution and intensity of the glycocalyx. It would be interesting to investigate the rate of change of the glycocalyx exposed to oscillating shear stress, for example at 2 hourly intervals.

It is of interest to observe the changes in anti-adhesive properties related to the thickness of the glycocalyx because this is linked to disease and pathological responses, such as inflammation and atherosclerosis. Studies could then look at specific processes, such as NO mechanotransduction or capsule/drug delivery, and test the impact of damage to the glycocalyx on these processes.

Sensitivity of the experimental results to small temperature differentials, such as experienced in vivo during the body's natural immune responses to infection, is of interest for future study and could be investigated by making small changes to the settings of the heater. Changes in cell attachment and growth have been observed in samples at 37°C, compared with samples at 32°C (Kushida, Yamato et al. 1999, Yamato, Akiyama et al. 2007).

The study could profitably be extended by comparison with ex vivo models, firstly of healthy tissue (for instance, comparison of glycocalyx damage and regeneration in cells taken from vascular tissue of varying vessel types, sizes, diameters and thicknesses; comparison of vascular tissue from vessels of similar diameter but from varying locations in the body such as liver, brain; and comparison of vascular tissue from different regions such as straight vessels or tissue from junction regions) and then subsequently for tissue affected by different disease models such as atherosclerotic tissue, tissue from subjects affected by inflammatory disease. This would enable further understanding of differences in structure and function between healthy endothelium/healthy glycocalyx, and endothelium/glycocalyx in diseased vascular tissue.

7. References:

Adams, R. H., G. A. Wilkinson, C. Weiss, F. Diella, N. W. Gale, U. Deutsch, W. Risau and R. Klein (1999). "Roles of ephrinB ligands and EphB receptors in cardiovascular development: demarcation of arterial/venous domains, vascular morphogenesis, and sprouting angiogenesis." Genes & development **13**(3): 295-306.

Adamson, R. and G. Clough (1992). "Plasma proteins modify the endothelial cell glycocalyx of frog mesenteric microvessels." The Journal of Physiology **445**: 473.

Aird, W. C. (2007). "Phenotypic heterogeneity of the endothelium I. Structure, function, and mechanisms." Circulation Research **100**(2): 158-173.

Aird, W. C. (2007). "Phenotypic heterogeneity of the endothelium II. Representative vascular beds." Circulation Research **100**(2): 174-190.

Aird, W. C. (2012). "Endothelial cell heterogeneity." Cold Spring Harbor perspectives in medicine **2**(1): a006429.

Arciniegas, E., A. B. Sutton, T. D. Allen and A. M. Schor (1992). "Transforming growth factor beta 1 promotes the differentiation of endothelial cells into smooth muscle-like cells in vitro." Journal of cell science **103**(2): 521-529.

Arras, M., W. D. Ito, D. Scholz, B. Winkler, J. Schaper and W. Schaper (1998). "Monocyte activation in angiogenesis and collateral growth in the rabbit hindlimb." Journal of Clinical Investigation **101**(1): 40.

Asada, H., J. Paszkowiak, D. Teso, K. Alvi, A. Thorisson, J. C. Frattini, F. A. Kudo, B. E. Sumpio and A. Dardik (2005). "Sustained orbital shear stress stimulates smooth muscle cell proliferation via the extracellular signal-regulated protein kinase 1/2 pathway." Journal of vascular surgery **42**(4): 772-780.

Auerbach, R., L. Alby, L. Morrissey, M. Tu and J. Joseph (1985). "Expression of organ-specific antigens on capillary endothelial cells." Microvascular research **29**(3): 401-411.

Bai, K. and W. Wang (2012). "Spatio-temporal development of the endothelial glycocalyx layer and its mechanical property in vitro." Journal of The Royal Society Interface: rsif20110901.

Bai, K. and W. Wang (2014). "Shear stress-induced redistribution of the glycocalyx on endothelial cells in vitro." Biomechanics and modeling in mechanobiology **13**(2): 303-311.

Barbee, K. A. (2002). "Role of subcellular shear–stress distributions in endothelial cell mechanotransduction." Annals of biomedical engineering **30**(4): 472-482.

Barker, A. L., O. Konopatskaya, C. R. Neal, J. V. Macpherson, J. L. Whatmore, C. P. Winlove, P. R. Unwin and A. C. Shore (2004). "Observation and characterisation of the glycocalyx of viable human endothelial cells using confocal laser scanning microscopy." Physical chemistry chemical physics **6**(5): 1006-1011.

Beatty, P. R., H. Puerta-Guardo, S. S. Killingbeck, D. R. Glasner, K. Hopkins and E. Harris (2015). "Dengue virus NS1 triggers endothelial permeability and vascular leak that is prevented by NS1 vaccination." Science translational medicine **7**(304): 304ra141-304ra141.

Bentz, G. L. and A. D. Yurochko (2008). "Human CMV infection of endothelial cells induces an angiogenic response through viral binding to EGF receptor and β1 and β3 integrins." Proceedings of the National Academy of Sciences **105**(14): 5531-5536.

Bernfield, M., M. Götte, P. W. Park, O. Reizes, M. L. Fitzgerald, J. Lincecum and M. Zako (1999). "Functions of cell surface heparan sulfate proteoglycans." Annual review of biochemistry **68**(1): 729-777.

Bilodeau, G. (1992). "Regular pyramid punch problem." Journal of applied mechanics **59**(3): 519-523.

Bombeli, T., B. R. Schwartz and J. M. Harlan (1998). "Adhesion of activated platelets to endothelial cells: evidence for a GPIIbIIIa-dependent bridging mechanism and novel roles for endothelial intercellular adhesion molecule 1 (ICAM-1), αvβ3 integrin, and GPIbα." The Journal of experimental medicine **187**(3): 329-339.

Braet, F. and E. Wisse (2002). "Structural and functional aspects of liver sinusoidal endothelial cell fenestrae: a review." Comparative hepatology **1**(1): 1.

Brambilla, R., K. Brückner, D. Orioli, A. D. Bergemann, J. G. Flanagan and R. Klein (1996). "Similarities and differences in the way transmembrane-type ligands interact with the Elk subclass of Eph receptors." Molecular and Cellular Neuroscience **8**(2): 199-209.

Briskin, M. J., L. M. McEvoy and E. C. Butcher (1993). "MAdCAM-1 has homology to immunoglobulin and mucin-like adhesion receptors and to IgA1." Nature **363**(6428): 461-464.

Cappella, B. and G. Dietler (1999). "Force-distance curves by atomic force microscopy." Surface science reports **34**(1): 1-104.

Carey, D. J. (1997). "Syndecans: multifunctional cell-surface co-receptors." Biochemical Journal **327**(1): 1-16.

Carmeliet, P. (2000). "Mechanisms of angiogenesis and arteriogenesis." Nature medicine **6**(4): 389-396.

Carmeliet, P., M.-G. Lampugnani, L. Moons, F. Breviario, V. Compernolle, F. Bono, G. Balconi, R. Spagnuolo, B. Oosthuyse and M. Dewerchin (1999). "Targeted deficiency or cytosolic truncation of the VE-cadherin gene in mice impairs VEGF-mediated endothelial survival and angiogenesis." Cell **98**(2): 147-157.

Ceriello, A., D. Giugliano, R. P. Dello, N. Passariello, F. Saccomanno and S. Sgambato (1983). "Glycosaminoglycans in human diabetes." Diabete & metabolisme **9**(1): 32-34.

Chappell, D., M. Jacob, O. Paul, M. Rehm, U. Welsch, M. Stoeckelhuber, P. Conzen and B. F. Becker (2009). "The glycocalyx of the human umbilical vein endothelial cell an impressive structure ex vivo but not in culture." Circulation research **104**(11): 1313-1317.

Chatterjee, S. and A. B. Fisher (2014). "Mechanotransduction in the endothelium: role of membrane proteins and reactive oxygen species in sensing, transduction, and transmission of the signal with altered blood flow." Antioxidants & redox signaling **20**(6): 899-913.

Chaudhuri, O., S. H. Parekh, W. A. Lam and D. A. Fletcher (2009). "Combined atomic force microscopy and side-view optical imaging for mechanical studies of cells." Nature methods **6**(5): 383-387.

Choi, K., M. Kennedy, A. Kazarov, J. C. Papadimitriou and G. Keller (1998). "A common precursor for hematopoietic and endothelial cells." Development **125**(4): 725-732.

Colman, P. M. (1994). "Influenza virus neuraminidase: structure, antibodies, and inhibitors." Protein Science **3**(10): 1687-1696.

Corle, T. and G. Kino (1996). "Confocal optic microscopy and related imaging systems." San Diego: Academic.

Curry, F. and C. Michel (1980). "A fiber matrix model of capillary permeability." Microvascular research **20**(1): 96-99.

Darling, E. M., S. Zauscher, J. A. Block and F. Guilak (2007). "A thin-layer model for viscoelastic, stress-relaxation testing of cells using atomic force microscopy: do cell properties reflect metastatic potential?" Biophysical journal **92**(5): 1784-1791.

Davidson, G. A., M. M. Truman, M. C. Fellers and M. S. Vinton (2007). Audio coding system using characteristics of a decoded signal to adapt synthesized spectral components, Google Patents.

Davies, P. F., A. Remuzzi, E. J. Gordon, C. F. Dewey and M. A. Gimbrone (1986). "Turbulent fluid shear stress induces vascular endothelial cell turnover in vitro." Proceedings of the National Academy of Sciences **83**(7): 2114-2117.

Davignon, J. and P. Ganz (2004). "Role of endothelial dysfunction in atherosclerosis." Circulation **109**(23 suppl 1): III-27-III-32.

De Keulenaer, G. W., D. C. Chappell, N. Ishizaka, R. M. Nerem, R. W. Alexander and K. K. Griendling (1998). "Oscillatory and steady laminar shear stress differentially affect human endothelial redox state role of a superoxide-producing NADH oxidase." Circulation research **82**(10): 1094-1101.

Deanfield, J., A. Donald, C. Ferri, C. Giannattasio, J. Halcox, S. Halligan, A. Lerman, G. Mancia, J. J. Oliver and A. C. Pessina (2005). "Endothelial function and dysfunction. Part I: Methodological issues for assessment in the different vascular beds: a statement by the Working Group on Endothelin and Endothelial Factors of the European Society of Hypertension." Journal of hypertension **23**(1): 7-17.

DePaola, N., P. F. Davies, W. F. Pritchard, L. Florez, N. Harbeck and D. C. Polacek (1999). "Spatial and temporal regulation of gap junction connexin43 in vascular endothelial cells exposed to controlled disturbed flows in vitro." Proceedings of the National Academy of Sciences **96**(6): 3154-3159.

DePaola, N., M. Gimbrone, P. F. Davies and C. Dewey (1992). "Vascular endothelium responds to fluid shear stress gradients." Arteriosclerosis, Thrombosis, and Vascular Biology **12**(11): 1254-1257.

Dewey, C., S. Bussolari, M. Gimbrone and P. F. Davies (1981). "The dynamic response of vascular endothelial cells to fluid shear stress." Journal of biomechanical engineering **103**(3): 177-185.

Dimitriadis, E. K., F. Horkay, J. Maresca, B. Kachar and R. S. Chadwick (2002). "Determination of elastic moduli of thin layers of soft material using the atomic force microscope." Biophysical journal **82**(5): 2798-2810.

Drake, B., C. Prater, A. Weisenhorn, S. Gould and T. Albrecht (1989). "Imaging crystals, polymers, and processes in water with the atomic force microscope." Science **243**(4898): 1586.

Du, X. L., D. Edelstein, S. Dimmeler, Q. Ju, C. Sui and M. Brownlee (2001). "Hyperglycemia inhibits endothelial nitric oxide synthase activity by posttranslational modification at the Akt site." The Journal of clinical investigation **108**(9): 1341-1348.

Ebong, E., D. Spray and J. Tarbell (2008). The role of the endothelial glycocalyx layer in transducing fluid shear stress into intracellular signaling events. Biorheology, IOS PRESS NIEUWE HEMWEG 6B, 1013 BG AMSTERDAM, NETHERLANDS.

Ebong, E. E., S. V. Lopez-Quintero, V. Rizzo, D. C. Spray and J. M. Tarbell (2014). "Shear-induced endothelial NOS activation and remodeling via heparan sulfate, glypican-1, and syndecan-1." Integrative Biology **6**(3): 338-347.

Ebong, E. E., F. P. Macaluso, D. C. Spray and J. M. Tarbell (2011). "Imaging the endothelial glycocalyx in vitro by rapid freezing/freeze substitution transmission electron microscopy." Arteriosclerosis, thrombosis, and vascular biology **31**(8): 1908-1915.

Elhadj, S., R. M. Akers and K. Forsten-Williams (2003). "Chronic pulsatile shear stress alters insulin-like growth factor-I (IGF-I) binding protein release in vitro." Annals of biomedical engineering **31**(2): 163-170.

Esmon, C. T. and W. G. Owen (1981). "Identification of an endothelial cell cofactor for thrombin-catalyzed activation of protein C." Proceedings of the National Academy of Sciences **78**(4): 2249-2252.

Fisher, T. E., P. E. Marszalek and J. M. Fernandez (2000). "Stretching single molecules into novel conformations using the atomic force microscope." Nature Structural & Molecular Biology **7**(9): 719-724.

Flaherty, J. T., J. E. Pierce, V. J. Ferrans, D. J. Patel, W. K. TUCKER and D. L. FRY (1972). "Endothelial nuclear patterns in the canine arterial tree with particular reference to hemodynamic events." Circulation Research **30**(1): 23-33.

Fletcher, N. F., G. K. Wilson, J. Murray, K. Hu, A. Lewis, G. M. Reynolds, Z. Stamataki, L. W. Meredith, I. A. Rowe and G. Luo (2012). "Hepatitis C virus infects the endothelial cells of the blood-brain barrier." Gastroenterology **142**(3): 634-643. e636.

Florian, J. A., J. R. Kosky, K. Ainslie, Z. Pang, R. O. Dull and J. M. Tarbell (2003). "Heparan sulfate proteoglycan is a mechanosensor on endothelial cells." Circulation research **93**(10): e136-e142.

Fransson, L.-Å., M. Belting, F. Cheng, M. Jönsson, K. Mani and S. Sandgren (2004). "Novel aspects of glypican glycobiology." Cellular and Molecular Life Sciences CMLS **61**(9): 1016-1024.

Furchgott, R. F. (1983). "Role of endothelium in responses of vascular smooth muscle." Circulation research **53**(5): 557-573.

Fux, L., N. Ilan, R. D. Sanderson and I. Vlodavsky (2009). "Heparanase: busy at the cell surface." Trends in biochemical sciences **34**(10): 511-519.

Gao, L. and H. H. Lipowsky (2010). "Composition of the endothelial glycocalyx and its relation to its thickness and diffusion of small solutes." Microvascular research **80**(3): 394-401.

Gawaz, M., H. Langer and A. E. May (2005). "Platelets in inflammation and atherogenesis." The Journal of clinical investigation **115**(12): 3378-3384.

Geary, R. L., N. Koyama, T. W. Wang, S. Vergel and A. W. Clowes (1995). "Failure of Heparin to Inhibit Intimal Hyperplasia in Injured Baboon Arteries The Role of Heparin-Sensitive and-Insensitive Pathways in the Stimulation of Smooth Muscle Cell Migration and Proliferation." Circulation **91**(12): 2972-2981.

Girard, J.-P. and T. A. Springer (1995). "High endothelial venules (HEVs): specialized endothelium for lymphocyte migration." Immunology today **16**(9): 449-457.

Grammas, P. (2011). "Neurovascular dysfunction, inflammation and endothelial activation: implications for the pathogenesis of Alzheimer's disease." Journal of neuroinflammation **8**(1): 1.

Grundy, J. E., K. M. Lawson, L. P. MacCormac, J. M. Fletcher and K. L. Yong (1998). "Cytomegalovirus-infected endothelial cells recruit neutrophils by the secretion of CXC chemokines and transmit virus by direct neutrophil-endothelial cell contact and during neutrophil transendothelial migration." Journal of Infectious Diseases **177**(6): 1465-1474.

Guck, J., S. Schinkinger, B. Lincoln, F. Wottawah, S. Ebert, M. Romeyke, D. Lenz, H. M. Erickson, R. Ananthakrishnan and D. Mitchell (2005). "Optical deformability as an inherent cell marker for testing malignant transformation and metastatic competence." Biophysical journal **88**(5): 3689-3698.

Guilak, F., W. R. Jones, H. P. Ting-Beall and G. M. Lee (1999). "The deformation behavior and mechanical properties of chondrocytes in articular cartilage." Osteoarthritis and Cartilage **7**(1): 59-70.

Gustafsson, M. G. (2005). "Nonlinear structured-illumination microscopy: wide-field fluorescence imaging with theoretically unlimited resolution." Proceedings of the National Academy of Sciences of the United States of America **102**(37): 13081-13086.

Guzik, T., R. Korbut and T. Adamek-Guzik (2003). "Nitric oxide and superoxide in inflammation." Journal of physiology and pharmacology **54**: 469-487.

Hürlimann, D., R. Weber, F. Enseleit and T. F. Lüscher (2005). "HIV-Infektion, antiretrovirale Therapie und Endothel." Herz Kardiovaskuläre Erkrankungen **30**(6): 472-480.

Halden, Y., R. Angelika, W. Atzenhofer, L. Szilak, A. Wabnig and J. Andreas (2004). "Interleukin-8 binds to syndecan-2 on human endothelial cells." Biochemical Journal **377**(2): 533-538.

Haldenby, K., D. Chappell, C. Winlove, K. Parker and J. Firth (1994). "Focal and regional variations in the composition of the glycocalyx of large vessel endothelium." Journal of vascular research **31**(1): 2-9.

Hamai, A., N. Hashimoto, H. Mochizuki, F. Kato, Y. Makiguchi, K. Horie and S. Suzuki (1997). "Two distinct chondroitin sulfate ABC lyases an endoeliminase yielding tetrasaccharides and an exoeliminase preferentially acting on oligosaccharides." Journal of Biological Chemistry **272**(14): 9123-9130.

Hamel, R., O. Dejarnac, S. Wichit, P. Ekchariyawat, A. Neyret, N. Luplertlop, M. Perera-Lecoin, P. Surasombatpattana, L. Talignani and F. Thomas (2015). "Biology of Zika virus infection in human skin cells." Journal of virology **89**(17): 8880-8896.

Hayashida, K., W. C. Parks and P. W. Park (2009). "Syndecan-1 shedding facilitates the resolution of neutrophilic inflammation by removing sequestered CXC chemokines." Blood **114**(14): 3033-3043.

Hecker, M., A. Mulsch, E. Bassenge and R. Busse (1993). "Vasoconstriction and increased flow: two principal mechanisms of shear stress-dependent endothelial autacoid release." American Journal of Physiology-Heart and Circulatory Physiology **265**(3): H828-H833.

Heemskerk, J. W., E. M. Bevers and T. Lindhout (2002). "Platelet activation and blood coagulation." THROMBOSIS AND HAEMOSTASIS-STUTTGART- **88**(2): 186-194.

Henderson, E. (1994). "Imaging of living cells by atomic force microscopy." Progress in surface science **46**(1): 39-60.

Henry, C. B. and B. R. Duling (1999). "Permeation of the luminal capillary glycocalyx is determined by hyaluronan." American Journal of Physiology-Heart and Circulatory Physiology **277**(2): H508-H514.

Henry, C. B. and B. R. Duling (2000). "TNF-α increases entry of macromolecules into luminal endothelial cell glycocalyx." American Journal of Physiology-Heart and Circulatory Physiology **279**(6): H2815-H2823.

Hertz, H. (1882). "Ueber die Verdunstung der Flüssigkeiten, insbesondere des Quecksilbers, im luftleeren Raume." Annalen der Physik **253**(10): 177-193.

Hsiai, T. K., S. K. Cho, H. M. Honda, S. Hama, M. Navab, L. L. Demer and C.-M. Ho (2002). "Endothelial cell dynamics under pulsating flows: significance of high versus low shear stress slew rates ($\partial \tau/\partial \tau$)." Annals of biomedical engineering **30**(5): 646-656.

Hu, X. and S. Weinbaum (1999). "A new view of Starling's hypothesis at the microstructural level." Microvascular research **58**(3): 281-304.

Ihrcke, N. S., L. E. Wrenshall, B. J. Lindman and J. L. Platt (1993). "Role of heparan sulfate in immune system-blood vessel interactions." Immunology today **14**(10): 500-505.

Jackson, R. L., S. J. Busch and A. D. Cardin (1991). "Glycosaminoglycans: molecular properties, protein interactions, and role in physiological processes." Physiological reviews **71**(2): 481-539.

Jarvis, M. A. and J. A. Nelson (2007). "Human cytomegalovirus tropism for endothelial cells: not all endothelial cells are created equal." Journal of virology **81**(5): 2095-2101.

Jung, U. and K. Ley (1997). "Regulation of E‐selectin, P‐selectin, and intercellular adhesion molecule 1 expression in mouse cremaster muscle vasculature." Microcirculation **4**(2): 311-319.

Kang, H., Q. Wen, P. A. Janmey, J. X. Tang, E. Conti and F. C. MacKintosh (2009). "Nonlinear elasticity of stiff filament networks: Strain stiffening, negative normal stress, and filament alignment in fibrin gels†." The Journal of Physical Chemistry B **113**(12): 3799-3805.

Kansas, G. S., K. B. Saunders, K. Ley, A. Zakrzewicz, R. M. Gibson, B. C. Furie, B. Furie and T. F. Tedder (1994). "A role for the epidermal growth factor-like domain of P-selectin in ligand recognition and cell adhesion." The Journal of cell biology **124**(4): 609-618.

Kataoka, N., K. Iwaki, K. Hashimoto, S. Mochizuki, Y. Ogasawara, M. Sato, K. Tsujioka and F. Kajiya (2002). "Measurements of endothelial cell-to-cell and cell-to-substrate gaps and micromechanical properties of endothelial cells during monocyte adhesion." Proceedings of the National Academy of Sciences **99**(24): 15638-15643.

Kemeny, S. F., D. S. Figueroa, A. M. Andrews, K. A. Barbee and A. M. Clyne (2011). "Glycated collagen alters endothelial cell actin alignment and nitric oxide release in response to fluid shear stress." Journal of biomechanics **44**(10): 1927-1935.

Komarova, Y. and A. B. Malik (2010). "Regulation of endothelial permeability via paracellular and transcellular transport pathways." Annual review of physiology **72**: 463-493.

Kushida, A., M. Yamato, C. Konno, A. Kikuchi, Y. Sakurai and T. Okano (1999). "Decrease in culture temperature releases monolayer endothelial cell sheets together with deposited fibronectin matrix from temperature‐responsive culture surfaces." Journal of biomedical materials research **45**(4): 355-362.

Lafrenie, R. M., M. R. Buchanan and F. W. Orr (1993). "Adhesion molecules and their role in cancer metastasis." Cell biophysics **23**(1-3): 3-89.

Lee, J., S. Kotliarova, Y. Kotliarov, A. Li, Q. Su, N. M. Donin, S. Pastorino, B. W. Purow, N. Christopher and W. Zhang (2006). "Tumor stem cells derived from glioblastomas cultured in bFGF and EGF more closely mirror the phenotype and genotype of primary tumors than do serum-cultured cell lines." Cancer cell **9**(5): 391-403.

Lehr, H., J. Seemüller, C. Hübner, M. Menger and K. Messmer (1993). "Oxidized LDL-induced leukocyte/endothelium interaction in vivo involves the receptor for platelet-activating factor." Arteriosclerosis, Thrombosis, and Vascular Biology **13**(7): 1013-1018.

Levesque, M. and R. Nerem (1985). "The elongation and orientation of cultured endothelial cells in response to shear stress." Journal of biomechanical engineering **107**(4): 341-347.

Levick, J. R. and C. C. Michel (2010). "Microvascular fluid exchange and the revised Starling principle." Cardiovascular research: cvq062.

Li, J., L. F. Brown, R. J. Laham, R. Volk and M. Simons (1997). "Macrophage-dependent regulation of syndecan gene expression." Circulation research **81**(5): 785-796.

Liao, L. and D. N. Granger (1995). "Modulation of oxidized low-density lipoprotein-induced microvascular dysfunction by nitric oxide." American Journal of Physiology-Heart and Circulatory Physiology **268**(4): H1643-H1650.

Linhardt, R., J. E. Turnbull, H. Wang, D. Loganathan and J. T. Gallagher (1990). "Examination of the substrate specificity of heparin and heparan sulfate lyases." Biochemistry **29**(10): 2611-2617.

Lipowsky, H. H. (2011). "Protease activity and the role of the endothelial glycocalyx in inflammation." Drug Discovery Today: Disease Models **8**(1): 57-62.

Lipowsky, H. H., L. Gao and A. Lescanic (2011). "Shedding of the endothelial glycocalyx in arterioles, capillaries, and venules and its effect on capillary hemodynamics during inflammation." American Journal of Physiology-Heart and Circulatory Physiology **301**(6): H2235-H2245.

Lopes, C. C., C. P. Dietrich and H. B. Nader (2006). "Specific structural features of syndecans and heparan sulfate chains are needed for cell signaling." Brazilian journal of medical and biological research **39**(2): 157-167.

Lopez-Quintero, S. V., R. Amaya, M. Pahakis and J. M. Tarbell (2009). "The endothelial glycocalyx mediates shear-induced changes in hydraulic conductivity." American Journal of Physiology-Heart and Circulatory Physiology **296**(5): H1451-H1456.

Lorant, D. E., K. D. Patel, T. M. McIntyre, R. P. McEver, S. M. Prescott and G. A. Zimmerman (1991). "Coexpression of GMP-140 and PAF by endothelium stimulated by histamine or thrombin: a juxtacrine system for adhesion and activation of neutrophils." The Journal of Cell Biology **115**(1): 223-234.

Lortat-Jacob, H., A. Grosdidier and A. Imberty (2002). "Structural diversity of heparan sulfate binding domains in chemokines." Proceedings of the National Academy of Sciences **99**(3): 1229-1234.

Luft, J. H. (1966). Fine structures of capillary and endocapillary layer as revealed by ruthenium red. Federation proceedings.

Müller, A. M., M. I. Hermanns, C. Cronen and C. J. Kirkpatrick (2002). "Comparative study of adhesion molecule expression in cultured human macro-and microvascular endothelial cells." Experimental and molecular pathology **73**(3): 171-180.

Masters, B. R. (2006). Confocal microscopy and multiphoton excitation microscopy: the genesis of live cell imaging, SPIE Washington, DC.

Masuda, H., K. Kawamura, K. Tohda, T. Shozawa, M. Sageshima and A. Kamiya (1989). "Increase in endothelial cell density before artery enlargement in flow-loaded

canine carotid artery." Arteriosclerosis, Thrombosis, and Vascular Biology **9**(6): 812-823.

Megens, R., S. Reitsma, P. Schiffers, R. Hilgers, J. De Mey, D. Slaaf and M. van Zandvoort (2006). "Two-photon microscopy of vital murine elastic and muscular arteries." Journal of vascular research **44**(2): 87-98.

Merks, R. M., S. V. Brodsky, M. S. Goligorksy, S. A. Newman and J. A. Glazier (2006). "Cell elongation is key to in silico replication of in vitro vasculogenesis and subsequent remodeling." Developmental biology **289**(1): 44-54.

Michel, C. and F. Curry (1999). "Microvascular permeability." Physiological reviews **79**(3): 703-761.

Michel, T. and O. Feron (1997). "Nitric oxide synthases: which, where, how, and why?" Journal of Clinical Investigation **100**(9): 2146.

Michiels, C. (2003). "Endothelial cell functions." Journal of cellular physiology **196**(3): 430-443.

Mikliaev, I. and S. Asselborn (2007). Method for obtaining a high resolution image, Google Patents.

Mironov, A., M. Rekhter, V. Kolpakov, E. Andreeva, R. Polishchuk, S. Bannykh, S. Filippov, L. Peretjatko, L. Kulida and A. Orekhov (1995). "Heterogeneity of smooth muscle cells in embryonic human aorta." Tissue and Cell **27**(1): 31-38.

Mochizuki, S., H. Vink, O. Hiramatsu, T. Kajita, F. Shigeto, J. A. Spaan and F. Kajiya (2003). "Role of hyaluronic acid glycosaminoglycans in shear-induced endothelium-derived nitric oxide release." American Journal of Physiology-Heart and Circulatory Physiology **285**(2): H722-H726.

Moerner, W. E. (2015). "Single‐Molecule Spectroscopy, Imaging, and Photocontrol: Foundations for Super‐Resolution Microscopy (Nobel Lecture)." Angewandte Chemie International Edition **54**(28): 8067-8093.

Moncada, S., A. Herman, E. A. HIGGs and J. Vane (1977). "Differential formation of prostacyclin (PGX or PGI 2) by layers of the arterial wall. An explanation for the anti-thrombotic properties of vascular endothelium." Thrombosis research **11**(3): 323-344.

Moon, J. J., M. Matsumoto, S. Patel, L. Lee, J. L. Guan and S. Li (2005). "Role of cell surface heparan sulfate proteoglycans in endothelial cell migration and mechanotransduction." Journal of cellular physiology **203**(1): 166-176.

Mulivor, A. W. and H. H. Lipowsky (2002). "Role of glycocalyx in leukocyte-endothelial cell adhesion." American Journal of Physiology-Heart and Circulatory Physiology **283**(4): H1282-H1291.

Mulivor, A. W. and H. H. Lipowsky (2004). "Inflammation-and ischemia-induced shedding of venular glycocalyx." American Journal of Physiology-Heart and Circulatory Physiology **286**(5): H1672-H1680.

Murdoch, A. D., G. Dodge, I. Cohen, R. Tuan and R. Iozzo (1992). "Primary structure of the human heparan sulfate proteoglycan from basement membrane (HSPG2/perlecan). A chimeric molecule with multiple domains homologous to the low density lipoprotein receptor, laminin, neural cell adhesion molecules, and epidermal growth factor." Journal of Biological Chemistry **267**(12): 8544-8557.

Nader, H., C. Dietrich, V. Buonassisi and P. Colburn (1987). "Heparin sequences in the heparan sulfate chains of an endothelial cell proteoglycan." Proceedings of the National Academy of Sciences **84**(11): 3565-3569.

Nader, H. B., M. A. Porcionatto, I. Tersariol, M. Pinhal, F. W. Oliveira, C. T. Moraes and C. P. Dietrich (1990). "Purification and substrate specificity of heparitinase I and heparitinase II from Flavobacterium heparinum. Analyses of the heparin and heparan sulfate degradation products by 13C NMR spectroscopy." Journal of Biological Chemistry **265**(28): 16807-16813.

Nandi, A., P. Estess and M. H. Siegelman (2000). "Hyaluronan anchoring and regulation on the surface of vascular endothelial cells is mediated through the functionally active form of CD44." Journal of Biological Chemistry **275**(20): 14939-14948.

Nishida, N., H. Yano, T. Nishida, T. Kamura and M. Kojiro (2006). "Angiogenesis in cancer." Vascular health and risk management **2**(3): 213.

Norvell, S. M., S. M. Ponik, D. K. Bowen, R. Gerard and F. M. Pavalko (2004). "Fluid shear stress induction of COX-2 protein and prostaglandin release in cultured MC3T3-E1 osteoblasts does not require intact microfilaments or microtubules." Journal of applied physiology **96**(3): 957-966.

O'Callaghan, R., K. M. Job, R. O. Dull and V. Hlady (2011). "Stiffness and heterogeneity of the pulmonary endothelial glycocalyx measured by atomic force microscopy." American Journal of Physiology-Lung Cellular and Molecular Physiology **301**(3): L353-L360.

Oberleithner, H., W. Peters, K. Kusche-Vihrog, S. Korte, H. Schillers, K. Kliche and K. Oberleithner (2011). "Salt overload damages the glycocalyx sodium barrier of vascular endothelium." Pflügers Archiv-European Journal of Physiology **462**(4): 519-528.

Okegawa, T., R.-C. Pong, Y. Li and J.-T. Hsieh (2004). "The role of cell adhesion molecule in cancer progression and its application in cancer therapy." Acta Biochimica Polonica-English Edition- **51**: 445-458.

Oohira, A., T. N. Wight and P. Bornstein (1983). "Sulfated proteoglycans synthesized by vascular endothelial cells in culture." Journal of Biological Chemistry **258**(3): 2014-2021.

Orr, F. W., H. H. Wang, R. M. Lafrenie, S. Scherbarth and D. M. Nance (2000). "Interactions between cancer cells and the endothelium in metastasis." The Journal of pathology **190**(3): 310-329.

Pahakis, M. Y., J. R. Kosky, R. O. Dull and J. M. Tarbell (2007). "The role of endothelial glycocalyx components in mechanotransduction of fluid shear stress." Biochemical and biophysical research communications **355**(1): 228-233.

Palmer, R. M., A. Ferrige and S. Moncada (1987). "Nitric oxide release accounts for the biological activity of endothelium-derived relaxing factor."

Parish, C. R. (2006). "The role of heparan sulphate in inflammation." Nature Reviews Immunology **6**(9): 633-643.

Park, S., D. Koch, R. Cardenas, J. Käs and C. Shih (2005). "Cell motility and local viscoelasticity of fibroblasts." Biophysical journal **89**(6): 4330-4342.

Patel, K. D., M. U. Nollert and R. P. McEver (1995). "P-selectin must extend a sufficient length from the plasma membrane to mediate rolling of neutrophils." The Journal of Cell Biology **131**(6): 1893-1902.

Pawley, J. (1995). Handbook of confocal microscopy. Pawley JB, Plenum, New York.

Perelygina, L., Q. Zheng, M. Metcalfe and J. Icenogle (2013). "Persistent infection of human fetal endothelial cells with rubella virus." PloS one **8**(8): e73014.

Pohl, U., K. Herlan, A. Huang and E. Bassenge (1991). "EDRF-mediated shear-induced dilation opposes myogenic vasoconstriction in small rabbit arteries." American Journal of Physiology-Heart and Circulatory Physiology **261**(6): H2016-H2023.

Ponik, S. M. and F. M. Pavalko (2004). "Formation of focal adhesions on fibronectin promotes fluid shear stress induction of COX-2 and PGE2 release in MC3T3-E1 osteoblasts." Journal of Applied Physiology **97**(1): 135-142.

Potter, D. R. and E. R. Damiano (2008). "The hydrodynamically relevant endothelial cell glycocalyx observed in vivo is absent in vitro." Circulation research **102**(7): 770-776.

Potter, D. R., J. Jiang and E. R. Damiano (2009). "The recovery time course of the endothelial cell glycocalyx in vivo and its implications in vitro." Circulation research **104**(11): 1318-1325.

Presta, M., M. Statuto, A. Isacchi, P. Caccia, A. Pozzi, A. Gualandris, M. Rusnati, L. Bergonzoni and P. Sarmientos (1992). "Structure-function relationship of basic fibroblast growth factor: site-directed mutagenesis of a putative heparin-binding and receptor-binding region." Biochemical and biophysical research communications **185**(3): 1098-1107.

Pries, A., T. W. Secomb and P. Gaehtgens (2000). "The endothelial surface layer." Pflügers Archiv **440**(5): 653-666.

Qiao, L., T. Nishimura, L. Shi, D. Sessions, A. Thrasher, J. R. Trudell, G. J. Berry, R. G. Pearl and P. N. Kao (2014). "Endothelial fate mapping in mice with pulmonary hypertension." Circulation **129**(6): 692-703.

Raines, E. W. and R. Ross (1992). "Compartmentalization of PDGF on extracellular binding sites dependent on exon-6-encoded sequences." The Journal of cell biology **116**(2): 533-543.

Rapraeger, A., M. Jalkanen and M. Bernfield (1986). "Cell surface proteoglycan associates with the cytoskeleton at the basolateral cell surface of mouse mammary epithelial cells." The Journal of cell biology **103**(6): 2683-2696.

Reitsma, S., D. W. Slaaf, H. Vink, M. A. van Zandvoort and M. G. oude Egbrink (2007). "The endothelial glycocalyx: composition, functions, and visualization." Pflügers Archiv-European Journal of Physiology **454**(3): 345-359.

Reitsma, S., H. Vink, B. M. van den Berg, V. Lima Passos, W. Engels, D. Slaaf and M. van Zandvoort (2011). "Endothelial glycocalyx structure in the intact carotid artery: a two-photon laser scanning microscopy study." Journal of vascular research **48**(4): 297-306.

Reymann, J., D. Baddeley, M. Gunkel, P. Lemmer, W. Stadter, T. Jegou, K. Rippe, C. Cremer and U. Birk (2008). "High-precision structural analysis of subnuclear complexes in fixed and live cells via spatially modulated illumination (SMI) microscopy." Chromosome Research **16**(3): 367-382.

Rico, F., P. Roca-Cusachs, N. Gavara, R. Farré, M. Rotger and D. Navajas (2005). "Probing mechanical properties of living cells by atomic force microscopy with blunted pyramidal cantilever tips." Physical Review E **72**(2): 021914.

Risau, W. and I. Flamme (1995). "Vasculogenesis." Annual review of cell and developmental biology **11**(1): 73-91.

Romero, L. I., D. N. Zhang, G. S. Herron and M. A. Karasek (1997). "Interleukin‐1 induces major phenotypic changes in human skin microvascular endothelial cells." Journal of cellular physiology **173**(1): 84-92.

Rosenberg, E. S., J. M. Billingsley, A. M. Caliendo, S. L. Boswell, P. E. Sax, S. A. Kalams and B. D. Walker (1997). "Vigorous HIV-1-specific CD4+ T cell responses associated with control of viremia." Science **278**(5342): 1447-1450.

Sasaki, K., Y. Okouchi, H.-J. Rothkötter and R. Pabst (1998). "Three-dimensional distribution of intercellular adhesion molecule-1 on lymphocytes in the high endothelial venule analyzed by backscatter electron imaging." Cells Tissues Organs **162**(1): 33-39.

Satcher, R., C. F. Dewey and J. H. Hartwig (1997). "Mechanical remodeling of the endothelial surface and actin cytoskeleton induced by fluid flow." Microcirculation **4**(4): 439-453.

Sato, H., M. Katano, T. Takigawa and T. Masuda (2001). "Estimation for the elasticity of vascular endothelial cells on the basis of atomic force microscopy and Young's modulus of gelatin gels." Polymer Bulletin **47**(3-4): 375-381.

Sato, H., N. Kataoka, F. Kajiya, M. Katano, T. Takigawa and T. Masuda (2004). "Kinetic study on the elastic change of vascular endothelial cells on collagen matrices by atomic force microscopy." Colloids and Surfaces B: Biointerfaces **34**(2): 141-146.

Savery, M. D. and E. R. Damiano (2008). "The endothelial glycocalyx is hydrodynamically relevant in arterioles throughout the cardiac cycle." Biophysical journal **95**(3): 1439-1447.

Schmidt, E. P., Y. Yang, W. J. Janssen, A. Gandjeva, M. J. Perez, L. Barthel, R. L. Zemans, J. C. Bowman, D. E. Koyanagi and Z. X. Yunt (2012). "The pulmonary endothelial glycocalyx regulates neutrophil adhesion and lung injury during experimental sepsis." Nature medicine **18**(8): 1217-1223.

Scott, P. (1989). "The role of TH1 and TH2 cells in experimental cutaneous leishmaniasis." Experimental parasitology **68**(3): 369-372.

Secomb, T. W., R. Hsu and A. Pries (2001). "Motion of red blood cells in a capillary with an endothelial surface layer: effect of flow velocity." American Journal of Physiology-Heart and Circulatory Physiology **281**(2): H629-H636.

Segarini, P. R., D. M. Rosen and S. M. Seyedin (1989). "Binding of transforming growth factor-β to cell surface proteins varies with cell type." Molecular Endocrinology **3**(2): 261-272.

Shalaby, F., J. Rossant, T. P. Yamaguchi, M. Gertsenstein, X.-F. Wu, M. L. Breitman and A. C. Schuh (1995). "Failure of blood-island formation and vasculogenesis in Flk-1-deficient mice." Nature **376**(6535): 62-66.

Sheetz, M. P. (1995). "Cellular plasma membrane domains." Molecular membrane biology **12**(1): 89-91.

Sheppard, C. (1997). "Effects of specimen refractive index on confocal imaging." Journal of microscopy **185**(3): 366-374.

Shin, D. and K. Athanasiou (1999). "Cytoindentation for obtaining cell biomechanical properties." Journal of Orthopaedic Research **17**(6): 880-890.

Shyy, Y.-J., H.-J. Hsieh, S. Usami and S. Chien (1994). "Fluid shear stress induces a biphasic response of human monocyte chemotactic protein 1 gene expression in vascular endothelium." Proceedings of the National Academy of Sciences **91**(11): 4678-4682.

Silva, M. E. and C. P. Dietrich (1974). "Isolation and partial characterization of three induced enzymes from Flavobacterium heparinum involved in the degradation of heparin and heparitin sulfates." Biochemical and biophysical research communications **56**(4): 965-972.

Singh, A., J. D. Van Hamme and O. P. Ward (2007). "Surfactants in microbiology and biotechnology: Part 2. Application aspects." Biotechnology advances **25**(1): 99-121.

Skogsberg, J., J. Lundström, A. Kovacs, R. Nilsson, P. Noori, S. Maleki, M. Köhler, A. Hamsten, J. Tegnér and J. Björkegren (2008). "Transcriptional profiling uncovers a network of cholesterol-responsive atherosclerosis target genes." PLoS Genet **4**(3): e1000036.

Smith, M. L., D. S. Long, E. R. Damiano and K. Ley (2003). "Near-wall μ-PIV reveals a hydrodynamically relevant endothelial surface layer in venules in vivo." Biophysical journal **85**(1): 637-645.

Sperandio, M. (2006). "Selectins and glycosyltransferases in leukocyte rolling in vivo." Febs Journal **273**(19): 4377-4389.

Squire, J. M., M. Chew, G. Nneji, C. Neal, J. Barry and C. Michel (2001). "Quasi-periodic substructure in the microvessel endothelial glycocalyx: a possible explanation for molecular filtering?" Journal of structural biology **136**(3): 239-255.

Starling, E. H. (1896). "On the absorption of fluids from the connective tissue spaces." Classic Papers in Critical Care **19**: 303.

Stern, D., P. Nawroth, D. Handley and W. Kisiel (1985). "An endothelial cell-dependent pathway of coagulation." Proceedings of the National Academy of Sciences **82**(8): 2523-2527.

Stevens, T., J. G. Garcia, D. M. Shasby, J. Bhattacharya and A. B. Malik (2000). "Mechanisms regulating endothelial cell barrier function." American Journal of Physiology-Lung Cellular and Molecular Physiology **279**(3): L419-L422.

Sumpio, B. E., J. T. Riley and A. Dardik (2002). "Cells in focus: endothelial cell." The international journal of biochemistry & cell biology **34**(12): 1508-1512.

Svoboda, K. and S. M. Block (1994). "Force and velocity measured for single kinesin molecules." Cell **77**(5): 773-784.

Tarbell, J. M. and M. Pahakis (2006). "Mechanotransduction and the glycocalyx." Journal of internal medicine **259**(4): 339-350.

Tedder, T., D. Steeber, A. Chen and P. Engel (1995). "The selectins: vascular adhesion molecules." The FASEB Journal **9**(10): 866-873.

Thi, M. M., J. M. Tarbell, S. Weinbaum and D. C. Spray (2004). "The role of the glycocalyx in reorganization of the actin cytoskeleton under fluid shear stress: a "bumper-car" model." Proceedings of the National Academy of Sciences of the United States of America **101**(47): 16483-16488.

Tkachenko, E., J. M. Rhodes and M. Simons (2005). "Syndecans new kids on the signaling block." Circulation Research **96**(5): 488-500.

Tricot, O., Z. Mallat, C. Heymes, J. Belmin, G. Leseche and A. Tedgui (2000). "Relation between endothelial cell apoptosis and blood flow direction in human atherosclerotic plaques." Circulation **101**(21): 2450-2453.

Ushiyama, S., T. M. Laue, K. L. Moore, H. Erickson and R. McEver (1993). "Structural and functional characterization of monomeric soluble P-selectin and comparison with membrane P-selectin." Journal of Biological Chemistry **268**(20): 15229-15237.

Van De Voorde, J. and I. Leusen (1983). "Role of the endothelium in the vasodilator response of rat thoracic aorta to histamine." European journal of pharmacology **87**(1): 113-120.

van den Berg, B. M., J. A. Spaan, T. M. Rolf and H. Vink (2006). "Atherogenic region and diet diminish glycocalyx dimension and increase intima-to-media ratios at murine carotid artery bifurcation." American Journal of Physiology-Heart and Circulatory Physiology **290**(2): H915-H920.

van den Berg, B. M., J. A. Spaan and H. Vink (2009). "Impaired glycocalyx barrier properties contribute to enhanced intimal low-density lipoprotein accumulation at the carotid artery bifurcation in mice." Pflügers Archiv-European Journal of Physiology **457**(6): 1199-1206.

van den Berg, B. M., H. Vink and J. A. Spaan (2003). "The endothelial glycocalyx protects against myocardial edema." Circulation research **92**(6): 592-594.

van Deurs, B., K. Roepstorff, A. M. Hommelgaard and K. Sandvig (2003). "Caveolae: anchored, multifunctional platforms in the lipid ocean." Trends in cell biology **13**(2): 92-100.

van Golen, R. F., T. M. van Gulik and M. Heger (2012). "Mechanistic overview of reactive species-induced degradation of the endothelial glycocalyx during hepatic ischemia/reperfusion injury." Free Radical Biology and Medicine **52**(8): 1382-1402.

van Haaren, P. M., E. VanBavel, H. Vink and J. A. Spaan (2003). "Localization of the permeability barrier to solutes in isolated arteries by confocal microscopy." American Journal of Physiology-Heart and Circulatory Physiology **285**(6): H2848-H2856.

Varki, A. (2008). "Sialic acids in human health and disease." Trends in molecular medicine **14**(8): 351-360.

Vink, H. and B. R. Duling (2000). "Capillary endothelial surface layer selectively reduces plasma solute distribution volume." American Journal of Physiology-Heart and Circulatory Physiology **278**(1): H285-H289.

Visser, M. R., P. B. Tracy, G. M. Vercellotti, J. L. Goodman, J. G. White and H. S. Jacob (1988). "Enhanced thrombin generation and platelet binding on herpes simplex virus-infected endothelium." Proceedings of the National Academy of Sciences **85**(21): 8227-8230.

Wang, H. U., Z.-F. Chen and D. J. Anderson (1998). "Molecular distinction and angiogenic interaction between embryonic arteries and veins revealed by ephrin-B2 and its receptor Eph-B4." Cell **93**(5): 741-753.

Wang, L., M. Fuster, P. Sriramarao and J. D. Esko (2005). "Endothelial heparan sulfate deficiency impairs L-selectin-and chemokine-mediated neutrophil trafficking during inflammatory responses." Nature immunology **6**(9): 902-910.

Wedmore, C. V. and T. Williams (1981). "Control of vascular permeability by polymorphonuclear leukocytes in inflammation." Nature **289**(5799): 646.

Weigel, P. H. and P. L. DeAngelis (2007). "Hyaluronan synthases: a decade-plus of novel glycosyltransferases." Journal of Biological Chemistry **282**(51): 36777-36781.

Weinbaum, S. (1998). "1997 Whitaker distinguished lecture: models to solve mysteries in biomechanics at the cellular level; a new view of fiber matrix layers." Annals of biomedical engineering **26**(4): 627-643.

Weinbaum, S., X. Zhang, Y. Han, H. Vink and S. C. Cowin (2003). "Mechanotransduction and flow across the endothelial glycocalyx." Proceedings of the National Academy of Sciences **100**(13): 7988-7995.

Wiedeman, M. P. (1963). "Dimensions of blood vessels from distributing artery to collecting vein." Circulation research **12**(4): 375-378.

Xiong, J. P., T. Stehle, S. Goodman and M. Arnaout (2003). "Integrins, cations and ligands: making the connection." Journal of Thrombosis and Haemostasis **1**(7): 1642-1654.

Yamagata, T., H. Saito, O. Habuchi and S. Suzuki (1968). "Purification and properties of bacterial chondroitinases and chondrosulfatases." Journal of Biological Chemistry **243**(7): 1523-1535.

Yamato, M., Y. Akiyama, J. Kobayashi, J. Yang, A. Kikuchi and T. Okano (2007). "Temperature-responsive cell culture surfaces for regenerative medicine with cell sheet engineering." Progress in Polymer Science **32**(8): 1123-1133.

Yamazaki, D., S. Kurisu and T. Takenawa (2005). "Regulation of cancer cell motility through actin reorganization." Cancer science **96**(7): 379-386.

Yano, K., D. Gale, S. Massberg, P. K. Cheruvu, R. Monahan-Earley, E. S. Morgan, D. Haig, U. H. von Andrian, A. M. Dvorak and W. C. Aird (2007). "Phenotypic heterogeneity is an evolutionarily conserved feature of the endothelium." Blood **109**(2): 613-615.

Yao, Y., A. Rabodzey and C. F. Dewey (2007). "Glycocalyx modulates the motility and proliferative response of vascular endothelium to fluid shear stress." American Journal of Physiology-Heart and Circulatory Physiology **293**(2): H1023-H1030.

Yen, W.-Y., B. Cai, M. Zeng, J. M. Tarbell and B. M. Fu (2012). "Quantification of the endothelial surface glycocalyx on rat and mouse blood vessels." Microvascular research **83**(3): 337-346.

Yoneda, A. and J. R. Couchman (2003). "Regulation of cytoskeletal organization by syndecan transmembrane proteoglycans." Matrix biology **22**(1): 25-33.

Yuan, L., A. Le Bras, A. Sacharidou, K. Itagaki, Y. Zhan, M. Kondo, C. V. Carman, G. E. Davis, W. C. Aird and P. Oettgen (2012). "ETS-related gene (ERG) controls endothelial cell permeability via transcriptional regulation of the claudin 5 (CLDN5) gene." Journal of Biological Chemistry **287**(9): 6582-6591.

Zarins, C. K., D. P. Giddens, B. Bharadvaj, V. S. Sottiurai, R. F. Mabon and S. Glagov (1983). "Carotid bifurcation atherosclerosis. Quantitative correlation of plaque localization with flow velocity profiles and wall shear stress." Circulation research **53**(4): 502-514.

Zeng, Y., R. Adamson, F.-R. Curry and J. Tarbell (2013). "Plasma protein protects endothelial glycocalyx mediated by sphingosine-1-phosphate." The FASEB Journal **27**(1 Supplement): 896.891-896.891.

Zeng, Y. and J. M. Tarbell (2014). "The adaptive remodeling of endothelial glycocalyx in response to fluid shear stress." PloS one **9**(1): e86249.

Zetter, B. (1993). Adhesion molecules in tumor metastasis. Seminars in cancer biology.

Zhao, Y., S. Chien and S. Weinbaum (2001). "Dynamic contact forces on leukocyte microvilli and their penetration of the endothelial glycocalyx." Biophysical journal **80**(3): 1124-1140.